

AD/A-000 893

STABILIZATION OF EXTERNALLY SLUNG  
HELICOPTER LOADS

T. C. Watkins, et al

Northrop Corporation

Prepared for:

Army Air Mobility Research and  
Development Laboratory

August 1974

DISTRIBUTED BY:

**NTIS**

National Technical Information Service  
U. S. DEPARTMENT OF COMMERCE

### EUSTIS DIRECTORATE POSITION STATEMENT

The analytical techniques developed under this helicopter external load stabilization program represent a significant contribution to assist in future investigations of this type. The investigation was somewhat narrowed by the lack of dynamic data pertaining to typical external loads; however, dynamic data on the MILVAN container was obtained experimentally by the contractor and formed the basis for this investigation. The load stabilization concepts investigated herein were verified by piloted flight simulation on Northrop's Large Amplitude Moving Base Simulator.

This report has been reviewed by this Directorate and is considered to be technically sound. The technical monitor for this contract was Mr. Richard E. Lane, Military Operations Technology Division.

#### DISCLAIMERS

The findings in this report are not to be construed as an official Department of the Army position unless so designated by other authorized documents.

When Government drawings, specifications, or other data are used for any purpose other than in connection with a definitely related Government procurement operation, the United States Government thereby incurs no responsibility nor any obligation whatsoever; and the fact that the Government may have formulated, furnished, or in any way supplied the said drawings, specifications, or other data is not to be regarded by implication or otherwise as in any manner licensing the holder or any other person or corporation, or conveying any rights or permission, to manufacture, use, or sell any patented invention that may in any way be related thereto.

Trade names cited in this report do not constitute an official endorsement or approval of the use of such commercial hardware or software.

#### DISPOSITION INSTRUCTIONS

Destroy this report when no longer needed. Do not return it to the originator.

BY D	DISTRIBUTION/AVAILABILITY CODES	BY D	ACCESSION BY	RTIS	WTR Section
			0 0	0 0	0 0
Dist.	AVAIL. and/or SPECIAL	BY D	UNCLASSIFIED	UNCLASSIFIED	UNCLASSIFIED
			UNCLASSIFIED	UNCLASSIFIED	UNCLASSIFIED
BY D	DISTRIBUTION/AVAILABILITY CODES	BY D	JUSTIFICATION	UNCLASSIFIED	UNCLASSIFIED
			UNCLASSIFIED	UNCLASSIFIED	UNCLASSIFIED

Unclassified

SECURITY CLASSIFICATION OF THIS PAGE (When Data Entered)

REPORT DOCUMENTATION PAGE		READ INSTRUCTIONS BEFORE COMPLETING FORM
1. REPORT NUMBER USAAMRDL-TR-74-42	2. GOVT ACCESSION NO.	3. RECIPIENT'S CATALOG NUMBER ADIA 000 893
4. TITLE (and Subtitle)  STABILIZATION OF EXTERNALLY SLUNG HELICOPTER LOADS		5. TYPE OF REPORT & PERIOD COVERED FINAL REPORT 7/1/72 thru 10/31/73
		6. PERFORMING ORG. REPORT NUMBER
7. AUTHOR(s)  T.C. Watkins, J.B. Sinacori, and D.F. Kesler		8. CONTRACT OR GRANT NUMBER(s)  DAAJ02-72-C-0047
9. PERFORMING ORGANIZATION NAME AND ADDRESS Northrop Corporation, Electronics Division 2301 West 120th Street Hawthorne, California 90250		10. PROGRAM ELEMENT, PROJECT, TASK AREA & WORK UNIT NUMBERS  1F162207AA33
11. CONTROLLING OFFICE NAME AND ADDRESS Eustis Directorate U.S. Army Air Mobility R&D Laboratory Fort Eustis, Virginia 23604		12. REPORT DATE August 1974
		13. NUMBER OF PAGES 129
14. MONITORING AGENCY NAME & ADDRESS (if different from Controlling Office)		15. SECURITY CLASS. (of this report)  Unclassified
		15a. DECLASSIFICATION/DOWNGRADING SCHEDULE
16. DISTRIBUTION STATEMENT (of this Report)  Approved for public release; distribution unlimited.		
17. DISTRIBUTION STATEMENT (of the abstract entered in Block 20, if different from Report)		
18. SUPPLEMENTARY NOTES  Reproduced by NATIONAL TECHNICAL INFORMATION SERVICE U S Department of Commerce Springfield VA 22151		
19. KEY WORDS (Continue on reverse side if necessary and identify by block number)  Loads (Forces) Helicopters Stabilization Systems Slings		
20. ABSTRACT (Continue on reverse side if necessary and identify by block number) The stability of external loads carried by helicopters is examined and analyzed. Use is made of experimental data and theoretical analyses to understand why load carrying speed is limited, and an attempt is made to identify promising stabilization concepts and to determine their capability to extend carrying speed. This effort is concentrated on the 8-by-8-by-20-foot cargo container; however, implications relating to other loads are given. An attempt is made to select the appropriate combination of analysis techniques that will yield a practical solution to the problem.		

DD FORM 1 JAN 73 1473

EDITION OF 1 NOV 68 IS OBSOLETE

Unclassified

SECURITY CLASSIFICATION OF THIS PAGE (When Data Entered)

Unclassified

SECURITY CLASSIFICATION OF THIS PAGE(When Data Entered)

20. (Continued)

The dynamics of the 8-by-8-by-20 container are dominated by unsteady aerodynamic effects and as such require additional experiments and associated computer analysis. The motions of this load are modeled, and this model is used in an analysis of stabilization systems designed to extend the carrying speed limitations. Several stabilization concepts are explored that show promise of extending carrying speed to 200 knots.

11  
Unclassified

SECURITY CLASSIFICATION OF THIS PAGE(When Data Entered)



## PREFACE

This final technical report covers the work performed by the Northrop Corporation, Aircraft Division, under Contract DAAJ02-72-C-0047, DA Project 1F162207AA33, during the period from July 1972 to October 1973. It was sponsored by the Eustis Directorate, U.S. Army Air Mobility Research and Development Laboratory, Ft. Eustis, Va., and was monitored by Mr. R.E. Lane. J.B. Sinacori served as principal investigator.

This program was a follow-on effort to Contract DAAJ02-70-C-0067, "In-Flight Stabilization of Externally Slung Helicopter Loads" (USAAMRDL TR 73-5). In the final report for the previous contract, various conclusions were reached regarding many different types of loads including the 8-by-8-by-20-foot cargo container. Recommendations were also submitted that urged the acquisition of load wind tunnel data in order to improve the accuracy of the analysis employed in that work.

Wind tunnel tests were performed on the cargo container during the follow-on effort, but their use did not improve the accuracy of the analysis. Unsteady aerodynamic effects were present which required additional dynamic wind tunnel tests in order to understand them. These tests were performed for only the 8-by-8-by-20-foot container. So while the analysis of this container is now accurate, a more comprehensive study of other loads is not warranted until confidence can be gained that their behavior is not also dominated by unsteady aerodynamic effects. A case in point is the unsuccessful attempt during this study to predict the dynamics of an 8-by-8-by-40-foot container using the results for the 20-foot container.

The present study defined the "weathercock stability" and other parameters described in the previous study and shows how they may be controlled. While specific carrying, speed boundaries for the 20-foot container could not be established in the previous study, they have been during this one through the use of a sophisticated flight simulation of the 347 helicopter prototype.

In the present study, the emphasis has been placed on achieving a reasonable mix of analysis and test that give credible results as compared with flight test. As such, only one load was treated and no general conclusions were reached regarding the overall problem of allowable sling load-carrying speed.

## TABLE OF CONTENTS

	<u>Page</u>
PREFACE . . . . .	1
LIST OF ILLUSTRATIONS . . . . .	5
LIST OF TABLES . . . . .	8
INTRODUCTION . . . . .	9
PRELIMINARY ANALYSIS . . . . .	11
Pilot Interview Results . . . . .	11
Static Wind Tunnel Tests and Aerodynamic Analysis . . . . .	11
Linear Stability Analysis . . . . .	21
Flight Data Correlations . . . . .	38
DYNAMIC WIND TUNNEL TEST . . . . .	41
Test Scope . . . . .	41
Test Results . . . . .	43
Wind Tunnel Speed Scaling . . . . .	44
NONLINEAR ANALYSIS OF THE 8-BY-8-BY-20-FOOT CONTAINER . . . . .	46
Interpretation of the Dynamic Wind Tunnel Test Results . . . . .	46
The Analog Matching Study . . . . .	46
Description of the Dynamic Model and Its Predictions . . . . .	49
CARRYING SPEED CRITERIA AND LIMITATIONS . . . . .	54
EXTENDING CARRYING SPEEDS AND EFFECTS OF VARIOUS STABILIZATION CONCEPTS . . . . .	58
Suspension System Optimization . . . . .	60
Maneuvering the Helicopter . . . . .	63
Modifying the Container Shape . . . . .	63
Active Stability Augmentation Using Cable Actuators . . . . .	64
Modifying the Helicopter Stability Augmentation System . . . . .	65
Active Stability Augmentation Using Auxiliary Airfoils . . . . .	65
SUMMARY . . . . .	66
CONCLUSIONS AND RECOMMENDATIONS . . . . .	68
LITERATURE CITED . . . . .	69

**Preceding page blank**

Page

**APPENDIXES**

A	Pilot Interview Data . . . . .	70
B	Analog Computer Mechanization Diagrams . . . . .	116
C	Dynamic Wind Tunnel Test Run Log . . . . .	120
D	Flight Simulator Description . . . . .	126
LIST OF SYMBOLS . . . . .		128

# LIST OF ILLUSTRATIONS

<u>Figure</u>		<u>Page</u>
1	Cargo Container (Box) . . . . .	12
2	Tracked Carrier Command Post (Command Car). . . . .	13
3	Cargo Truck . . . . .	14
4	Tracked Carrier Command Post Sting - Mounted Backwards. .	15
5	Model Axes and Sign Convention . . . . .	17
6	Moment Center of Cargo Container . . . . .	18
7	Moment Center of Tracked Carrier Command Post . . . . .	19
8	Moment Center of 6 x 6 Truck . . . . .	20
9	Typical Root Plot From the Linear Analysis . . . . .	23
10	Cable Suspension and Characteristic Frequencies . . . . .	24
11	Lateral Directional Char. in Sideslip Cargo Carrier Q = 50. . . . .	26
12	Lateral Directional Char. in Sideslip Cargo Carrier Q = 75. . . . .	32
13	Flight Data-Analysis Comparison of an 8-by-8-by-20-Foot Empty Container on a Two-Point Suspension . . . . .	39
1	Flight Data-Analysis Comparison for a Mobile Home on a Single-Point Suspension. . . . .	40
15	0.1 Scale MILVAN Dynamic Wind Tunnel Test Setup . . . . .	42
16	Dynamic (Unsteady) Yawing Moment Function . . . . .	47
17	Block Diagram of the Dynamic Model of the 8-by-8-by-20- Foot Container for the Limit Cycle Class of Motions . . .	50
18	Effect of Angle of Attack and Fins . . . . .	51
19	Comparison of Computer Model Data With Flight Results (OC = 0). . . . .	53
20	Three Classes of Load Motions . . . . .	54

<u>Figure</u>		<u>Page</u>
21	Carrying Speed vs Allowable Limit Cycle Amplitude and Frequency . . . . .	57
22	8-by-8-by-20-Foot Container Carrying Speed Limitation . . .	59
23	Key Properties of Stabilization Systems Studied . . . . .	61
24	Fin Configurations That Suppress the Unsteady Yaw Moment . . . . .	64
A-1	Summary of Army Aviator Rotary-Wing Flying Time . . . . .	75
A-2	Years of Rated Service . . . . .	75
A-3	Combat Experience as Army Aviator . . . . .	76
A-4	Combat Experience as Army Aviator . . . . .	77
A-5	Military Education . . . . .	78
A-6	Instrument Qualification . . . . .	79
A-7	Composite of Army Sling Load Experience . . . . .	80
A-8	Airspeed Range for Vehicular Load CH-47 (1-1/2-Ton Water Trailer). . . . .	85
A-9	Altitude Range for Vehicular Load CH-47 (1-1/2-Ton Water Trailer). . . . .	86
A-10	Airspeed Range for Vehicular Load CH-47 (Downed Aircraft) . . . . .	87
A-11	Altitude Range for Vehicular Load CH-47 (Downed Aircraft) . . . . .	88
A-12	M102 Howitzer With Piggyback. . . . .	90
A-13	Airspeed Range for Artillery Load CH-47 (Howitzer, 105mm Towed, M102) . . . . .	91
A-14	Altitude Range for Artillery Load CH-47 (Howitzer, 105mm Towed, M102) . . . . .	92
A-15	Airspeed Range for Artillery Load CH-47 (155 Howitzer, Towed, M114A1) . . . . .	93
A-16	Altitude Range for Artillery Load CH-47 (155mm Howitzer). .	94

<u>Figure</u>		<u>Page</u>
A-17	Airspeed Range for POL Load CH-47 (55-Gallon Drums - Gasoline) . . . . .	95
A-18	Altitude Range for POL Load CH-47 (55-Gallon Drums - Gasoline) . . . . .	96
A-19	Airspeed Range for POL Load CH-54 (500-Gallon Collapsible Bags - Gasoline) . . . . .	97
A-20	Altitude Range for POL Load CH-54 (500-Gallon Collapsible Bags - Gasoline) . . . . .	98
A-21	Airspeed Range for Container Load CH-47 (Conex) . . . . .	99
A-22	Altitude Range for Container Load CH-47 (Conex) . . . . .	100
A-23	Airspeed Range for Container Load CH-54 (Conex) . . . . .	101
A-24	Altitude Range for Container Load CH-54 (Conex) . . . . .	102
A-25	CH-47 Average Load Weights and Airspeeds . . . . .	104
A-26	CH-54 Average Load Weights and Airspeeds . . . . .	105
B-1	Sling Load Analysis (Dynamics) . . . . .	116
B-2	Sling Load Analysis (Aerodynamics). . . . .	117
B-3	Sling Load Analysis (Aerodynamics). . . . .	118
B-4	Sling Load Analysis (Engineering Computation) . . . . .	119
D-1	Key Properties of the 347 Flight Simulation . . . . .	126

## LIST OF TABLES

<u>Table</u>		<u>Page</u>
1	Simulator Results of Allowable Carrying Speed . . . . .	67
A-1	CH-47 Vehicular Sling Loads . . . . .	81
A-2	CH-54 Vehicular Sling Loads . . . . .	81
A-3	CH-47 Artillery Sling Loads . . . . .	82
A-4	CH-54 Artillery Sling Loads . . . . .	82
A-5	CH-47 POL Sling Loads . . . . .	82
A-6	CH-54 POL Sling Loads . . . . .	82
A-7	CH-47 Container Sling Loads . . . . .	83
A-8	CH-54 Container Sling Loads . . . . .	83
A-9	Slings and Nets . . . . .	103
A-10	Load Stabilization Devices and Rigging Techniques . . . . .	106
A-11	Individual Load Stability . . . . .	106
A-12	Load Stability Ranking (Tandem Rotor Configuration) . . . . .	107
A-13	Load Stability Ranking (Single Main Rotor Configuration) . . . . .	107
A-14	Single-Main-Rotor Optimum Sling Lengths . . . . .	108
A-15	Tandem-Rotor Optimum Sling Lengths . . . . .	108

## INTRODUCTION

When external loads are carried beneath helicopters, a dynamic interaction takes place which can severely limit the speed at which the load can safely be carried. Since a variety of methods exist by which the load may be attached to the helicopter, a variety of variables are present that affect the problem. The interaction of some of the more important of these variables is brought out and their effects on the problem are presented. Both single- and multi-cable suspensions are treated. In this work, a mathematical model is created which describes the motions of the container when it is attached to a helicopter of infinite mass. The effects of attaching this load to a finite mass helicopter are explored in order to determine the applicable range of the model. The load motions fall into two broad classes: those characterized by linear properties such as convergent or divergent sinusoids, and those dominated by nonlinear action, such as a limit cycle. Stability is the main consideration for those motions with linear properties. For the limit cycle motions, a carrying speed limitation concept based on energy is presented, together with some experimental data to support it.

A helicopter flight simulation with a two-cable suspension sling load model based on the above results was used to investigate the effects of the various stabilization concepts on the handling and ride qualities of the helicopter.

The work statement of the present effort specified the use of static wind tunnel data in the dynamic analysis, and such an analysis was found to be inadequate to describe the real-world effects. Consequently, a change of direction was made, and a dynamic wind tunnel test was conducted. The results were incorporated into a dynamic model which described the observational evidence reasonably well.

The important dynamics of the 8-by-8-by-20-foot cargo container on a two-point suspension are dominated by unsteady flow effects which give rise to limit cycle motions about the yaw axis. The effects are apparently caused by the flow's transition from a partially separated to a fully separated state, and they manifest themselves in the form of yawing moments proportional to sideslip rate in a hysteresis-type fashion. These moments increase with speed and cause the limit cycle motions to occur at nearly the resonant frequency of the load-suspension combination and increase in magnitude as speed increases.

The original purpose of this effort was to conduct studies to determine the best stabilization concepts for use by the Army for a broad spectrum of loads. As it turned out, however, the dominance of the unsteady flow effects of the 8-by-8-by-20-foot container threw open to doubt the results of any analysis of a bluff body that did not consider these effects. Since they are difficult to measure and even more difficult



to estimate, the scope of the present effort was considerably narrowed so that a relevant study of the 8-by-8-by-20-foot container could be made.

This report presents: (1) the results of a pilot interview survey; (2) static wind tunnel results, together with a brief description of attempts to estimate these data; (3) dynamic analysis based on the static wind tunnel data; (4) a correlation study with flight data; (5) descriptions of the dynamic wind tunnel test results; (6) the nonlinear dynamic analysis; and (7) discussions of stabilization concepts and carrying speed criteria.

## PRELIMINARY ANALYSIS

### PILOT INTERVIEW RESULTS

Appendix A contains the results of a pilot interview survey which was conducted in order to demonstrate the operational aspects of the problem. The purpose of this study was to accomplish a subjective appraisal of aircraft responses and load behavior during operations involving Army cargo helicopters carrying externally slung loads.

The effort was accomplished in three phases. Phase I entailed the preparation of a questionnaire covering four broad categories of sling loads: vehicles, artillery (including ammo), POL, and containers. These categories were further definitized utilizing specific items of Army equipment that are continually lifted as sling loads. Phase II consisted of interviews, using a prepared questionnaire, with 40 experienced Army aviators at Fort Rucker, Alabama, and Fort Eustis, Virginia. The aviator responses were evaluated during Phase III by equally experienced, retired master Army aviators.

The output from the study effort provided the following: First, it was possible to model a typical Army cargo helicopter aviator in terms of education, years of rated service, and instrument and flying time experience. Secondly, the data were obtained on single-main and tandem-rotor helicopter response, load behavior, and aviator techniques for resolving load instability problems. Finally, aviator recommendations were obtained concerning the optimum number of load suspension points, methods of stabilizing loads, and development of aviator sling load flying proficiency.

### STATIC WIND TUNNEL TESTS AND AERODYNAMIC ANALYSIS

A wind tunnel test was conducted in the Northrop 7-by-10-foot wind tunnel. The test program results can be obtained under separate cover on request.

Three models were fabricated and tested. They were 0.10 scale representations of a standard U.S. Army 7-by-8-by-20-foot cargo container, a tracked carrier command post, and a cargo truck (Figures 1, 2, and 3).

The models were sting mounted on the two-parameter sting support with image strut. The tracked carrier command post and a cargo truck model were constructed so as to be able to accept the sting from either the front or rear (Figures 2, 3, and 4). This was done to obtain sideslip angles greater than 180°.

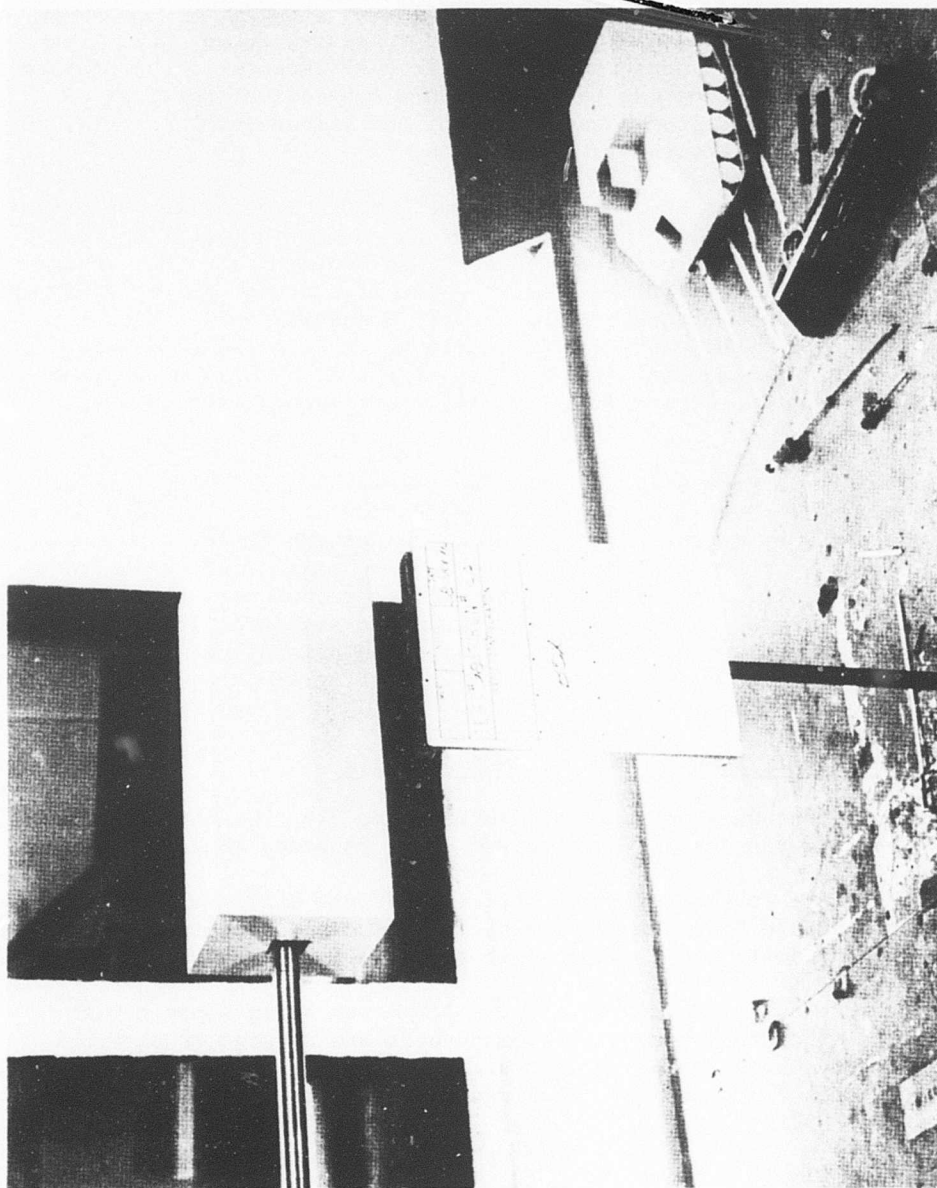


Figure 1. Cargo Container (Box).

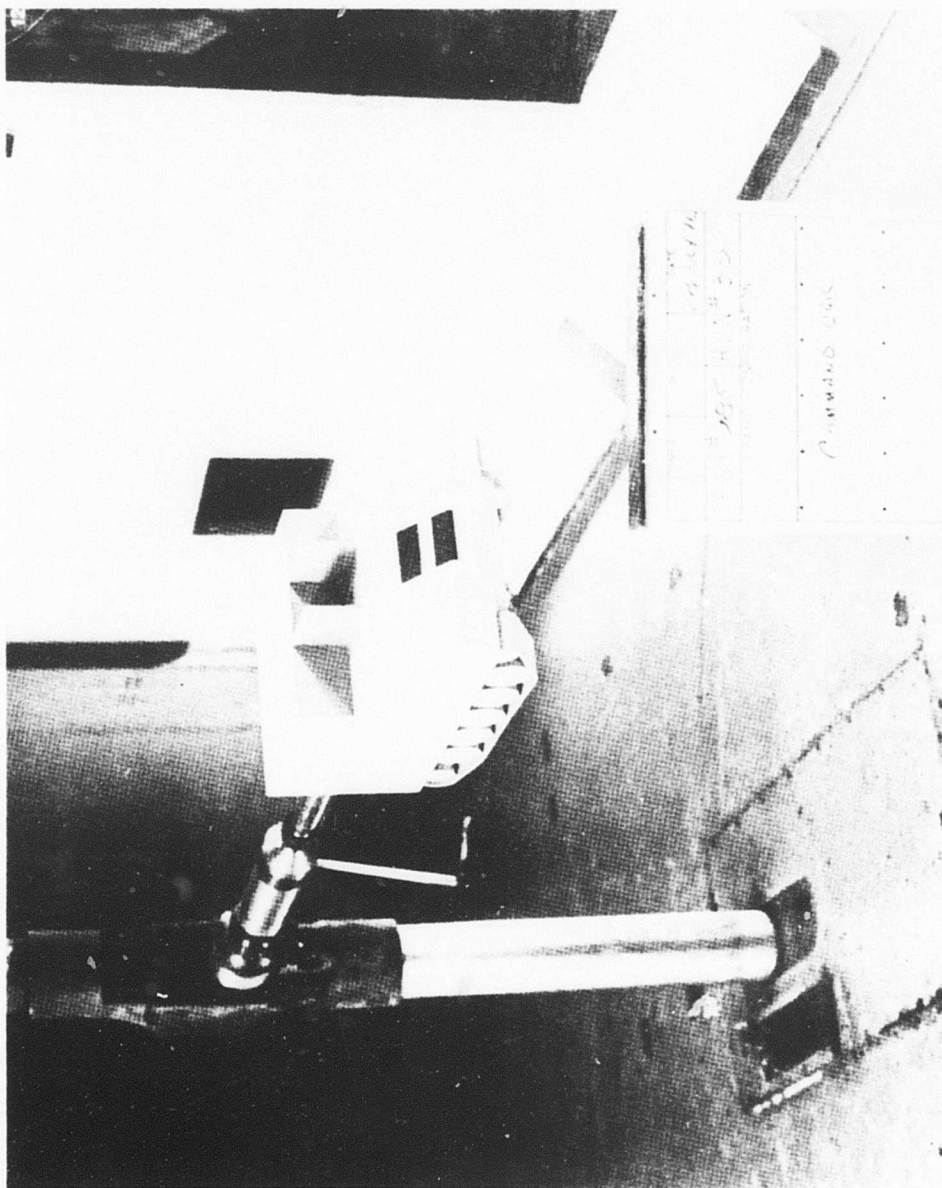


Figure 2. Tracked Carrier Command Post (Command Car).

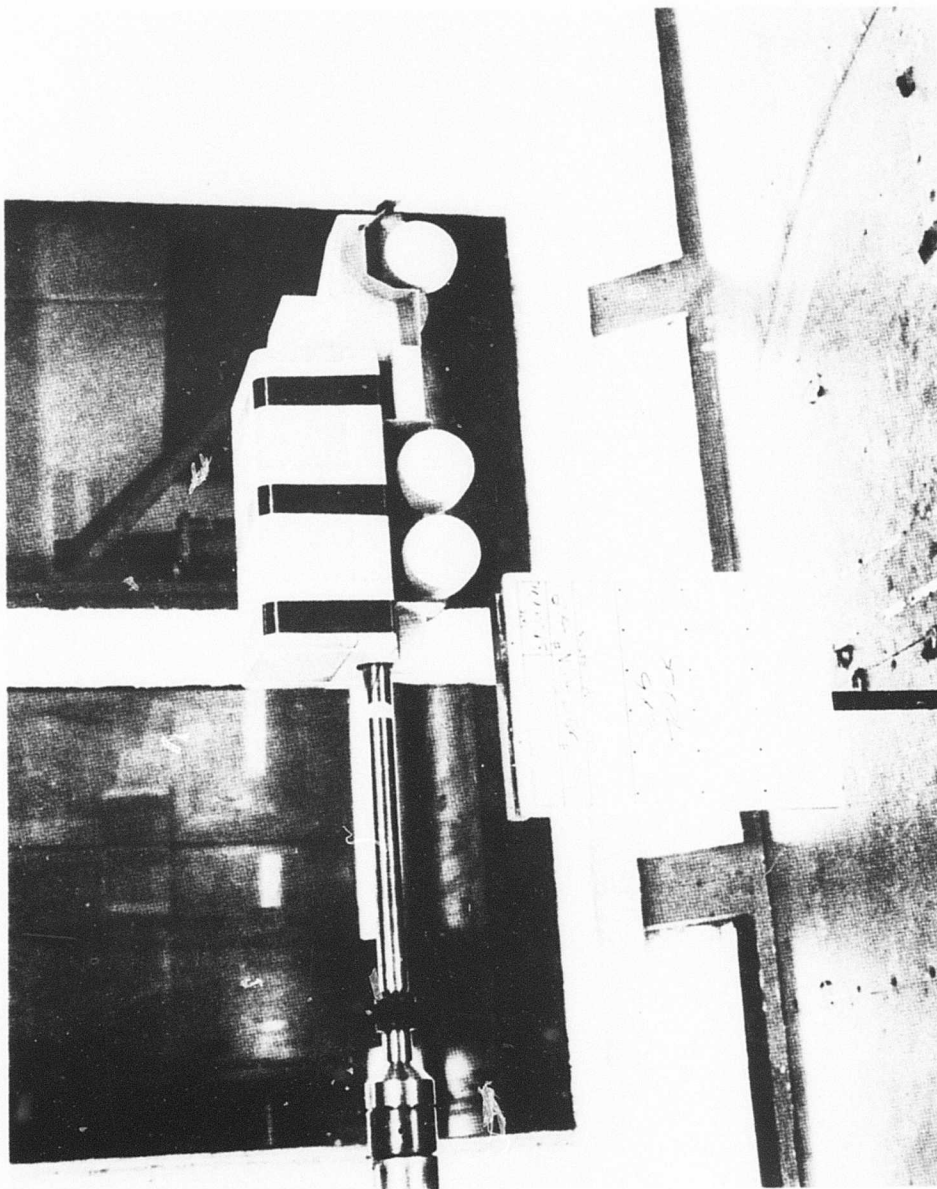


Figure 3. Cargo Truck.

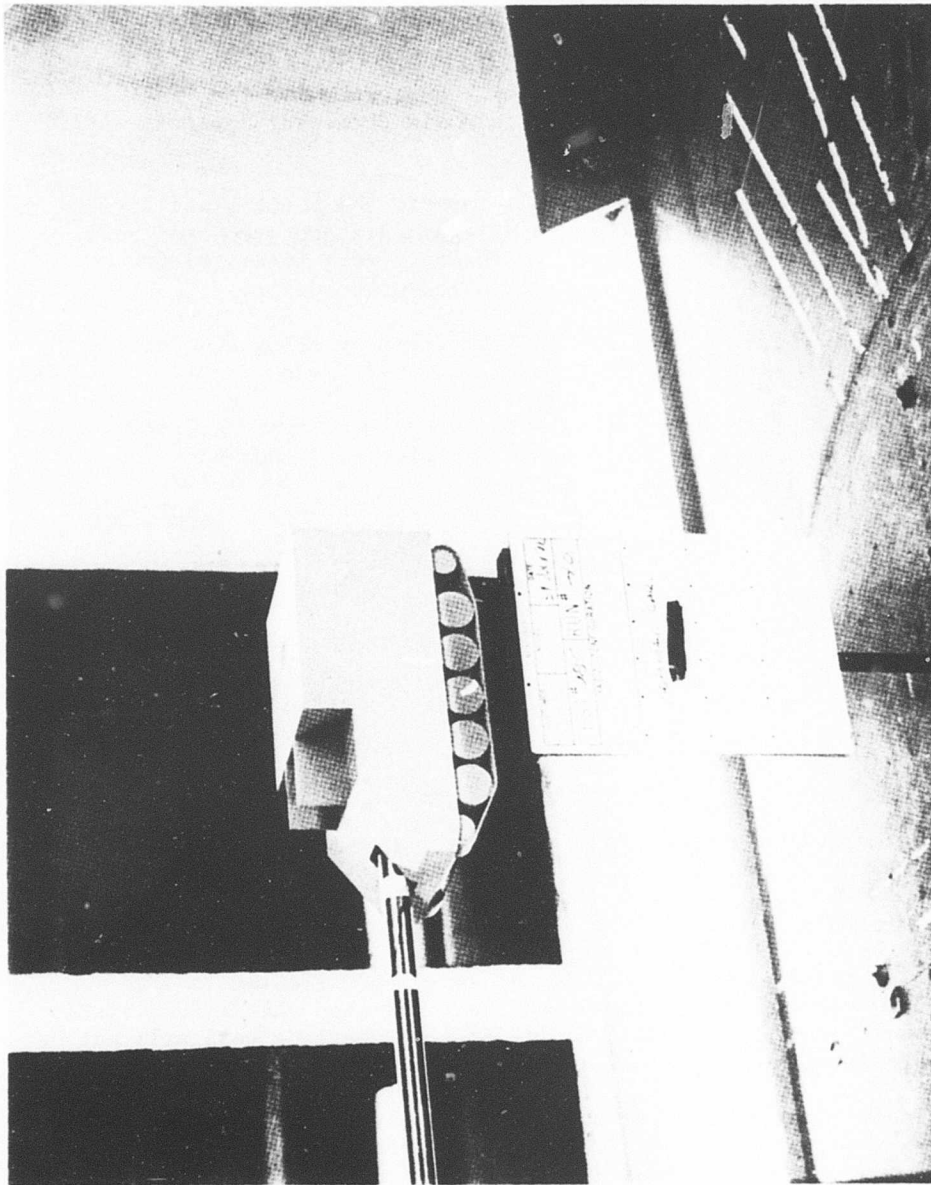


Figure 4. Tracked Carrier Command Post Sting-Mounted Backwards.



To obtain the required angles of attack and sideslip, the test was conducted at model roll angles of 0°, 90°, and 180°.

Boundary layer transition was not used.

The aerodynamic forces and moments were measured with the Task 1.25-inch-diameter (-61) balance. This is a six-component internal strain gage balance.

The data were reduced to coefficient form in the body, stability and wind axes systems; only body and wind axes data are presented here. Figure 5 shows these axes systems. The data were corrected for the effect of the presence of the model in the wind tunnel.

Model attitudes were corrected for the effect of sting and balance deflections due to airloads. No correction was made for base pressure.

The aerodynamic forces and moments were resolved about the following moment centers listed in model scale (Figures 6, 7, and 8):

<u>MODEL</u>	<u>STATION</u>	<u>WATERLINE</u>	<u>BUTTLINE</u>
Cargo Container	12.00	4.80	0
Tracked Carrier Command Post	10.38	4.70	0
Cargo Truck	13.30	4.90	0

The model reference dimensions used in the reduction of the data are as follows:

<u>MODEL</u>	<u>LENGTH (in.)</u>	<u>WIDTH (in.)</u>	<u>PLANFORM AREA (ft<sup>2</sup>)</u>
Cargo Container	24.00	9.60	1.60
Tracked Carrier Command Post	19.15	10.57	1.406
Cargo Truck	26.55	10.00	1.844

Since the static aerodynamics did not contribute greatly to the important dynamics of this load, the fact that the theoretical static aerodynamic analysis did not predict these properties well will not be elaborated upon here.

Specifically, application of the viscous cross-flow theory to the 8-by-8-by-20-foot container, the cargo truck, and the tracked command post carrier yielded a fair estimate of the force properties but a poor estimate of the moment characteristics. Apparently, the assumption of a fully separated flow pattern for all angle of attack and sideslip values is not a valid one.

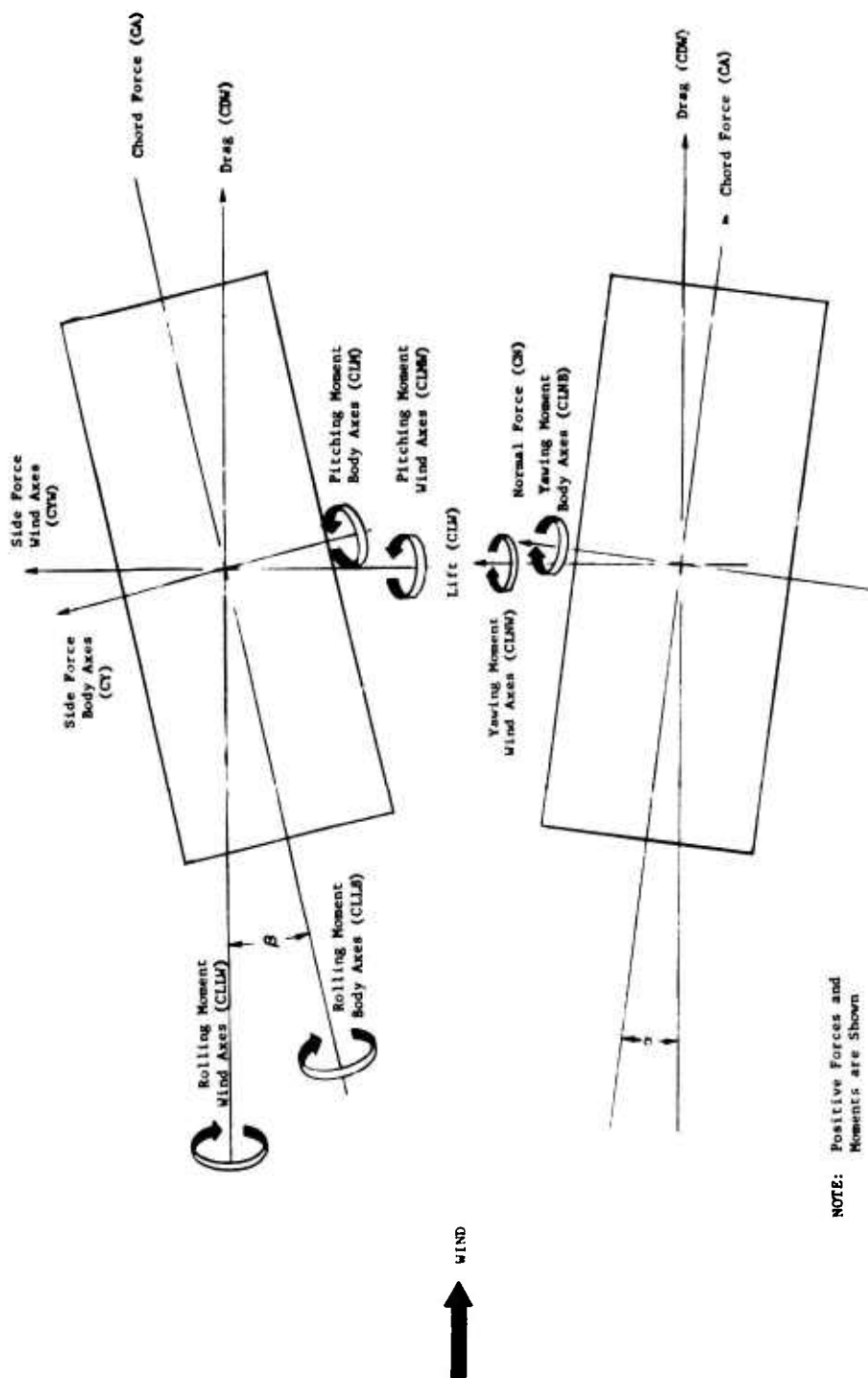
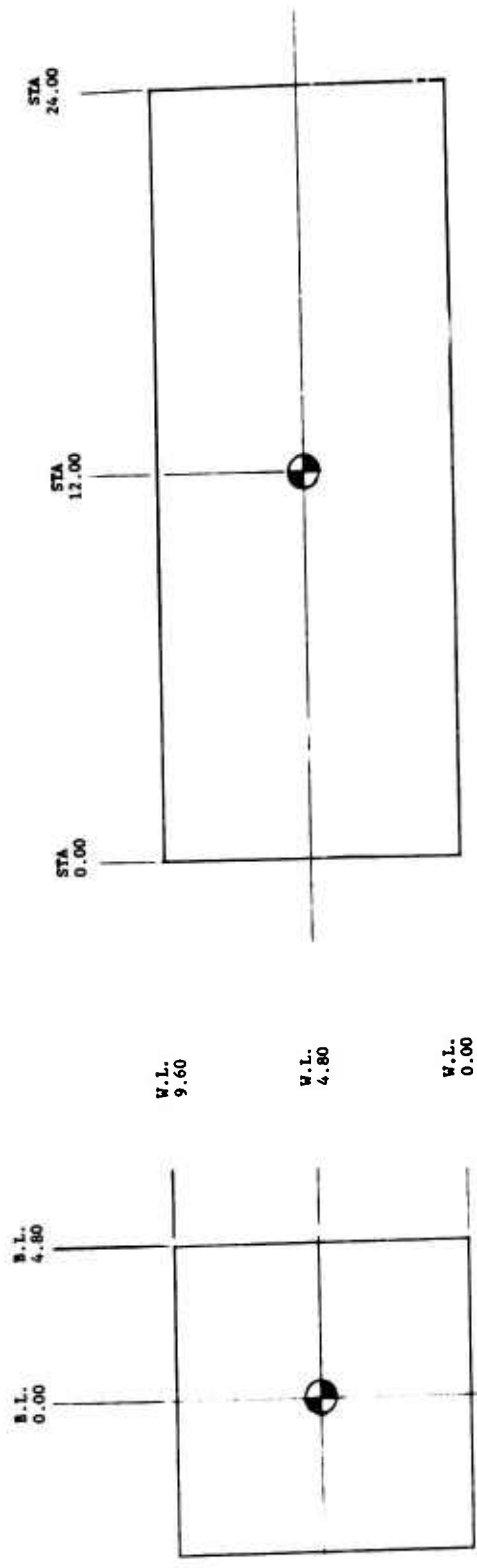


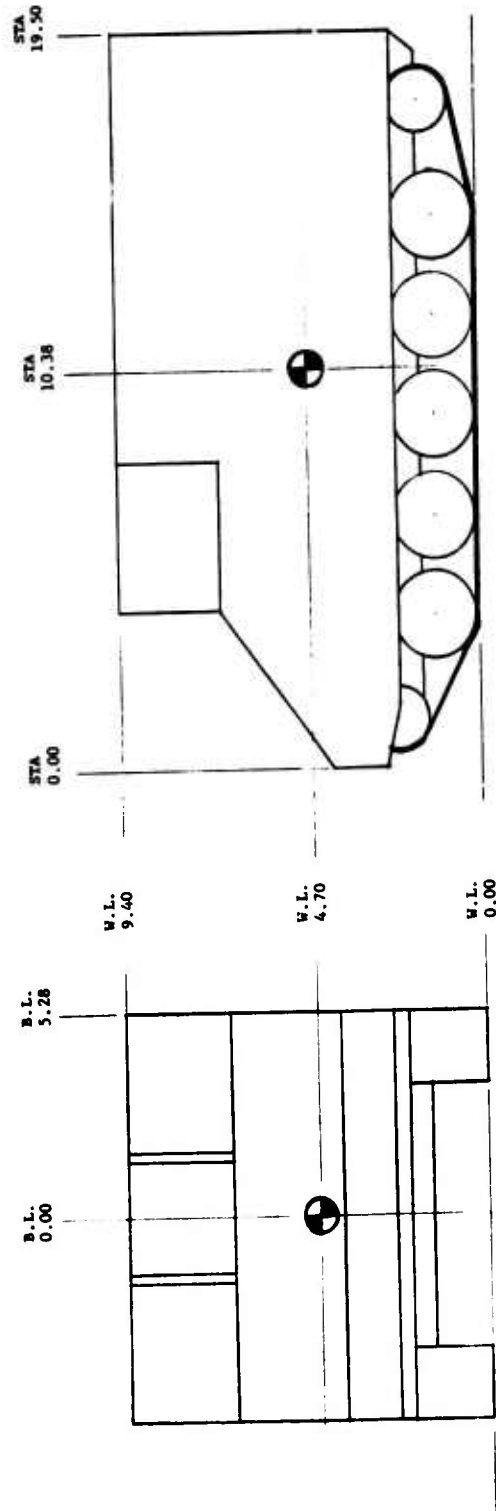
Figure 5. Model Axes and Sign Convention.






 Moment Center

Figure 6. Moment Center of Cargo Container.




 Moment Center

Figure 7. Moment Center of Tracked Carrier Command Post.

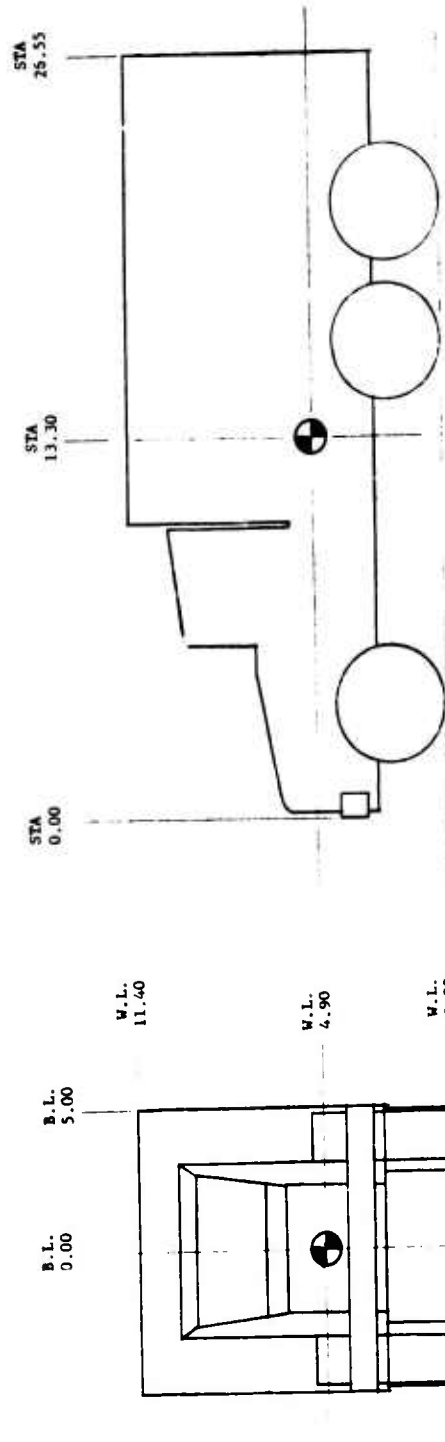


Figure 8. Moment Center of 6 x 6 Truck.

Comparison of the Northrop data for the smooth container with those from the corrugated container tests conducted by NASA-Ames revealed small differences that could be attributed to the model support system.

### LINEAR STABILITY ANALYSIS

A linear analysis was conducted initially which followed the procedure of Reference 1. It was hoped that this simple representation would suffice for the purposes of this study. The assumptions used for this analysis are:

1. The container and cables are rigid.
2. The cables are without mass.
3. No moments act at the cable attachment points.
4. All angles are small, i.e., less than  $10^\circ$ .
5. Fore-and-aft and heave motions relative to the helicopter may be neglected.
6. The upper attachment points move at constant velocity, i.e., the helicopter has infinite mass.
7. The relative pitch attitude of the load is a function of cable geometry only.

The analysis proceeded, using only two degrees of freedom: lateral sway of the load and load yaw, both relative to helicopter-fixed axes. Also, the aerodynamics of the load are linearized versions of the static wind tunnel results for small sideslip angles and a theoretical estimate for the yaw damping function:

1. Yawing moment due to sideslip.
2. Side force due to sideslip.
3. Yawing moment due to yaw rate.

The equations of motion for lateral sway and yaw are:

$$m l p \ddot{\phi} = - m g l p \phi + C_{Y\beta} q S l p \beta$$

$$I_z \ddot{\psi} = - \frac{m g}{l \beta} x_C^2 \psi + C_{N\beta} q S b \beta + C_{N_r} q S b \left( \frac{b \dot{\psi}}{2 V_0} \right)$$

$$q = \frac{p V_0^2}{2}, \beta \approx \frac{\phi l p}{V_0} - \psi$$

Since these equations are linear second-order differential equations, the roots of their characteristic equation will reveal much about the stability of the system. The characteristic equation is

$$\begin{aligned}
 & D^4 + \left[ -\frac{A}{V_0} C_{Y\beta} - \frac{bB}{2V_0} C_{N_r} \right] D^3 \\
 & + \left[ BC_{N\beta} + \frac{g}{\ell_P} + \frac{gmX_C^2}{\ell_B I_z} + \frac{ABb}{2V_0^2} C_{Y\beta} C_{N_r} \right] D^2 \\
 & + \left[ -\frac{A}{V_0} C_{Y\beta} \frac{g}{\ell_B} \frac{mX_C^2}{I_z} - \frac{bBg}{2V_0 \ell_P} C_{N_r} \right] D \\
 & + \frac{g}{\ell_P} \left[ BC_{N\beta} + \frac{g}{\ell_B} \frac{mX_C^2}{I_z} \right] = 0,
 \end{aligned}$$

$$A = \frac{qS}{m}, \quad B = \frac{qSb}{I_z}$$

When the roots of this equation are positive (or have positive real parts), the system is unstable. Consequently, a plot of the roots will suffice to demonstrate the interaction of the variables. A typical root plot is given in Figure 9. This graph shows the values of the positive complex roots as airspeed varies. For this example, the sway mode roots cross into the right-half (positive) plane at an airspeed of 68 knots. At this speed, the motion would be characterized by a divergent sway oscillation. If this is the correct representation of this load, the airspeed could not be increased beyond 68 knots without the sway mode amplitude building up to a dangerous level.

In the following paragraphs, an interpretation of the results of this analysis is given along with a description of the effects of the more important variables.

When an external load such as a cargo container is attached to a helicopter, it is generally done by an arrangement of cables and slings. In most instances, with the container, nylon slings are used to attach the upper corners to a central "doughnut" shackled to a short cable, which in turn is attached to a cargo hook. In this configuration, the degrees of freedom are limited to yaw, lateral sway and longitudinal

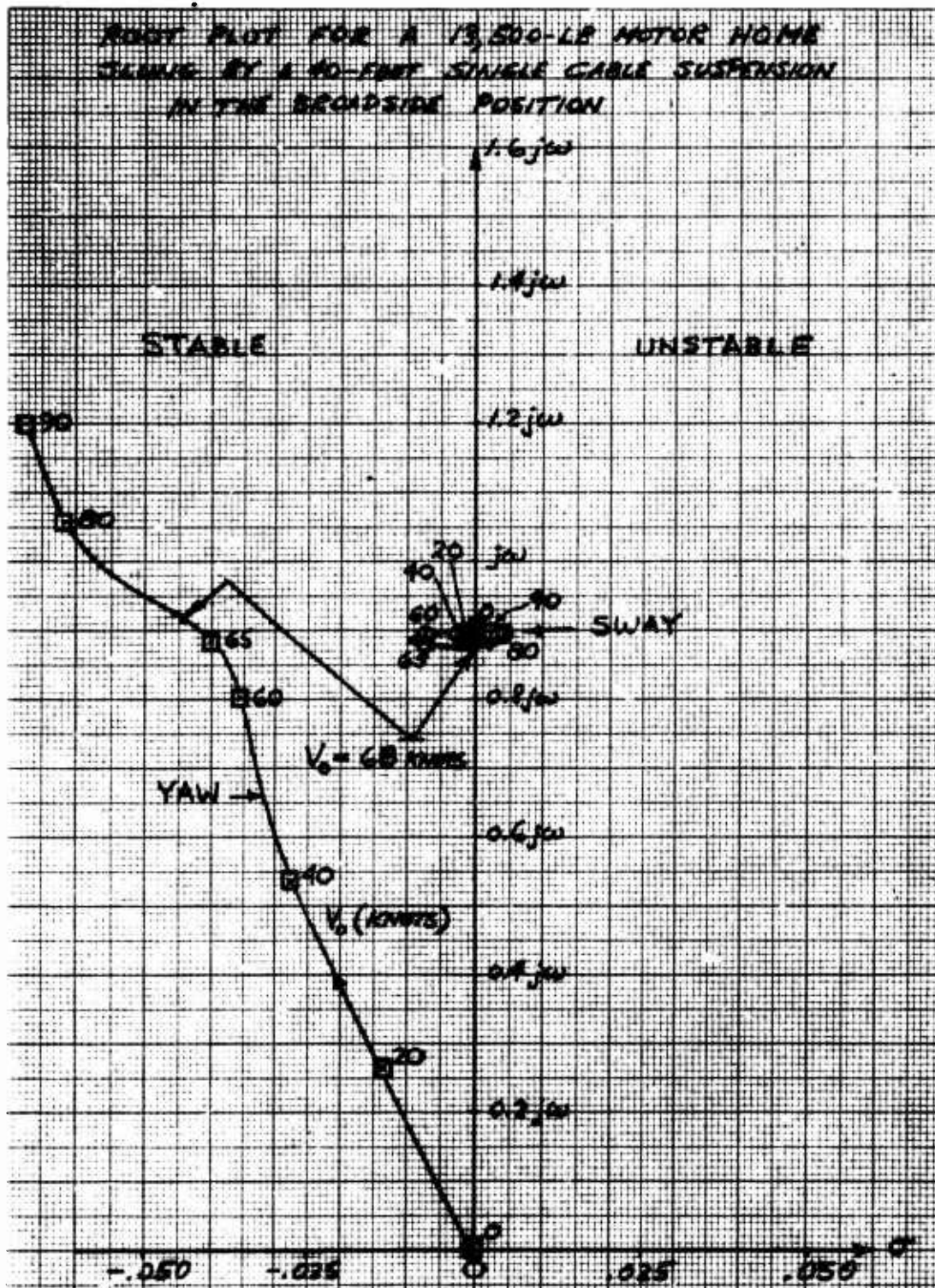


Figure 9. Typical Root Plot From the Linear Analysis.

surge angle, and the load roll angle is nearly equal to the lateral sway angle. With a two-cable suspension, the torsion moment produced by the two cables provides some "spring" in yaw. Moreover, the two-cable suspension ensures that the load pitch angle is directly related to the helicopter pitch attitude except when the cables are not parallel. In this case, load pitch is dependent on the longitudinal surge angle as well as helicopter pitch attitude.

It should be clear enough that at zero airspeed, the action of the cable tension forces that react against the gravitational force gives rise to restoring torques, which in turn produce oscillations in the longitudinal, lateral and yaw axes. The frequencies of these oscillations are important in a stability analysis, so they are described below.

The "pendulum" frequency,  $\omega_\phi$ , rad/sec, is simply  $\sqrt{\frac{g}{\ell_p}}$ , where  $g$  is the acceleration of gravity and  $\ell_p$  is the effective length from the upper attachment point to the load center of mass. This is the zero airspeed frequency of the longitudinal and lateral modes.

The yaw frequency in rad/sec, the so called "bifilar frequency",  $\omega_\psi$ ,

is slightly more complex; it is equal to  $\sqrt{\frac{mg X_c^2}{I_z \ell_B}}$ , where  $X_c$  is the horizontal spacing between each parallel cable and the center of mass,  $I_z$  is the yawing moment of inertia, and  $\ell_B$  is the "bifilar length" or the length of parallel cable that contributes to the yawing torque. This length, unless stated otherwise, is the length of cable between the upper attachment points and the effective lower attachment points. These lengths are illustrated in Figure 10.

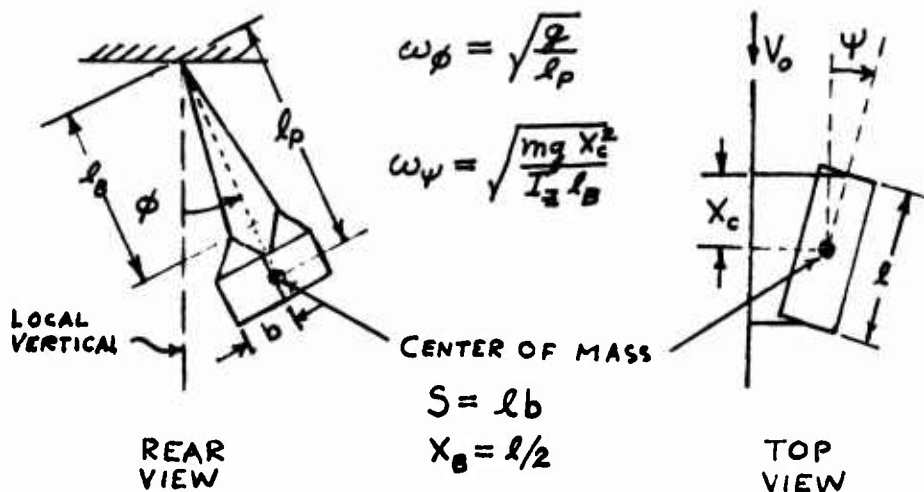


Figure 10. Cable Suspension and Characteristic Frequencies.

We have seen how the cables introduce "spring like" torques in the yaw, lateral sway, and longitudinal surge axes. Next, the important aerodynamics as determined from static wind tunnel tests will be discussed. The most important characteristic of these data is the yawing moment due to sideslip. See Figure 11. The yawing moment has null points, at  $0^\circ$ ,  $90^\circ$ ,  $180^\circ$ , and  $270^\circ$  sideslip angle. They are all statically stable; i.e., an increase in sideslip from these points results in a yawing moment change that tends to reduce the sideslip. The null points indicate that the container will stabilize either in a small-end-forward position or broadside (on a single-cable suspension). The side force data (Figure 11) indicates that there will be damping forces along the sway axis, and the assumption of a rotary damping characteristic suggests that the yaw axis by itself should be stable.

The drag data (Figure 12) suggests that the container will trail along the longitudinal axis as speed increases and that the drag varies with sideslip; thus a longitudinal motion should result from any lateral motions. Again, the linear analysis neglects the longitudinal forces; however, the effect that the trail angle has on the cable spring torques must be considered. A brief study of this effect revealed a small influence, so longitudinal trail effects on yawing torque have also been neglected.

The analysis proceeded using the cable torques and the aerodynamic yawing moment and side force characteristics previously discussed. The results indeed show that unstable motions do occur at certain airspeeds. This is illustrated in Figure 9, where it is seen that the sway mode becomes unstable at a speed of 68 knots. This is due to the aerodynamic yawing moment that acts through sideslip, which in turn is a function of yaw angle and sway rate. This fact introduces a phase shift in the yawing moment, which causes it to increase the amplitude of motion. An aerodynamic sensitivity analysis revealed the following effects:

1. Increasing  $C_{N_\beta}$  decreased the airspeed at which an instability appeared.
2. Increasing  $C_{Y_\beta}$  and  $C_{N_r}$  increased the airspeed at which an instability appeared.

Another way of stating the results is to describe what increases the speed at which an instability appears:

1. Decrease in cable lengths
2. Increase in cable separation
3. Decrease in yawing moment due to sideslip
4. Increase in side force and yaw damping characteristics
5. Increase in yawing moment of inertia

We shall see later how, in the practical sense, these variables may be changed to increase allowable carrying speed.









CONFIRMATION			
ANALYSIS			
SYN	CONF	10	10
1	SE	1.3	1.3
1	SE	1.3	1.3

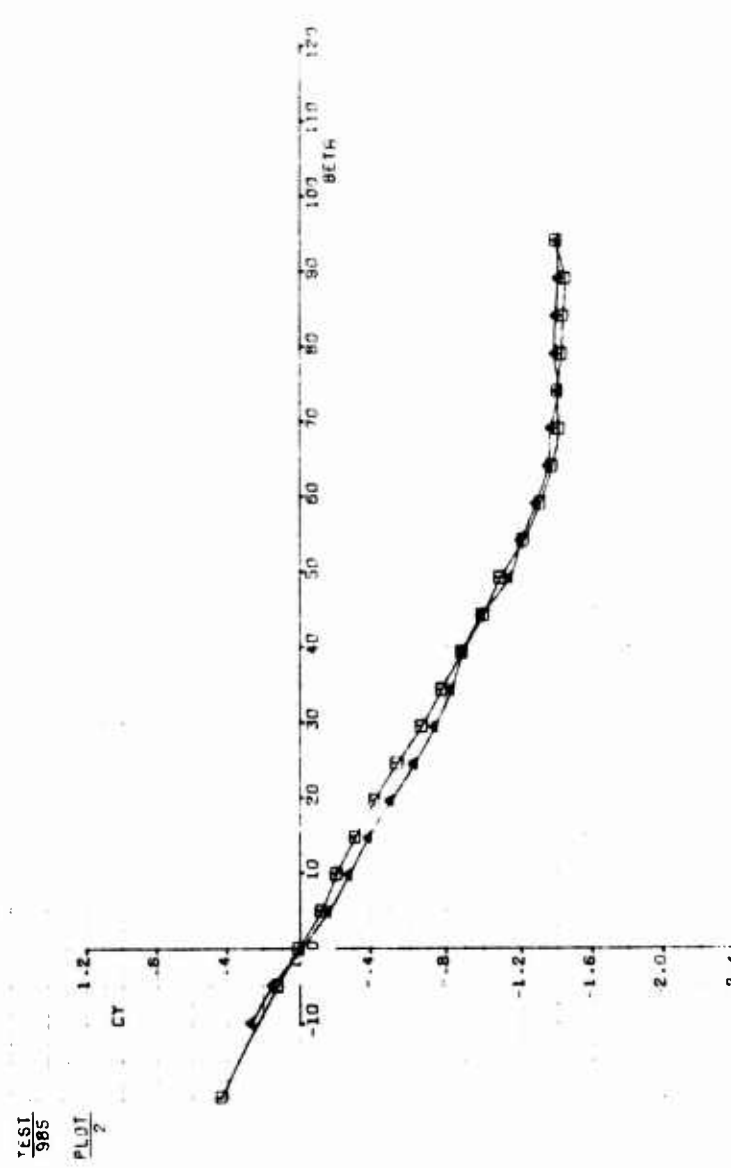


Figure 11. Lateral Directional Char. In Sideslip Cargo Carrier  $Q = 50$  (Continued).

TEST  
585  
PLOT  
Z

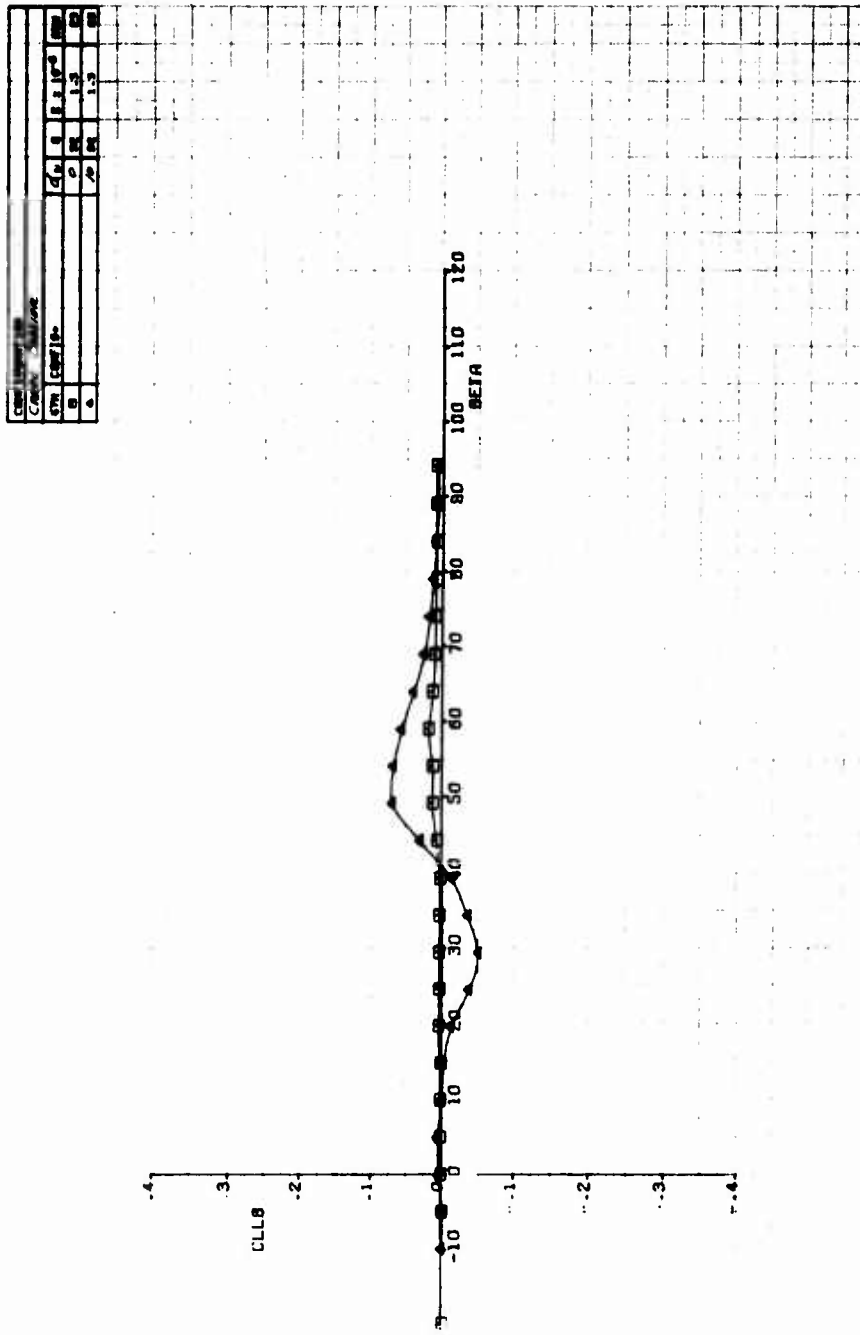


Figure 11. Lateral Directional Char. In Sideslip Cargo Carrier Q = 50 (Continued).

YESI  
985  
PLOT  
2

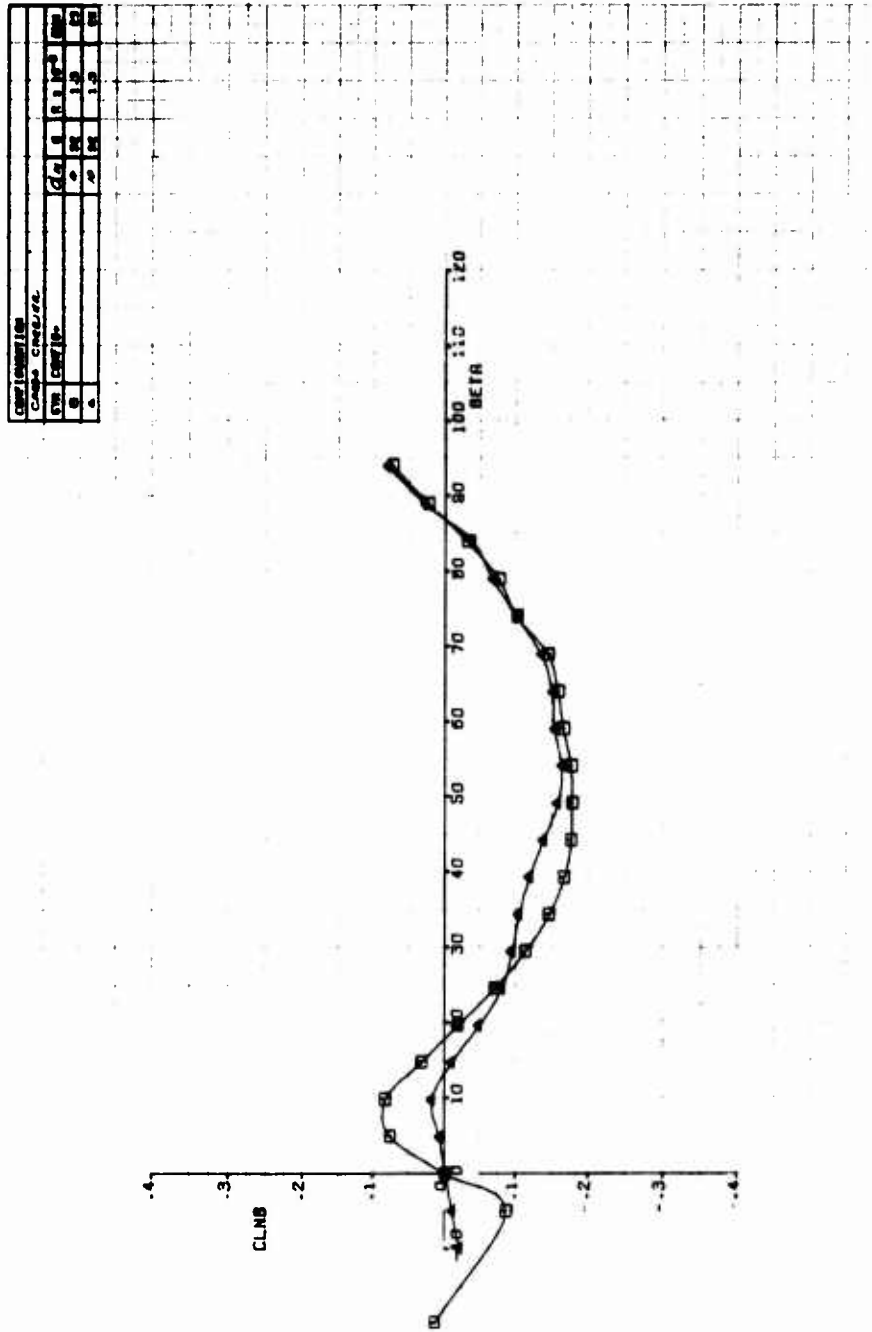
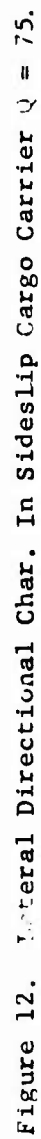


Figure 11. Lateral Directional Char. In Sideslip Cargo Carrier Q = 50 (Continued).



CONFIDENCE LIMITS				
CONFIDENCE LIMITS				
SYN	CONF	Q	R	QUM
0	1.0	75	1.0	22
1	1.0	75	1.0	22
2	1.0	75	1.0	22
3	1.0	75	1.0	22
4	1.0	75	1.0	22
5	1.0	75	1.0	22
6	1.0	75	1.0	22
7	1.0	75	1.0	22
8	1.0	75	1.0	22
9	1.0	75	1.0	22
10	1.0	75	1.0	22
11	1.0	75	1.0	22
12	1.0	75	1.0	22
13	1.0	75	1.0	22
14	1.0	75	1.0	22
15	1.0	75	1.0	22
16	1.0	75	1.0	22
17	1.0	75	1.0	22
18	1.0	75	1.0	22
19	1.0	75	1.0	22
20	1.0	75	1.0	22
21	1.0	75	1.0	22
22	1.0	75	1.0	22
23	1.0	75	1.0	22
24	1.0	75	1.0	22
25	1.0	75	1.0	22
26	1.0	75	1.0	22
27	1.0	75	1.0	22

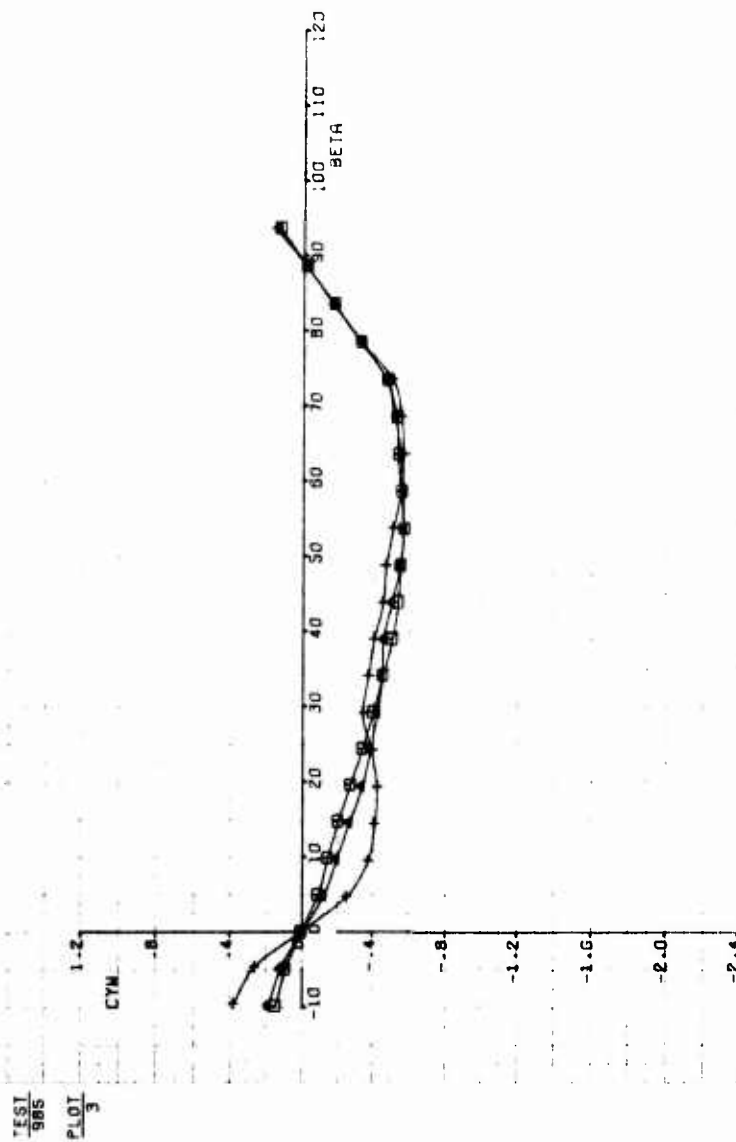


Figure 12. Lateral Directional Char. In Sideslip Cargo Carrier Q = 75 (Continued).



TEST  
985  
PLOT  
3

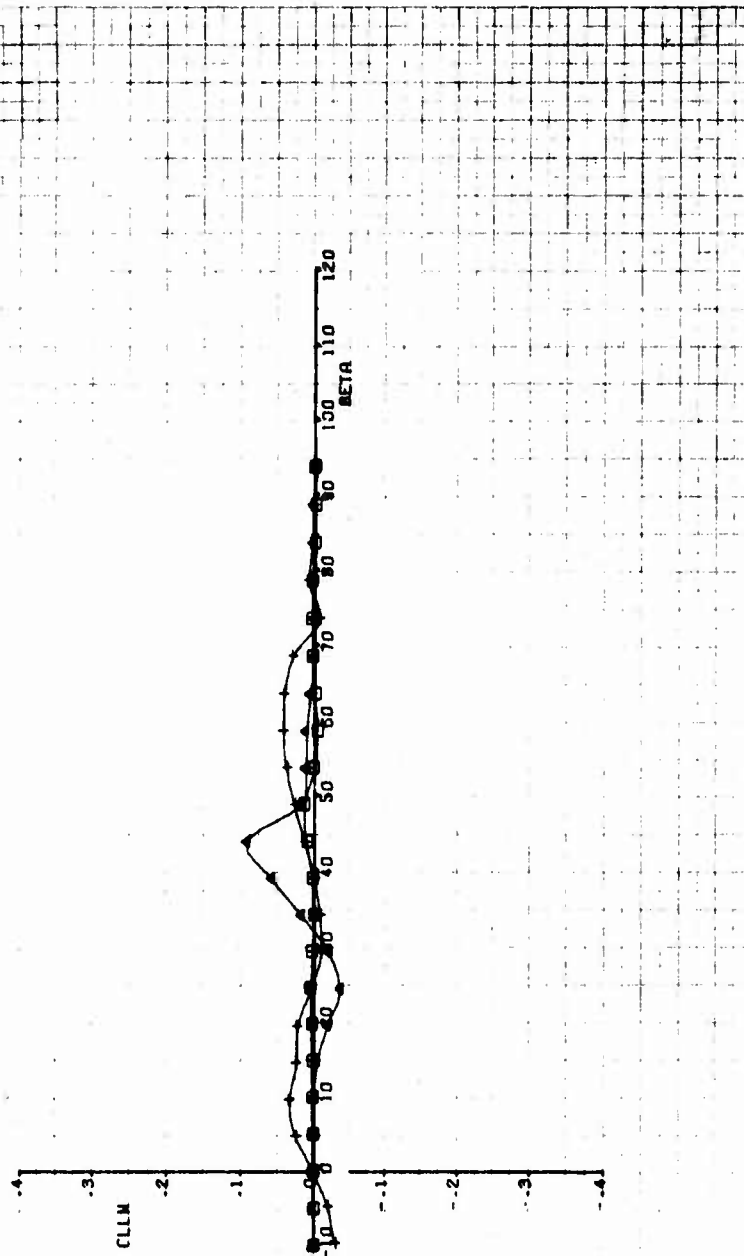


Figure 12. Lateral Directional Char. In Sideslip Cargo Carrier  $Q = 75$  (Continued).

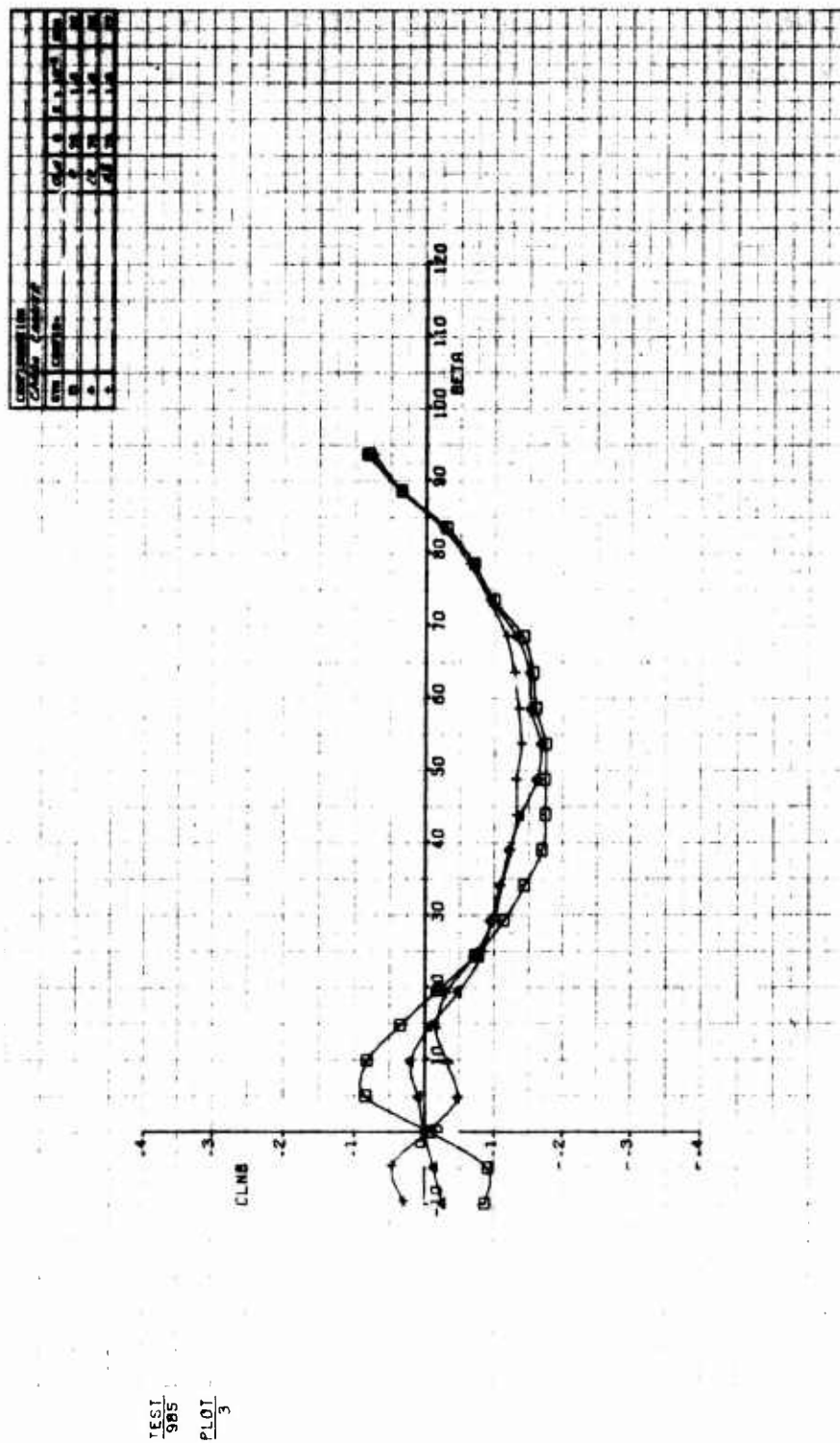


Figure 12. Lateral Directional Char. In Sideslip Cargo Carrier Q = 75 (Continued).





## FLIGHT DATA CORRELATIONS

Before the study proceeded further, the validity of the linear analysis was checked by comparing its results with flight data. Two cases were isolated for comparison after an examination of many candidates. The first and by far the most documented was a test of an empty MILVAN container carried on a two-cable suspension by a CH-47C helicopter (Reference 2). The container was carried small-end-into-the wind with a 24-foot spreader beam weighing 3505 lb. Pilot and observer reports about container motions are available with pilot judgements of maximum allowable carrying speed.

The second case is a lift made in Colorado by a CH-54 Tarhe. The load was a 13,500-lb mobile home slung on a single cable with cross slings and spreader bars. Observer reports (from a chase helicopter) were available as well as film records, and these were examined in detail. A summary of the important findings for these two comparisons is given in Figures 13 and 14. The other cases examined did not have sufficient documentation to make a comparison meaningful, so it was decided to rely more on a detailed study of a few cases rather than a broader study of a large number of more poorly documented cases.

In general, the comparisons are very poor, particularly when the container is carried small-end-forward on a two-point suspension. The linearized analysis predicts no instabilities with an increasing yaw frequency as airspeed increases, while the observations show sustained yaw oscillations at about the zero airspeed frequency (bifilar frequency). In the broadside case, no pilot reports of oscillatory frequency are available. Indeed, the analysis predicts a damped oscillatory motion which was not apparent in the film records. The comparison therefore is quantitatively inconclusive, but qualitatively interesting, because the load did stabilize to a broadside position and the airspeeds flown were less than the predicted maximum stable airspeed.

The generally poor correlation just discussed and the lack of good data for dynamic comparison prompted the setup of an analog computer for the purpose of conducting a nonlinear analysis. A parallel theoretical effort was also initiated. The simple linearized equations of motion previously described were programmed as before except the yaw axis was made continuous and the yawing moment data for any value of yaw and sideslip angle were incorporated. The mechanization diagrams for the program which evolved from this study are given in Appendix III. It is sufficient here to say that this extension of the analysis did not provide results that compared favorably with flight data. No sustained oscillation could be produced, although many of the properties of the broadside case could be reproduced.

At this point, it was obvious that before the contract work could be continued, a redirection of effort was necessary. This redirection is described in the following section.

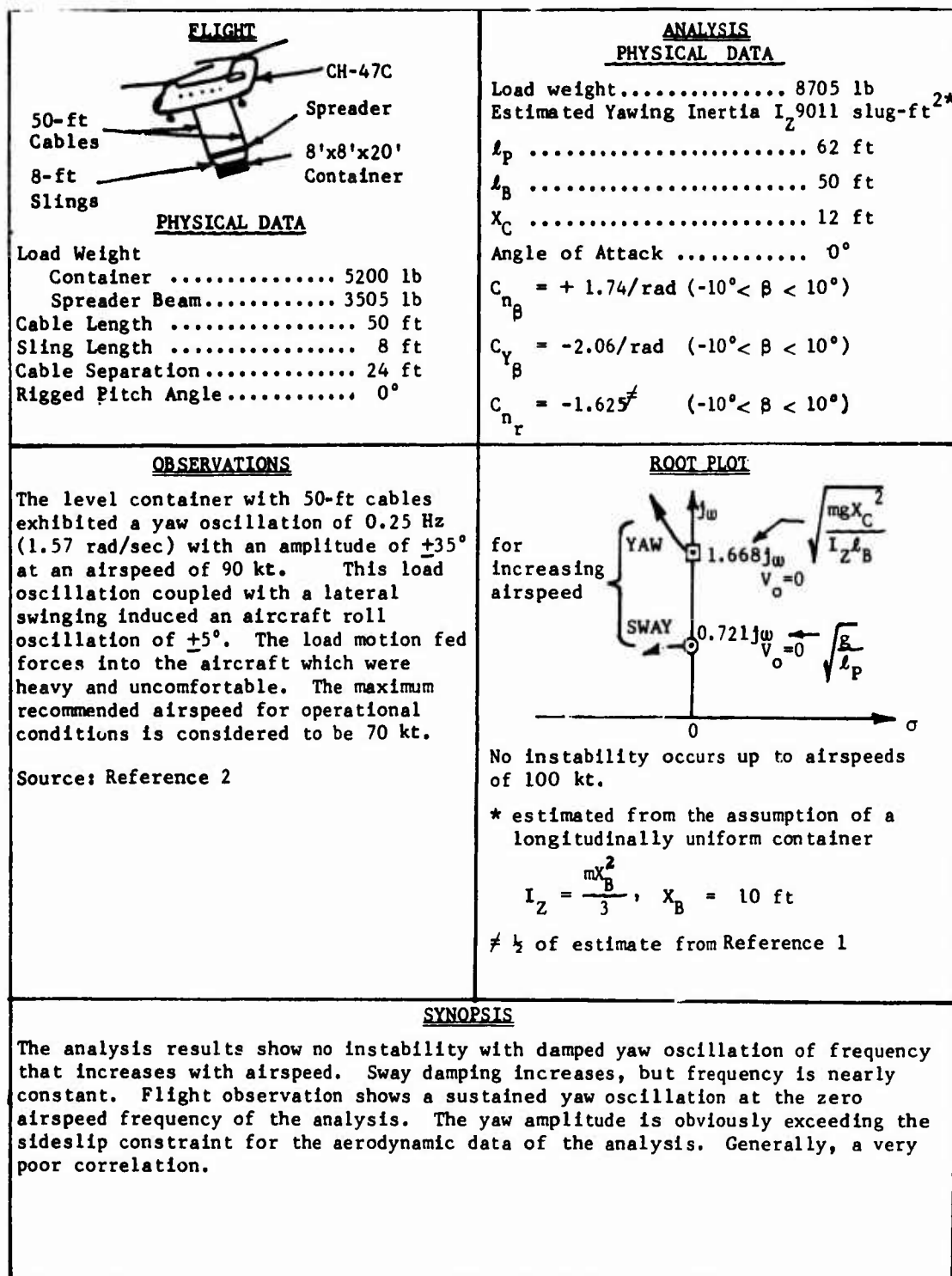


Figure 13. Flight Data-Analysis Comparison of an 8-by-8-by-20-Foot Empty Container on a Two-Point Suspension.

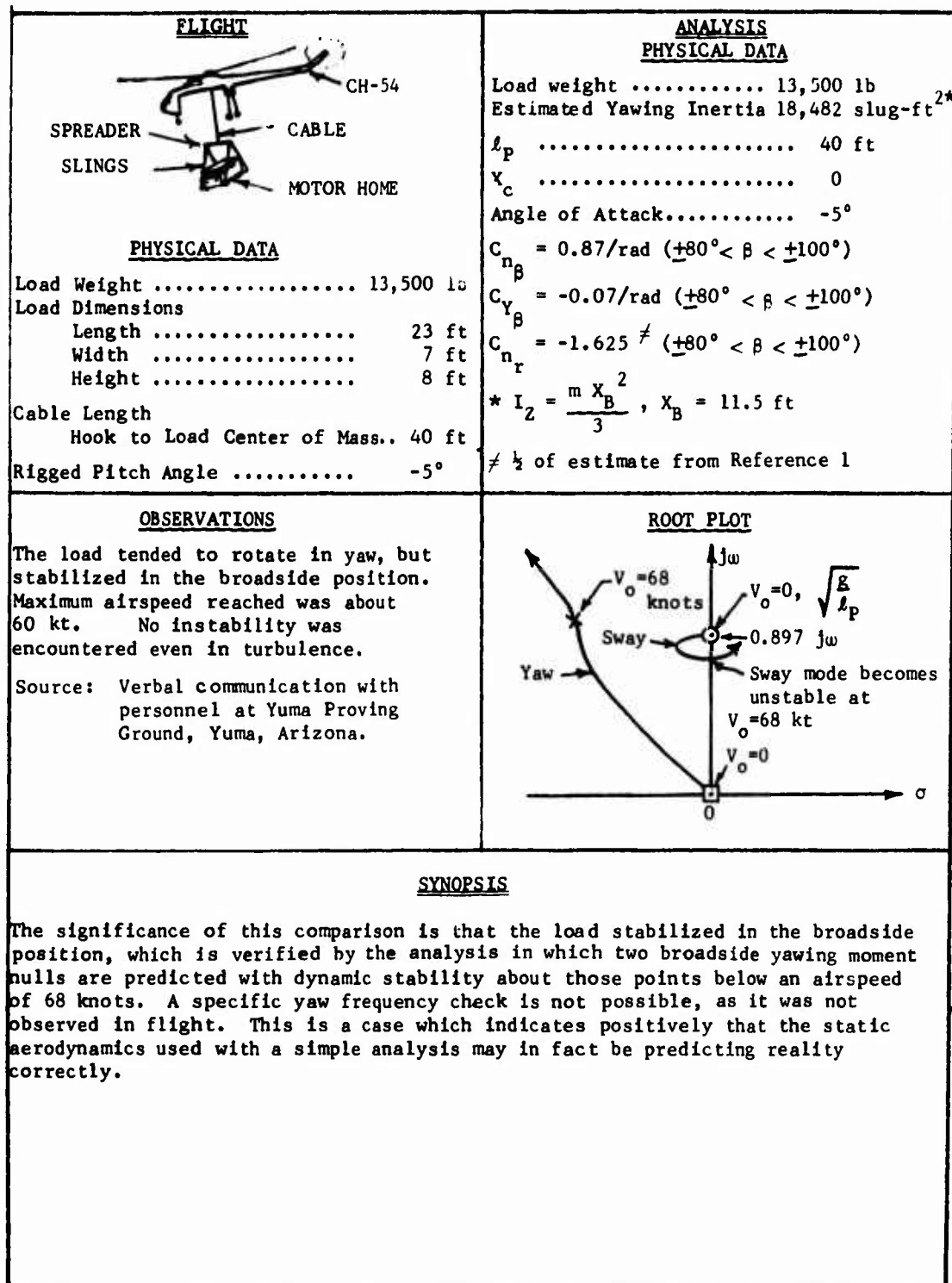


Figure 14. Flight Data-Analysis Comparison for a Mobile Home on a Single-Point Suspension.

## DYNAMIC WIND TUNNEL TEST

### TEST SCOPE

Up to this point, attempts have been made to describe the action of the load by a linearized dynamic model based on static wind tunnel data. We have seen that a poor prediction results from this for the small-end-forward case and that probably a better prediction can be made for the broadside case. Since the broadside case is not likely to be the candidate position for high-speed operations (due to drag), a better analysis is needed before an understanding of this load's behavior can be achieved. Certainly what has been learned up to now is not sufficient to justify mounting a "grand" study of all the variables and all the possible stabilization schemes just yet.

With this in mind, the effort was redirected so that a dynamic wind tunnel test could be performed. The suspicion at this point was that unsteady aerodynamic effects were present which dominated the dynamics, particularly for the more important small-end-forward case.

The 0.1 scale model of the 8-by-8-by-20-foot container used for the static tests was available, and it was modified slightly so that it could be hung in the tunnel test section. The suspension system consisted of two cables with end fittings that allowed the creation of a number of single- and two-point suspension systems. Attach points were available at 1, 3, 5, 7, and 9 inches on either side of center.

Tufts were taped to the model for airflow identification, and the floor of the tunnel was striped for a camera reference. All the pertinent variables were measured, such as yawing moment of inertia, weight and center-of-gravity location, cable length and cable separation. The primary instrumentation consisted of a 16 mm camera located above the tunnel as depicted in Figure 15. An airspeed cone was hung in the tunnel for a visual indication of airspeed.

Before the tests began, a rigorous analysis of the model was made using the linearized equations of motion and the static wind tunnel test results. It was planned to attempt to measure the yaw damping function  $C_{N_r}$ , and to this end, a variety of cases sensitive to this parameter were isolated and incorporated into the test plan.

The basic test procedure was to restrain the model by a makeshift hand-held fork, bring the tunnel up to speed, start the camera, and then release the model. The initial sway angle was set to either 0, 6, or 12 degrees. Zero was generally used for the more active conditions, and 6 degrees was generally used for the milder ones.



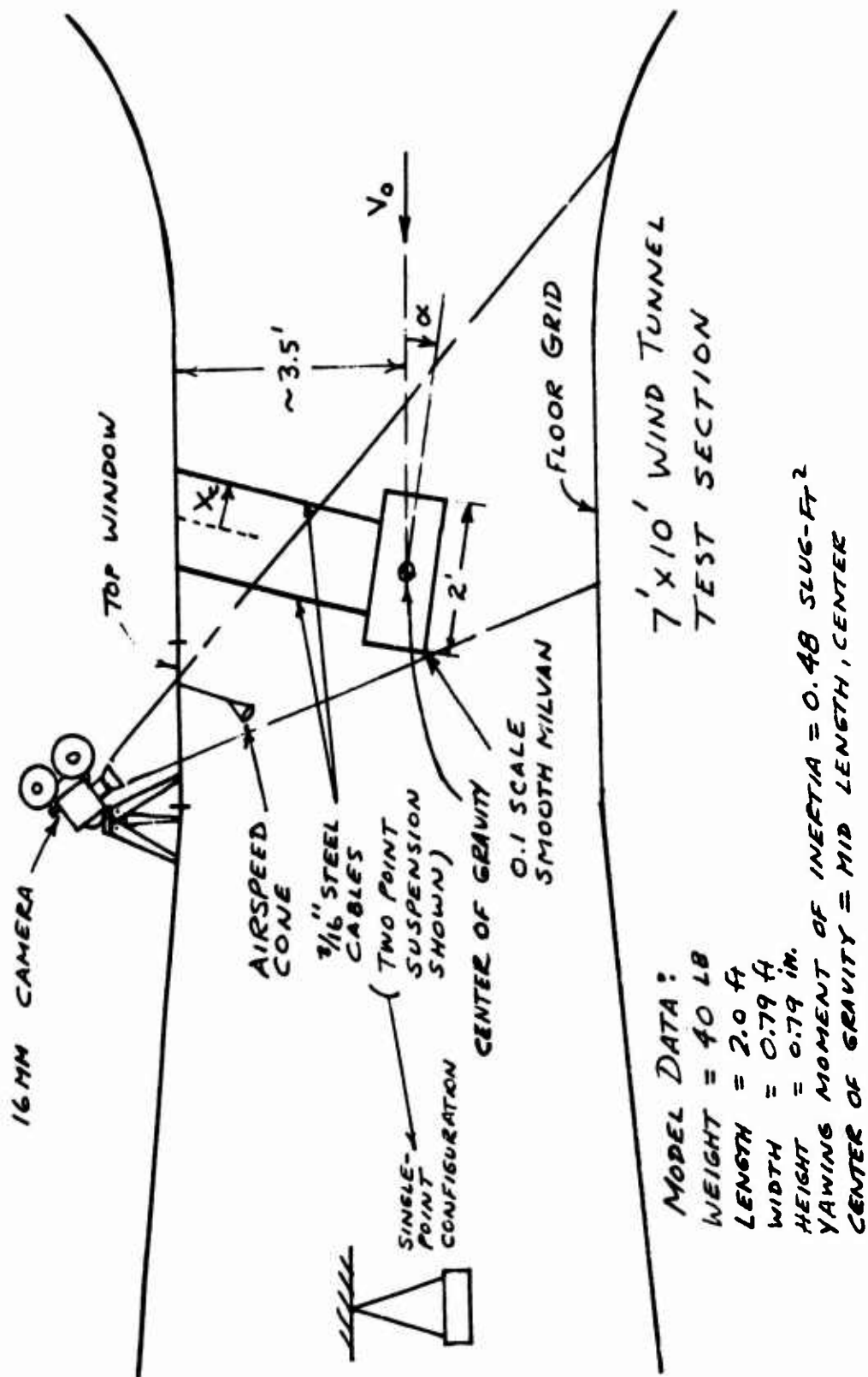


Figure 15. 0.1 Scale MILVAN Dynamic Wind Tunnel Test Setup.

Forty-seven documented runs were made. These included 3 calibration runs, 17 basic container runs, 22 with fixed fins added, 3 with drogue chutes, and 2 with smoke flow visualization tests. Included in the basic and finned tests were level and drooped runs (to vary angle of attack), narrow cable runs, unequally spaced cable, and single cable runs.

The run log corresponding to the film record is in Appendix IV. A generalized summary of the observations follows.

### TEST RESULTS

1. The first free model run at 20 knots tunnel speed for the level box showed a surprising disparity from the analog computer runs using the static aerodynamic data. There was obviously an energy-producing device that was causing a large yaw limit cycle of approximately  $\pm 20^\circ$  amplitude at the bifilar frequency. As the speed was increased to 40 knots, the amplitude increased and the fixed point of rotation moved forward to the front of the model. All stable limit cycle motions occurred at the bifilar frequency.

When hung from a single cable, the model turned broadside and developed a lateral swaying motion. With narrowly spaced cables, the center of rotation moved toward the rear of the model.

For angles of attack of -10 and -14 degrees, the model was almost completely still.

2. Light finned configurations were tested, three of which were quite still. The successful configurations incorporated a long fin projecting out of the center of the rear face (Runs 12-15) or two fins projecting back from the rear corners, simulating opening the rear doors of the MILVAN. The fin length was 20% of the length of the MILVAN. Fins of 10% length were not effective. Tilting the finned MILVAN 10 degrees down was even better, as the tunnel speed could be taken to 67 knots. Initial sway angles of 12 degrees were successfully tested at this speed.

3. Drogue chutes had little effect on the stability of the MILVAN. One drogue chute was simulated by a paint filter cone and was attached to the center of the rear of the MILVAN. This configuration showed almost no yaw amplitude reduction. When the chute was connected by two cables to the outer corners of the container, the yaw amplitude was reduced when no initial sway angle was introduced; however, it reached a stable limit cycle in yaw after a disturbance.

4. Smoke Tests (Runs 34 and 35). A smoke generator was hand-held in the vicinity of the model, and the path of the smoke was observed from above and the sides of the test section. Smoke released near the center of the forward face would billow out around the sides, revealing the separation pattern. As the model oscillated, the pattern alternated asymmetrically. The downstream side face exhibited a large separation plume, while the plume on the upstream side appeared to subside. Of more significance was the rapidity with which the plume changed. Smoke emitted just above the rear face followed one of two curved paths and appeared to snap from one to the other just after the sideslip angle passed through zero.

5. Tuft Study. Of considerable interest was the behavior of tufts on the rear face. They would snap back and forth just after sideslip passed through zero. For example, as the rear face proceeded to the left from a maximum right position (nose left), the tufts would point left. As the rear face passed through the neutral position (about  $-3^\circ$  sideslip), the tufts reversed quickly and pointed right. This action then reversed itself.

#### WIND TUNNEL SPEED SCALING

In dynamic wind tunnel tests, it is common practice to attempt to control certain parameters so that the results may be interpreted in light of the full-scale conditions. For most dynamic work, it is sufficient to consider three parameters: the Reynolds number, the Froude number, and the Strouhal number.

Reynolds number - This parameter represents the ratio of the pressure forces to the viscous forces and is important in flows where the onset of separation is caused by the properties of the boundary layer. For a bluff shape such as the cargo container, it is unlikely that the boundary layer will appear different in the range of Reynolds number of model to full scale ( $10^5$  to  $10^6$  respectively).

Froude number - This is the ratio of pressure to gravitational forces and is important here because these two kinds of forces dominate the dynamics. It is customary to hold Froude number constant from full scale to model by the proper choice of tunnel speed and the inertial properties of the model. In the present study, the use of the existing static model of the cargo container reduced model fabrication cost, but of course this meant that the full-scale container that was represented was not realistic ( $W=40,000$  lb,  $I=40,000$  slug-ft<sup>2</sup>). The rigorous interpretation of the model results is that it represented a geometrically similar model with the above inertial properties, with 31-foot cables. The speed scaling inferred by a constant Froude number is  $1/\sqrt{\text{scale factor}} = 1/\sqrt{0.1} = 3.16$ . This means that a tunnel speed of 20 knots corresponded

to a full-scale speed of  $3.16 \times 20 = 63.2$  knots. Since the bifilar frequency also scales at 3.16 (ratio of model to full scale), a model film record taken at a tunnel speed of, say, 20 knots, corresponds to a full-scale condition of 63.2 knots. If the film were shown at  $1/3.16$  the speed at which it was taken, the load motions it would show would be close to the full-scale motions at 63.2 knots.

Again, the unrealistic model conditions are not considered important because the model parameters were used during the analysis to extract the unsteady aerodynamics, and as it turned out, simply applying the results to the full-scale container gave good correlation with flight results.

Strouhal number - This is a nondimensional frequency that is used in dynamic tunnel testing. It is a frequency in radians/second or cycles per second multiplied by length and divided by velocity. Holding this number constant from model to full scale gives the same result as for the Froude number, namely, full-scale speed is 3.16 times model speed. Strouhal number is useful in describing vortex shedding and other properties of a turbulent wake. It is reasonable to hold it constant for dynamic wind tunnel testing of this kind because in doing so the relation between the wake motions (vorticity, etc.) and the model motions is maintained, thereby increasing the probability of correctly representing the unsteady aerodynamic effects.

## NONLINEAR ANALYSIS OF THE 8-BY-8-BY-20-FOOT CONTAINER

The poor correlation between flight data and the results of the linearized analysis prompted the initiation of a nonlinear analysis. It was decided to use a small analog computer so that on-line comparisons with film records could be made in real time, as was first mentioned in the section describing flight data-analysis comparisons. The incorporation of the nonlinear aerodynamic yawing moment and the extension of the yaw degree of freedom to continuous operation did not produce results that compared with flight data, particularly for the small-end-forward case.

## INTERPRETATION OF THE DYNAMIC WIND TUNNEL TEST RESULTS

It was obvious from the beginning of these tests that a dynamic yawing moment was present beyond the simple concept of damping moments due to yaw rate. The formulation of this additional dynamic moment began with a detailed examination of the tuft behavior on the rear face. It is very probable that the "switching" back and forth of the tufts was caused by a rapidly reversing flow pattern which in turn was caused by the transition of the flow back and forth between a partially separated state to a fully separated one. The resulting flow required time to establish itself, and in the process of doing so, unsteady flow effects were generated. For example, when a two-dimensional airfoil is oscillated in a wind tunnel, a vortex is generated on the suction side during the time when angle of attack is increasing. This vortex precedes the separation and is accompanied by a low-pressure region. This low-pressure region propagates downstream and in doing so creates a "pulse" of pitching moment.

It is suspected that this is the mechanism occurring with the container. Specifically, as sideslip reaches about  $3^\circ$  and is increasing, a vortex propagates downstream along the downstream side. When it reaches the rear face where the vortex can now "draw in" more flow, it does so, and a small sharp pulse of negative pressure appears on that side of the rear face, causing the tufts to reverse and creating a small pulse of yawing moment that reinforces the oscillation. With this hypothesis in mind, the reader may now turn to Figure 16, where he may find the dynamic yawing moment evolved from the analog matching study. Note that a moment hysteresis is present; i.e., a dynamic moment is present only when the product of sideslip and sideslip rate is positive and sideslip remains within certain limits.

## THE ANALOG MATCHING STUDY

The motion of the tufts and smoke pattern suggested that a vortex was being shed as the model rotated through nearly zero sideslip. The purpose of the analog matching study was to find a vortex model that could be added to the wind tunnel static aerodynamics and conventional rotary derivatives which would satisfactorily match the observed dynamic tunnel test results over a wide range of conditions. A set of ground rules was set for the vortex model.

UNSTEADY YAWING MOMENT  
OF A  $3\frac{1}{4}' \times 3\frac{1}{4}' \times 2'$  BOX

MODELED FROM THE RESULTS  
OF A DYNAMIC WIND  
TUNNEL TEST  
(STROUHAL NUMBER  
 $\approx 0.1$  RADIAN,  
BASED ON WIDTH,  $b$ )

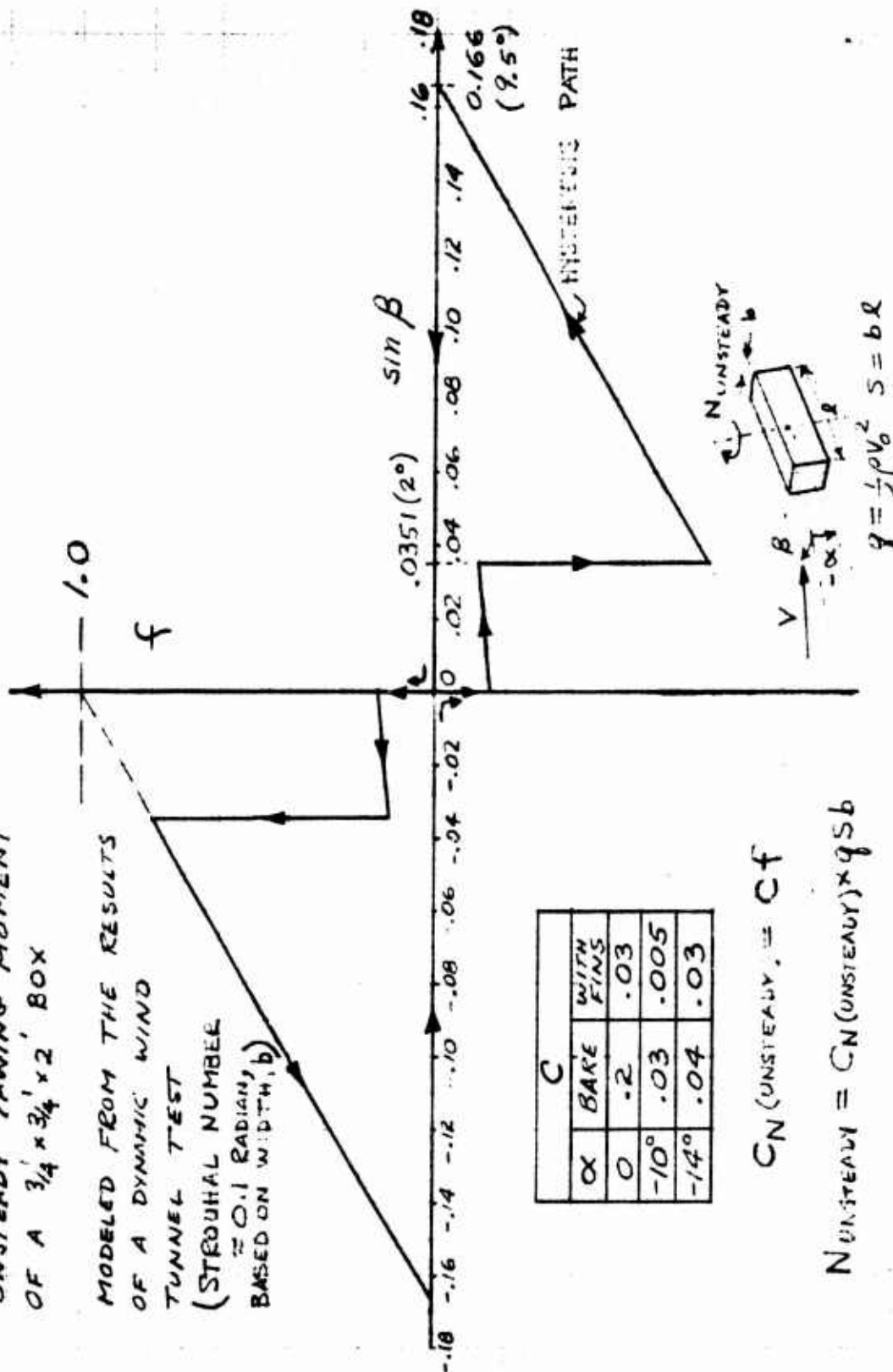


Figure 16. Dynamic (Unsteady) Yawing Moment Function.

1. The model should be compatible with established concepts of unsteady flow effects.
2. No changes would be necessary to accommodate a match at different speeds.
3. Changes could be made to accommodate different angles of attack and the addition of fins.

The matching conditions consist of first generating an oscilloscope display representing the centerline of the MILVAN scaled such that the sway and yaw modes appeared as if viewed from above. Next to the oscilloscope, the films of the tests were projected at approximately the same size. When the movie project was started, the computer, with the appropriate initial conditions, was set to compute when the film showed the model being released.

From the beginning, it was obvious that an exact match, movement for movement, could not be made; therefore, an attempt was made to match the limit cycle frequency, growth and decay rates, and fixed point of rotation or phasing of the modes. Since  $C_{N_r}$  was an unknown parameter,

initial attempts were made to match using this parameter. It was found that a match could be made at various levels of  $C_{N_r}$ . Hence, it was set to

a "reasonable" level and not changed. The larger the  $C_{N_r}$ , the larger the

value of the unsteady moment that was required to match the wind tunnel data. This led to the energy balance concept presented in the following section. The shape and magnitude of the unsteady moment function had a large influence on the growth and steady-state magnitude of the limit cycle. The shape could not be defined precisely due to the inaccuracy of the test data and the use of an eyeball match; however, as more test runs were matched, more confidence was gained in the model.

Some of the conditions that have a severe impact on the shape of the unsteady function (Figure 6) are illustrated by the following examples. Runs 25, 26 and 27 (see Appendix C) displayed an extreme speed sensitivity and a dual mode stability. These cases and others tended to have a small-amplitude stable limit cycle with no initial disturbance, and when disturbed, a large-amplitude limit cycle. An increase in speed in Run 25 caused the change in limit cycle. There were no cases of limit cycle amplitudes between approximately  $\pm 2$  and  $\pm 10$  degrees. The above conditions were met by reducing the magnitude of the unsteady function at sideslip angles near zero, and forcing it to zero beyond  $\pm 9.5^\circ$  sideslip. After this form of unsteady moment function was used, only changes in the magnitude were required to match the various configurations. The fact that the unsteady function was zero beyond  $\pm 10^\circ$  sideslip and the fact that the container had its best stability at angles of attack of  $\pm 10^\circ$  are probably related.

It is interesting to note that the fixed point of rotation\* of the container was near the front and moved forward with increased speed, for  $X_c = .75'$ ; however, with the reduced cable separation ( $X_c = .417'$ ), the fixed point was near the rear of the container.

In all cases with the wide cable separation, the sway mode quickly dissipated and the sway motion was forced by the yaw mode. With the cable separation such that the yaw frequency and sway frequency are nearly the same, the modes couple and instability of the classical nature results.

The single-cable cases matched to near perfection.

The analog model matched quite well with the wind tunnel results. The limit cycle frequency matched to approximately  $1/4$  cycle in 10 cycles, or 2.5%. Nothing was done to the model to change the frequency because it was primarily controlled by the cable separation. With small-amplitude limit cycles, the static yawing moment had an effect; however, with large-amplitude limit cycles, it averaged out to nearly zero. The growth rate of the limit cycle is probably accurate to 10 - 20%. The amplitude of the limit cycle, while the most easily changed variable, is probably 15 - 20% in error due primarily to the camera angles not being vertical. Some correction was made for this effect, but it was not calibrated precisely.

The shape of the unsteady moment curve is undoubtedly in gross error due to the lack of precision of the data. The straight lines of the function do not reflect the lags associated with unsteady aerodynamics; however, the general characteristics of the unsteady moment which evolved must have some correlation with reality because the predicted MILVAN motions agreed well over a wide range of speeds and geometrical conditions.

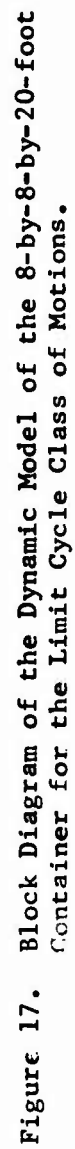
#### DESCRIPTION OF THE DYNAMIC MODEL AND ITS PREDICTIONS

Figure 17 contains a block diagram of the dynamic model. A logic representation of the unsteady yawing moment function is shown, and the static yawing moment is also included. Note that the model is a single-degree-of-freedom one, describing the motions about the yaw axis only, which is usually a stable limit cycle. This model is valid as long as the yawing limit cycle frequency (the bifilar frequency) is significantly greater than the sway pendulum frequency. If, for example, the bifilar frequency is lowered to about 1.5 times the sway pendulum frequency, the sway mode will be unduly perturbed by yaw and a classical instability usually begins to appear. The mechanization diagrams for the complete two-degree-of-freedom analysis are given in Appendix B.

---

\* Due to the phasing of the sway and yaw motions, one point on the container appeared to be fixed relative to the tunnel. This is referred to as the "fixed point of rotation".





An attempt was made to estimate the yaw limit cycle amplitude based on the concept of conservation of energy. Specifically, the yaw motion is assumed to be a stable limit cycle at the bifilar frequency, and the energy added to the system by the unsteady aerodynamics is exactly removed by the damping function  $C_{N_r}$  with the assumption of sinusoidal motion. The integration of the unsteady moment function into energy is complex for amplitudes less than  $\pm 9.5^\circ$ ; however, for larger amplitudes, a closed-form solution can be derived which is given below.

$$\psi_{\max} = \pm \sqrt{\frac{-.1126C}{\pi C_{N_r}}} \frac{2V_o}{b\omega_\psi} \quad (|\psi_{\max}| \geq .166 \text{ rad})$$

In this expression, the negative sign reflects the damping offered by  $C_{N_r}$  which is usually taken as minus, .1126 is the integral value of the unsteady moment function, and  $C$  is the normalized value of the unsteady function and is a function of fins and angle of attack. For a peak amplitude greater than 0.166 rad,  $C$  is a function only of angle of attack, and this function is given in Figure 18. A straight-line function was assumed between the measured points.

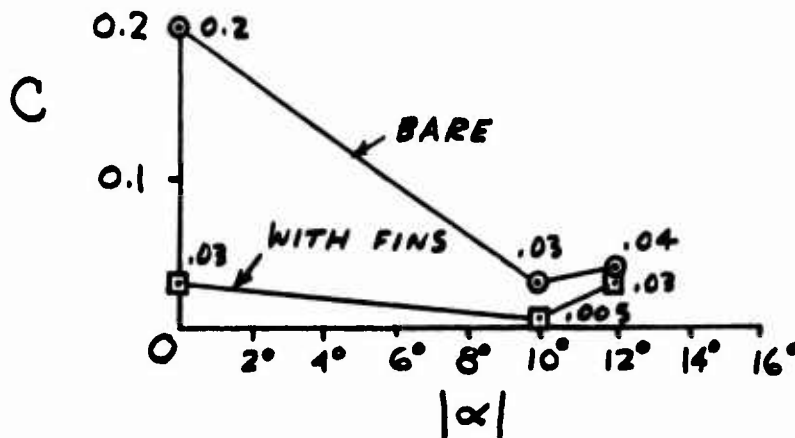


Figure 18. Effect of Angle of Attack and Fins.

It is convenient to express the relation in terms of the Strouhal number ( $S_T = \omega_\psi b/V_o$ ) thus:

$$\psi_{\max} = \sqrt{\frac{-2C \times .1226}{\pi C_{N_r}}} \sqrt{\frac{1}{S_T}}$$

where  $b$  is container width,  $\omega_\psi$  is the bifilar frequency in rad/sec, and  $V_o$  is forward speed in ft/sec. The value of  $C_{N_r}$  derived from the analog

matching study is -0.94. When this is substituted into the equation, a relatively simple expression results:

$$\psi_{\max} = \sqrt{\frac{2 \times 1126}{\pi \times .94}} \times \sqrt{\frac{C}{S_T}} = 0.276 \sqrt{\frac{C}{S_T}}$$

Figure 19 shows the model data points, full-scale points from Reference 2, computer predictions, and the energy balance estimate. The agreement between the computer results and the energy balance prediction is seen to be very good. The flight data from Reference 2 also shows good agreement with the model for short cables and low yaw amplitude ( $\pm 15^\circ$ ). The agreement between the energy balance prediction and flight data for large amplitude (long cables) is not as good. The reason for this is that the simple formula assumes the motion to be sinusoidal and the computer prediction shows it to be approaching a triangular form. This will certainly affect the calculation for the damping function  $C_{N_r}$ . The reasonably good match

between the model prediction of flight results and the flight results themselves is remarkable, considering the strong effect of angle of attack and the lack of documentation of angle of attack in the flight data.



### CARRYING SPEED CRITERIA AND LIMITATIONS

Up to this point, we have seen how the motions of the container may be calculated for any combination of airspeed, weight, moment of inertia, cable geometry, and angle of attack. The effects of aft fins are included in this method. We have also seen that when the bifilar frequency lies

close to the sway pendulum frequency, i.e.,  $0.6 < \frac{\omega_\psi}{\omega_\phi} < 1.5$ , a classical instability usually results. When these frequencies are widely separated, i.e.,  $0.6 > \frac{\omega_\psi}{\omega_\phi} > 1.5$ , generally a stable limit cycle dominates the dynamics.

This is illustrated in Figure 20, below the root plot sketches of the three regions.

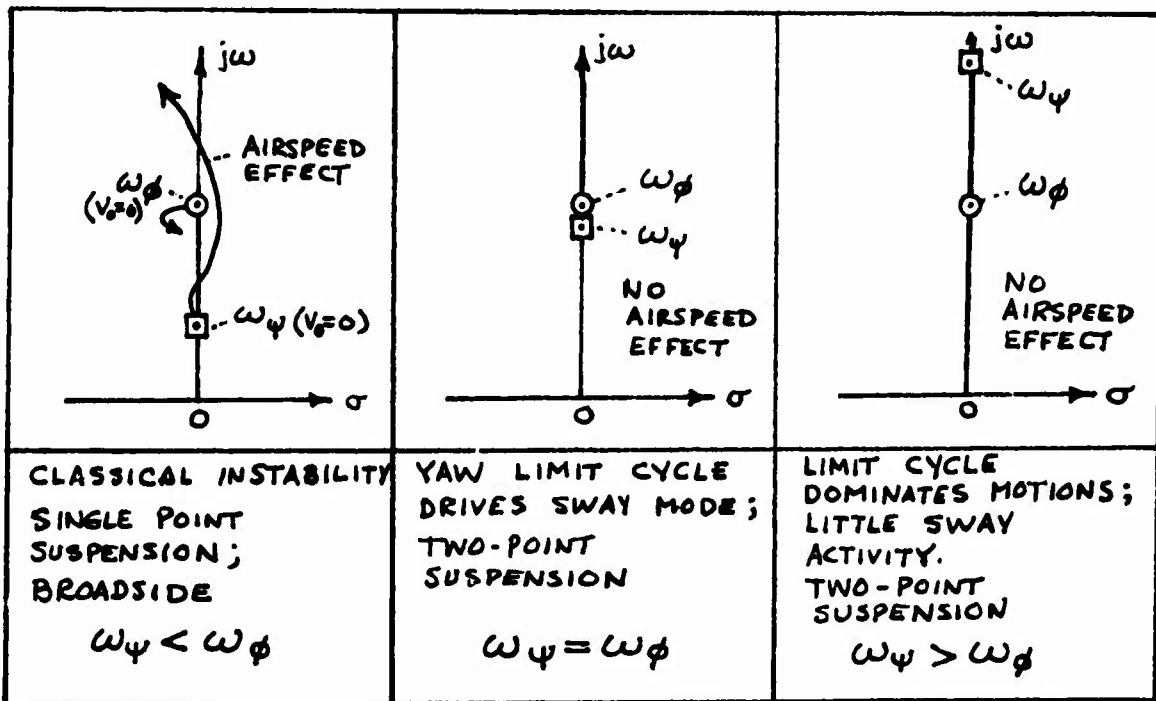


Figure 20. Three Classes of Load Motions.

Drooping the container with an asymmetric sling system helps considerably because the angle of attack of the container may be held near the optimum value of  $10^\circ$  in cruise flight. Apparently, an angle of attack of  $\pm 10^\circ$  ensures that the flow has stabilized to a fully separated state and that no unsteady moments exist beyond this value. A reexamination of the unsteady

yawing moment function (Figure 16) will show that the function is zero beyond  $9.5^\circ$  sideslip. This is undoubtedly caused by the same separation phenomenon that causes the angle-of-attack variation. At an angle of attack of approximately zero, the addition of rear-mounted fins (simulating the doors opened  $90^\circ$ ) reduces the limit cycle amplitude to the value when angle of attack is set to the optimum of  $10^\circ$ .

Now that the capability exists for calculating the motions of the container with confidence, the next question naturally arises: what motions can be handled?

For the cases involving classical stability, the answer is simply "no instability shall exist". This typifies the single cable cases, which are known to have oscillatory motions at higher speeds that prevent the pilots from carrying them any faster. For the cases where the yaw limit cycle dominates the dynamics (two-cycle suspensions, small-end-forward), the answer is not so clear. As speed increases, the limit cycle amplitude increases, but so does the drag, so that with two cable suspensions, the nose-down attitude of the helicopter constrains a similar attitude in the load. The resulting increased angle of attack of the load decreases the limit cycle amplitude. The inducement of sideslip angles greater than  $10^\circ$  also reduces the amplitude, as would climbs and descents.

With so many influences on the limit cycle amplitude, many answers undoubtedly exist. In an attempt to begin to understand the effects of stabilization concepts varying from active "black box" types to passive configuration-oriented (fins, etc.) ones, included maneuvering (pilot training), a sophisticated simulation of the Model 347 helicopter was utilized. A more detailed description is contained in Appendix D. Linearized equations of motion for the sling load were used, and the dynamic model of the 8-by-8-by-20-foot container was incorporated into the simulation. A validation effort preceded the primary test phase, whose purpose was the establishment of confidence in the simulation. This consisted of setting in coefficients which produced a simulation of a known flight condition and allowing the same evaluation pilot who flew that flight condition to fly the simulator. The condition used for validation was one flown by Boeing-Vertol pilots using the Model 347 helicopter carrying an empty 8-by-8-by-20-foot container. This load was suspended on a two-point cable and sling system. The two parallel cables were each 7.5 feet long and were separated just above the load by a 24-foot-long spreader beam weighing 3505 pounds. Nylon slings, 8 feet long, attached the ends of the spreader to the upper corners of the container. In this configuration, the pitch attitude of the container was very nearly constrained to the helicopter's pitch attitude. This configuration's motions fall into the limit cycle class previously discussed. The bifilar frequency is 4.18 rad/sec and is greater than the lateral sway pendulum frequency of 1.49 rad/sec. Since the container tries to maintain its small end forward, a limit cycle yaw motion results at the bifilar frequency whose amplitude is strongly dependent on airspeed,

load angle-of-attack and load sideslip angle. It is sufficient to say that a remarkable agreement occurred immediately between the evaluation pilots' recollection of that flight condition and the simulation of that flight condition. Other configurations involving a cable length of 50 feet were also evaluated with similar good results.

When confidence in the simulation was established, a series of tests was made to determine the limit cycle amplitude that the pilots felt was the maximum allowable. To effect this test, the cable separation was varied so that the bifilar frequency could be controlled. Five data points were obtained for the range of bifilar frequency from 1.34 rad/sec to 5.22 rad/sec. For the spreader beam configuration with 7.5-foot cables mentioned previously, this corresponds to a cable separation range from 7.7 feet to 30 feet, respectively.

The five data points revealed that for a given airspeed, the pilot will accept large-amplitude limit cycle load motions provided these motions are slow, i.e., low bifilar frequency. Before he will carry the load any faster, the load motion amplitude must be made lower or its frequency reduced.

Curiously enough, these five data points can be fitted very well by the simple relation

$$\psi_{\max} = \frac{.091}{\sqrt{S_T}}$$

It can be recalled that this form resulted from an estimation of limit cycle amplitude considering that the energy added to the system by the unsteady aerodynamics was equal to that removed by the damping function.

This relation is clarified by the plot of Figure 21, in which the maximum allowable amplitude is plotted versus airspeed and bifilar frequency. The five simulation data points are also shown.

A minor point that affects these results is the effect of helicopter mass. The two-degree-of-freedom nonlinear analysis, while rigorous, does not predict the limit cycle amplitude precisely when the load is attached to a finite mass helicopter. For the empty MILVAN with spreader, the ratio of load mass to total mass is  $8705/37,000 + 8705 = 0.19$ . The ratio of load yawing inertia to helicopter inertia is even smaller,  $9500/367,000 = .026$ . It would seem that the condition of infinite helicopter mass is satisfied for the purpose of employing the two-degree-of-freedom analysis. As it turned out, however, when the dynamic model was incorporated into the simulation, the limit cycle amplitude matched the earlier model results precisely, but only if the helicopter was held fixed (by manipulating the computers). When the helicopter was released after trimming, the limit cycle amplitude



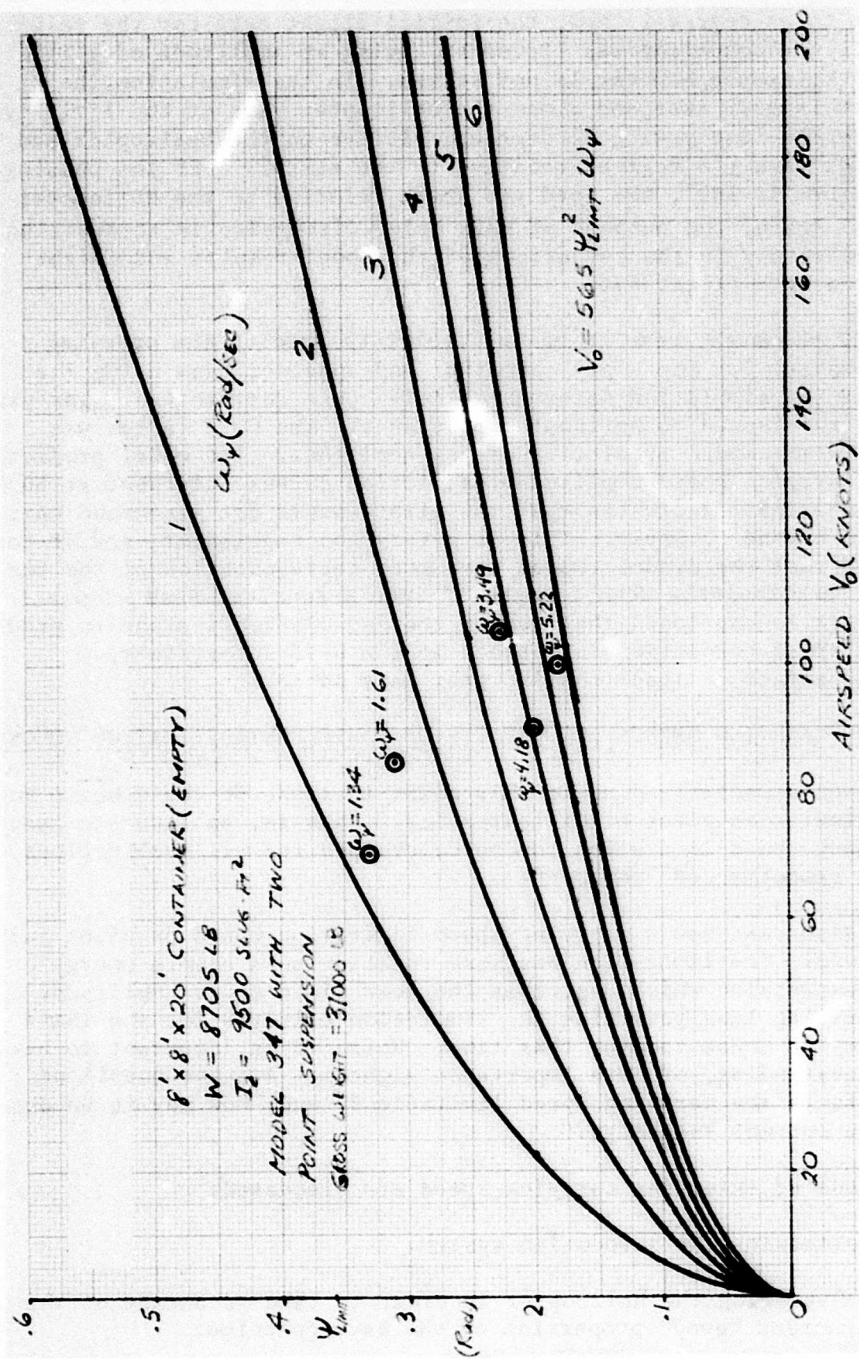


Figure 21. Carrying Speed vs Allowable Limit Cycle Amplitude and Frequency.



was reduced to .75 of the helicopter-fixed value. The difference amounted to about three degrees. Now, the initial flight data for the validation flight condition was listed as having an amplitude of  $\pm 15^\circ$ . The axes reference, however, is not stated. In the simulation, the reference is body axes; and since the helicopter yaws at the limit cycle frequency, the load yaws  $\pm 12$  degrees relative to the helicopter and the helicopter yaws  $\pm 3$  degrees relative to the earth. If the phasing between them is  $180^\circ$ , the load yaw angle relative to the helicopter is  $+15^\circ$ . Again, the purpose of this brief discussion is to describe an inconsistency in the comparison of the model results and flight simulation with flight data.

Figure 22 shows the results of an attempt to predict the carrying speed boundary for the empty container and spreader beam using the model and the simulation-determined limit cycle restriction. The yaw angle is referenced to helicopter body axes. The 0.75 factor was applied to the model prediction of yaw amplitude. The model prediction and the carrying speed amplitude restriction curves intersect at 60 knots. The flight report indicates that the pilots would not recommend carrying this load beyond 65 knots. This is a very good agreement, and it can be concluded that the dynamic model is a good representation of the real-world effects, particularly when integrated into a sophisticated simulation. However, it is cautioned that use of the dynamic model alone to predict carrying speed boundaries is subject to the 0.75 uncertainty, i.e., the effect of load-to-helicopter mass ratio.

#### EXTENDING CARRYING SPEEDS AND EFFECTS OF VARIOUS STABILIZATION CONCEPTS

It has been demonstrated up to this point that use of the dynamic model with a simulation gives credible results. That is, an accurate assessment of carrying speed limitation can be determined for all combinations of cable geometry and load mass.

We have also seen how a carrying speed limitation based on pilot judgement was evolved. The limitation has some relation to a simple energy balance expression which describes the load limit cycle amplitude. The underlying laws governing the limitation criteria for the limit cycle are not understood at this time. While it is important to have this understanding, of more importance right now are the questions "what affects the carrying speed limitation?" and "how may it be extended using the current knowledge?"

Six methods of extending carrying speed are discussed:

1. Optimizing the suspension system.
2. Maneuvering the helicopter in order to take advantage of the inherent "good" properties of the bare container.

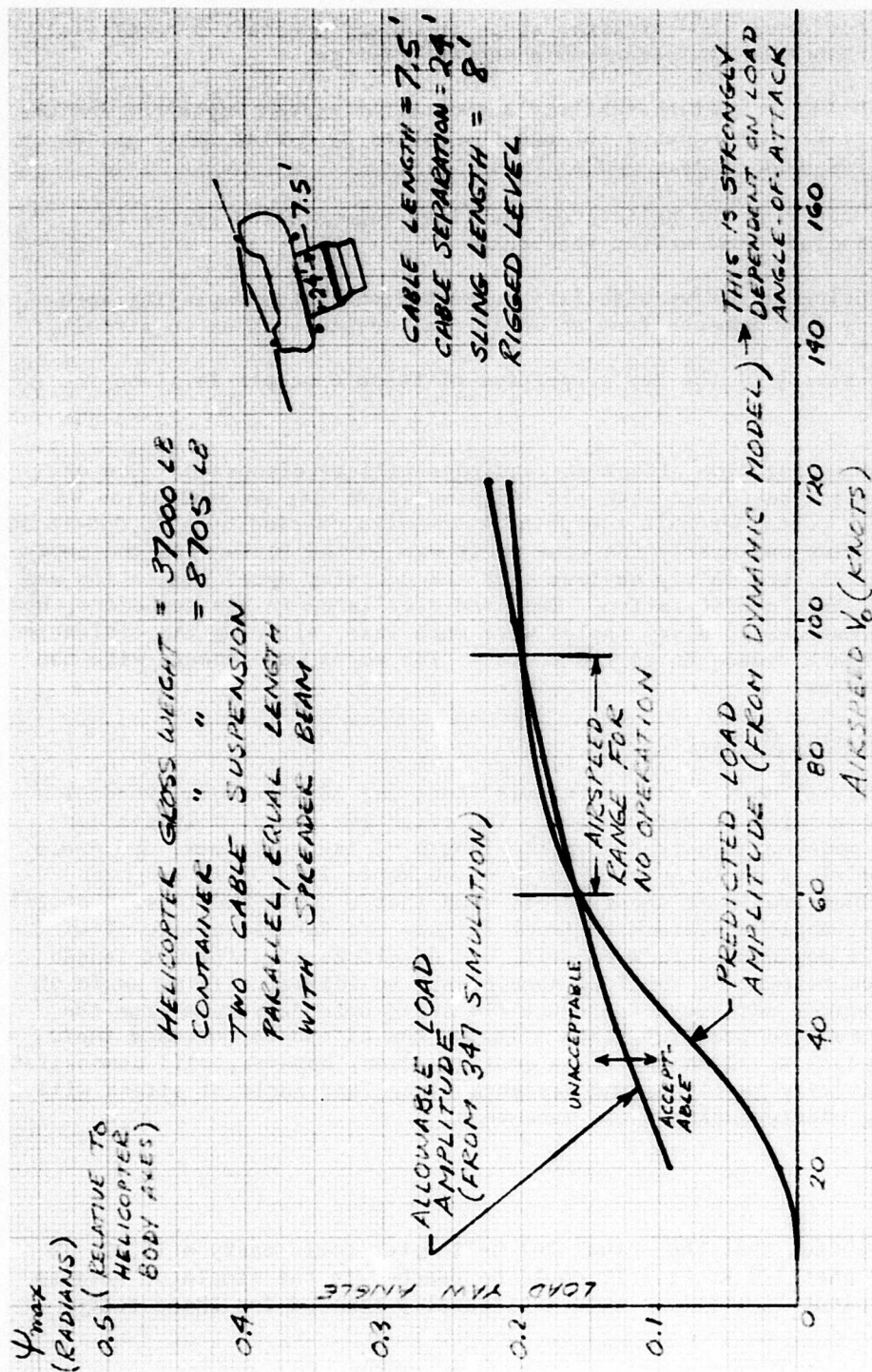


Figure 22. 8-by-8-by-20-Foot Container Carrying Speed Limitation.

3. Modifying the container shape in order to effect a beneficial change in its aerodynamic characteristics.
4. Using an active stability augmentation system employing devices generating moments through the cables by moving cable guides in the helicopter.
5. Modifying the helicopter stability augmentation system to include load motion feedback.
6. Using an active stability augmentation system employing aerodynamic moments from an additional device such as an airfoil.

A summary sketch of the key properties of these concepts is given in Figure 23.

Before proceeding, the effect of load mass will be discussed. One of the last tests performed with the 347 simulation was an evaluation of a 15,000-lb container on a two-point suspension carried by a 30,000-lb 347. The total mass was nearly the same as it was in the tests with the empty container. It was fairly obvious that the carrying speed limitation was higher for this configuration. The load oscillated in yaw as before, however, the maximum load yaw angles were much less, allowing the evaluation pilot to reach speeds up to 150 knots.\* The worst case occurs with the empty container.

#### SUSPENSION SYSTEM OPTIMIZATION

There is little more that can be said about the single-point suspension beyond the remarks in Reference 2. The effective pendulum length can rarely be made much shorter than the length of the container, and under these conditions an acceptable speed of 40 knots is usually recommended. The container trails at these speeds such that a small-end-forward position has a small angle of attack in level flight. To take advantage of the container's angle-of-attack benefit, use of slings of different length could allow rigging of the load nose-down. An initial rigging angle of about 5 degrees may serve to reduce the rapid nose departure from the small-end-forward position, thus allowing the pilots to increase their speed, perhaps to 50 knots. This configuration, however, will demonstrate high sensitivity to climbs and descents since load angle of attack will be varying widely during these maneuvers.

---

\*It is doubtful that the actual 347 helicopter could carry a 15,000-lb container past 120 knots. It could be reached in the simulator because the powerplant limitations were artificially removed for these tests.

<p>1</p> <p>REAR CABLE WINCH TO OPTIMIZE NOSE DOWN RIGGING ANGLE</p> <p><math>\alpha = 10^\circ</math></p>	<p>Optimized suspension; two-point, pendulum length less than 20 ft, 20 ft parallel cable separation. Aft winch to optimize angle of attack to <math>-10^\circ</math>. Sensitive to piloting technique.</p>
<p>2</p> <p>CRUISE ACCELERATE</p> <p>SLOW DESCENT, SIDESLIP</p> <p>STEEL CLIMB</p> <p>TAKE OFF</p> <p>STEEL APPROACH</p> <p>LANDING</p>	<p>Optimum maneuvering; carrying maneuver is designed to maintain an angle of attack or sideslip of <math>10^\circ</math> while minimizing mission time. Contingency maneuvers in case of emergency (collision avoidance, etc.), additional pilot training required.</p>
<p>3</p> <p>WAKE SPLITTER</p> <p>FINS</p> <p>CORNER DEFLECTORS</p> <p>ROUNDED NOSE</p>	<p>Modifying container shape; wake splitter plate aft fins, corner deflector, round nose all tend to reduce unsteady aerodynamic yaw moments. Sensitive to normal operational abuse.</p>
<p>4</p> <p>CABLE ANGLE SENSORS</p> <p>CABLE GUIDE ACTUATORS</p>	<p>Cable guide actuators; two cable guide actuators deflect the cables laterally (collectively) in response to load sway rate, and laterally (differentially) in response to load yaw rate (relative to helicopter). Desensitizes the problem, permits brisk maneuvering, but requires additional actuator and load motion sensor hardware.</p>
<p>5</p> <p>CABLE ANGLE + RATE SENSORS</p> <p>To SAS</p>	<p>Helicopter SAS inputs from load motion sensors; lateral sway rate <math>\rightarrow</math> lateral SAS; load yaw rate <math>\rightarrow</math> yaw SAS. Improves carrying speed slightly; degrades helicopter ride qualities.</p>
<p>6</p> <p>AUXILIARY AIRFOIL DRIVEN BY YAW RATE SENSOR</p>	<p>Auxiliary airfoil; driven by load yaw rate? May improve carrying speed if airfoil operates effectively in wake of container; airfoil may possibly be placed forward of load. Complex to handle; requires additional hardware.</p>

Figure 23. Key Properties of Stabilization Systems Studied.

There is a greater possibility for improvement with a suspension of two or more points. First of all, the bifilar and pendulum frequencies may be separated sufficiently that no classical sway mode instabilities appear. For the empty container, this requires a parallel cable separation of at least 12 feet, considering that in practical sling arrangements, the bifilar length,  $\ell_b$ , is generally less than the pendulum length,  $\ell_p$ .

Increasing cable separation to the maximum practical is also advisable. Furthermore, the container may be rigged such that at level cruise conditions, the load angle of attack is about  $-10^\circ$ . For the container and spreader beam, carried by a 37,000-lb 347, a nose-down rigging angle of  $2^\circ$  produces this condition at 180 knots. This angle will vary slightly with different helicopters. Another possibility is the winching up of the load so that the cable length is zero. The theoretical bifilar frequency is infinite, as the yaw stiffness is now provided by the triangular sling-box arrangement. The yaw stiffness will in practice be some large, but finite, value, and this should obviously allow higher speeds. There is a danger, however, that the increased bifilar frequency will now couple with the von Karman vortex shedding frequency. If this happens the problem may return much higher frequency range where vibration loads may be limiting. It is also not clear at this point that the slings will always remain taut for this configuration.

Some background on this problem will be useful here. It is well known that a body with an adverse pressure gradient causes the surrounding boundary layer to separate. This separation, however, proceeds through the mechanism of an alternating series of vortices moving downstream in the case of a blunt-ended body. A dominant frequency of shedding of this "vortex street" is measurable, and von Karman showed such a vortex system to be theoretically possible. The energy consumed in the creation of the vortex street is equal to the drag energy. Thus, if measurements of the geometry of the vortex street are available, it is then possible to calculate the drag without any reference to air viscosity. It is believed that this vortex street is the sound-producing mechanism in the Aeolian tones of telephone wires in winds. In the application to the present problem, the calculation of the vortex shedding frequency according to Hoerner's data\* gives a value of  $\frac{0.46 V_o}{b}$  cycles per second for the vortices shed on one side only.

Thus, for the container at, say, 60 knots, the frequency is  $\frac{0.46 \times 60 \times 1.69}{8} = 5.8$  cycles per second. At this speed, therefore, excitation frequencies of 5.8 and 11.7 Hz may be expected. Excitation frequencies of rotor wakes also occur in this range, and the question arises as to the interaction. Of prime importance with this point, however, is the fact that "tightening up" the sling system will undoubtedly raise the bifilar frequency near the values for the vortex street, which could cause resonance.

---

\*Reference 3, Hoerner, pages 3-6.

## MANEUVERING THE HELICOPTER

Maneuvering the helicopter in order to take advantage of the inherent "good" properties of the bare container offers a powerful method of extending allowable carrying speeds. For example, during the simulation of the empty container with spreader, a curious ambiguity appeared. When the container was rigged level, a speed limitation of 90 knots would be voiced by the evaluation pilot. On subsequent runs, he was able to reach a speed of 165 knots. Upon closer examination, it was found that on the higher speed run, he had accelerated through the region of 90 knots. Obviously, the nose-down attitude during acceleration caused the load to assume an angle of attack which reduced the limit cycle amplitude. Referring again to Figure 22, there is a region between 60 and 90 knots where no operation is expected. However, with an additional angle of attack, the two curves could not intersect until a much higher speed was reached. This point emphasizes the possibility of following a flight profile that minimizes the limit cycle amplitude. This could be achieved by climbing, descending, or introducing sideslip. It should be recalled that a sideslip of  $10^\circ$  or more suppresses the limit cycle. These properties make this case sensitive to pilot strategy, but of more importance is the possibility that a series of maneuvers could be followed that would allow the attainment of power-limited airspeeds for this container.

## MODIFYING THE CONTAINER SHAPE

Modifying the container shape in order to effect a beneficial change in its aerodynamic properties is also a powerful, although less practical, way of extending carrying speed. Specifically, it was found that the addition of a wake splitter plate or rear fins suppressed the unsteady moments (see Figure 16) as much as the introduction of the optimum angle of attack of  $10^\circ$ . The one configuration tested with fins could be carried to a speed of 120 knots as opposed to 90 knots without them. The fins and splitter plate required are modest. The fins could be the aft doors, and the splitter a plate about 10 feet in length mounted on the centerline of the aft face. These configurations are shown in Figure 24.

An additional benefit of the fins is the added static directional stability. This is expected to greatly aid the single-point suspension configuration. A test of this configuration during the dynamic wind tunnel tests revealed that the container would remain in the small-end-forward position even when started at  $90^\circ$  sideslip. The limits of stability for this configuration, however, were not explored in the tunnel. It is very likely that the addition of fins to a single-point suspension will increase the limiting carrying speed to perhaps 60 knots.

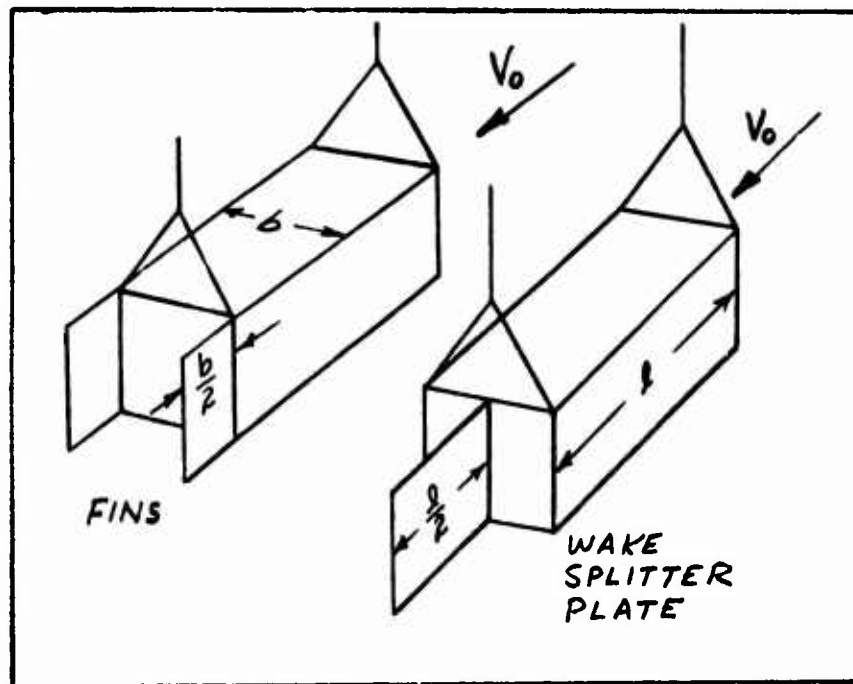


Figure 24. Fin Configurations That Suppress the Unsteady Yaw Moment.

#### ACTIVE STABILITY AUGMENTATION USING CABLE ACTUATORS

One form of an active stabilization device that was found to be highly effective is the concept of driving the cables in response to measured load motions. In its simplest form, a cable guide is moved in the horizontal plane by an actuator that is driven by load yaw rate with respect to the helicopter. This has the effect of damping the pendulum and bifilar modes. If gains are set such that a damping ratio of 0.5 is produced at hover, the configuration will be easily handled in forward flight to speeds approaching 200 knots. With a two-point suspension, such a device would incorporate two cable guides driving each cable laterally just below its attachment point to the helicopter. The guides would be driven laterally collectively in response to lateral sway rate and differentially in response to load yaw rate (relative to helicopter body axes). If the gains are set to produce a damping ratio of 0.5, the limit cycle amplitude is suppressed to less than 1/10 of its unaugmented value, thereby eliminating any load-carrying speed limitations. This device was incorporated into the 347 simulation, and the evaluations revealed that speeds up to 180 knots could be reached. The maximum lateral cable guide displacements called for were slightly greater than  $\pm 2$  feet for the transient following turn-on with large load motions, and less than  $\pm 1$  foot for normal maneuvering when the system was already turned on prior to acceleration to high speed.



The advantage of such a system is its ability to suppress the limit cycle for all conditions of load angle of attack and sideslip, thereby eliminating the sensitivity of the problem to maneuvering. A disadvantage is, of course, the added mechanisms required to sense the load motions and actuate the cable guides.

#### MODIFYING THE HELICOPTER STABILITY AUGMENTATION SYSTEM

Modifying the stability augmentation system (SAS) of the helicopter is an attractive way of stabilizing external loads. The 347 helicopter system was modified to include lateral SAS inputs from lateral cable sway rate and directional SAS inputs from load relative yaw rate. No shaping of these signals was incorporated, and the normal 347 low-authority SAS limits were retained. The gains were optimized based on improving the load yaw and sway damping ratios. Improvements were possible up to a point, and then high-frequency instabilities associated with reaching SAS limits were observed. The gains were reduced until a nominal damping ratio of 0.3 - 0.4 was obtained. This configuration was then evaluated and found to offer only slight increases in allowable carrying speed.

Closer examination of the records and pilot comment revealed that the helicopter's ride qualities were being compromised by the load motion inputs into the SAS. Specifically, the load yaw rates were commanding the helicopter to "follow" the load in an attempt to reduce the differential yaw motion. Since the pilot's station is about 23 feet forward of the helicopter center of gravity, this SAS activity showed up as a side force oscillation at the load yaw frequency (bifilar frequency). These side forces became uncomfortable with increasing speed and caused the pilot to downrate his judgement of allowable carrying speed. The lateral SAS input from load sway rate did not improve the situation. Other combinations of feedbacks incorporating combinations of load position and rate were attempted without noticeable improvements.

In a sense, attempting to use the relatively low bandwidth helicopter to suppress the relatively high bandwidth load yaw limit cycle motions does not appear to offer significant improvements in allowable carrying speed. This can be related to the cable guide concept, where now the inertial cable guide movements must be produced by moving the whole helicopter. These movements were found to be about  $\pm 1$  foot, which translate to  $\pm 5$  degrees of helicopter yaw angle for a cable separation of 24 feet.

#### ACTIVE STABILITY AUGMENTATION USING AUXILIARY AIRFOILS

The use of an active stability augmentation system employing aerodynamic surfaces driven by rate gyros is another interesting, but less practical, way of extending allowable carrying speed. This kind of device generally employs a servo-driven airfoil surface placed behind the load that introduces yawing moments proportional to yaw rate. Because the airfoil must operate in the wake of the load, predicting its moment characteristics



should be difficult. If a pure damping moment could be produced, the device has the effect of augmenting  $C_{N_r}$ , which directly reduces the limit

cycle amplitude. The amplitude is proportional to the reciprocal of the square root of  $C_{N_r}$ . For the device to be effective,  $C_{N_r}$  must be at least

doubled from its present value of -0.94. This is a decrement of about -1. A simple surface that is located a container length aft of the center of mass may work; however, this is considered to be doubtful because of the highly separated and turbulent wake that the surface must operate in. This judgement is based on drag chute test results with the 0.1 scale container model in the wind tunnel (see Runs 20, 21, and 22 in Appendix C). If a drag device could not stabilize the load, a lifting device such as an air-foil certainly will not do much better.

#### SUMMARY

Six methods of extending allowable carrying speed were discussed, and some evaluation data for five of them were given. It is seen that optimizing the suspension system to increase the bifilar frequency, and optimizing angle of attack and use of maneuvering techniques can effectively suppress the problem. It is also seen that the addition of fins greatly suppresses the unsteady aerodynamics, which is the primary cause of the problem. The use of more exotic devices such as active cable actuators can also eliminate the problem. Direct feedback to the onboard SAS without an extensive optimization effort produced only minor improvements.

The allowable carrying speeds as determined from the 347 simulation of the empty 8-by-8-by-20-foot container on a two-point suspension are listed in Table 1. These data are the result of the evaluation of one highly skilled pilot experienced in sling load flight. It is realized that a greater sample of pilot opinion would enhance the results.

TABLE 1 SIMULATOR RESULTS OF ALLOWABLE CARRYING SPEED							
Simulator Results of Allowable Carrying Speed for the 8-by-8-by-20-foot Container on a Two-Point Suspension with Spreader Carried by the Model 347 Helicopter; Total Weight 45,000 lb							
8-foot slings, container rigged level (NT = Not Tested)							
Cable and SAS Parameters	Cable Separation (ft)	Cable Length (ft)	Bare Container (kt)	With SAS Feedback (kt)	With Fins (kt)	With Cable Guide Stabilizer (kt)	
Configuration							
Container Weight, 8705 lb	24	7.5	90*	100	120	180	
	30	7.5	100*	100	NT	170	
Helicopter Weight, 36,000 lb	20	7.5	105* 150*	NT	NT	165	
	15	7.5	130*	160**	NT	160	
	24	50	85*	100	NT	150	
	20	50	70*	NT	NT	150	
	15	50	100*	90	NT	120	
Container Weight 15,000 lb	20	7.5	150*	NT	NT	160	
Helicopter Weight 30,000 lb							
* steady state							
**by accelerating, peak load yaw amplitude occurred at 110 kt.							

## CONCLUSIONS AND RECOMMENDATIONS

### CONCLUSIONS

Based on the results of this study, it is concluded that:

1. The important dynamics of the 8-by-8-by-20-foot container carried externally can be described by a nonlinear model.
2. The dynamics of this container are dominated by unsteady aerodynamic effects and require dynamic testing in order to describe them.
3. This dynamic model when incorporated into a sophisticated helicopter simulation can reveal data regarding allowable carrying speeds.
4. The empty 8-by-8-by-20-foot container may be carried to speeds approaching 180 knots, using various stabilization techniques ranging from:
  - suspension optimization
  - helicopter maneuvering
  - active cable actuators
  - container shape modification
5. The most effective method of stabilization found from the standpoint of overall elimination of any unwanted load motions was that of using an active cable actuator system.

### RECOMMENDATIONS:

1. Conduct research to determine ways of adapting the 8-by-8-by-20-foot container model to closed-loop analysis with any helicopter.
2. Develop a prototype cable actuator stabilization system.
3. Conduct flight and simulator research to determine optimum maneuvering that allows this container to be carried to high speeds.
4. Conduct dynamic wind tunnel tests on a variety of helicopter loads before proceeding with an analysis of their motions.

### LITERATURE CITED

1. Lin, David T., IN-FLIGHT STABILIZATION OF EXTERNALLY SLUNG HELICOPTER LOADS, Northrop Corporation; USAAMRDL Technical Report 73-5, Eustis Directorate, U.S. Army Air Mobility Research and Development Laboratory, Fort Eustis, Virginia, May 1973.
2. Midgett, J., and Hutto, A.J., FLIGHT TEST EVALUATION OF A TWO-POINT EXTERNAL LOAD SUSPENSION SYSTEM CONCEPT ON A CH-47 HELICOPTER, Boeing Vertol No. 114-FT-031-1, January 1970.
3. Hoerner, S.F., FLUID DYNAMIC DRAG, Published by the Author, 1958.
4. Cogan, C., Gajkowski, B.J., Garnett, T.S., FULL FLIGHT ENVELOPE MATH MODEL FOR 347/HLH CONTROL SYSTEM ANALYSIS - CONTROL DOCUMENT, Boeing Co., Philadelphia, Penn., Number D301-10148-1, July 1972.
5. Sinacori, J.B., A PRACTICAL APPROACH TO MOTION SIMULATION, AIAA Paper No. 73-931, September 1973.

## APPENDIX A

### PILOT INTERVIEW DATA

#### INTRODUCTION

In January 1972 the Northrop Corporation, Electronics Division completed a study, "In-Flight Stabilization of Externally Slung Helicopter Loads," Contract DAAJ02-70-C-0067, for the Eustis Directorate, U.S. Army Air Mobility Research and Development Laboratory, Fort Eustis, Virginia. The purpose of this study was to select the best technical approaches for stabilizing externally slung helicopter loads at forward speeds up to 150 knots equivalent airspeed (KEAS).

Conclusions reached during the above described study have been presented in Reference 1.

A decision was made to obtain additional real-world sling load data (by interviewing a cross section of Army aviators) and to correlate the collected data with the study conclusions. This, then, is the purpose of this appendix. The effort was accomplished in three phases, which are discussed herein.

## REFERENCE DOCUMENTS

### Studies

1. In-flight Stabilization of Externally Slung Helicopter Loads, Contract DAAJ02-70-C-0067 (Reference 1)
2. Unpublished Boeing-Vertol test data.

### Manuals

1. Special Text 57-210-1, Tactical Air Movement Guide, U.S. Army Aviation School, dated April 1968.
2. Handbook on CH-47 Employment and Utilization in Vietnam, Hq USARV, dated October 1968.

### SOP's

1. 1st Air Cavalry Division Sling Load Standing Operating Procedures, dated February 1966 and June 1969.
2. U.S. Army Field Force I Sling Load SOP, dated July 1968.

### After Action Report

Evaluation of Off-Shore Discharge of Containerships, Hq U.S. Army Transportation Center and Fort Eustis, Fort Eustis, Virginia, dated 5-9 December 1970.

## PHASE I (QUESTIONNAIRE PREPARATION)

Phase I Activity was accomplished during the period of 11-22 September 1972.

### Preparation of Questionnaire

The main task completed during Phase I was preparation of a questionnaire on helicopter externally slung loads. Tailoring the questionnaire was facilitated by research of several Army cargo helicopter unit Standing Operating Procedures (SOP) manuals on sling loads, as augmented by Army helicopter combat operations expertise of Northrop personnel.

The questionnaire was structured to maximize the injection of individual aviator flying experience with sling loads into the answers. Questions 1 and 2 relate to flying time, civilian and military education, and aircraft and instrument qualification. These data permitted the construction of a model of a type Army cargo helicopter aviator.

Question 3 was selected with the objective of reducing the scope of externally slung load operations to a manageable level within the study time/manpower constraints. Army helicopters lift a myriad variety of sling loads. These loads vary from live water buffaloes to CONEX containers, and are lifted under an equally myriad quantity of density altitude conditions. Analysis of these variables in conjunction with Army aviation unit Standing Operating Procedures (SOP) permitted the selection of four broad categories of sling loads: vehicles, artillery (including ammo), POL, and containers. Further analysis permitted allocation of specific items of Army equipment to the four broad categories.

Subelements of Question 3 provide data on slings/nets, stabilization devices, cable and sling lengths, load shape stability, and aviator flying techniques when lifting external loads.

Question 4 of the questionnaire solicits information on maximum sling load weighting and "vertical bounce."

The last question provides information on multi-point suspension of external loads.

#### PHASE II (AVIATOR INTERVIEWS)

Phase II was accomplished during the period 24-29 September 1972.

Coordination with aviation elements of the U. S. Army Continental Army Command (USCONARC) revealed that the majority of Army cargo helicopter experienced aviators were located at Fort Rucker, Alabama, and Fort Eustis, Virginia. Accordingly, liaison was established with both sides and command concurrence was obtained for aviator interviews.

Personnel interviewed at Fort Rucker were assigned to the cargo helicopter training division at Hanchey, AAF. Aviators at Fort Eustis were assigned to the CH-54 "Crane" Company. Forty Army aviators participated in the exercise.

#### PHASE III (STUDY FINDINGS)

Phase III was accomplished during the period 2-27 October 1972.

### Data Reduction and Analysis

The Army aviator data were reduced and analyzed by personnel of Maintainability and System Support, Aircraft Division, Northrop Corporation. Subsequent to reduction, the data were correlated with other Army aviation studies in the Northrop data bank.

### Aviator Data

A recapitulation of the aviators interviewed by grade is outlined below.

<u>Grade</u>	<u>Number</u>
Colonel	1
LTC	2
Major	2
Captain	4
LT	1
CWO	<u>30</u>
Total	40

### Army Aviator Profile

The first usage of the interview data was to model a type Army cargo helicopter aviator. Figures A-1 and A-2 provide a summary of rotary-wing flying time and years of rated service. The significant points derived from these charts are that Army aviation personnel are younger but, at the same time, are very experienced aviators. These factors indicate that the Department of the Army program to achieve a young Army is working and, spurred by the recent heavy flying hour program in Southeast Asia, the young aviators rapidly accumulate hundreds of flying hours. Figure A-3 reinforces these conclusions, since 95% of the aviators interviewed have completed one to three tours in Southeast Asia. It is also clear that attrition has depleted individuals with Korean and World War II experience.

Figures A-4 and A-5 present statistics on military and civilian education. The aviators are doing well in selection for service schools vis-a-vis their nonrated contemporary, and are ahead of the national average in the civilian field.

Figure A-6 outlines the status of aviator instrument qualification. This chart reflects the decreasing involvement of the Army with fixed-wing aircraft pursuant to the 1966 Memorandum of Understanding with the U.S. Air Force, whereby the Army will concentrate Role and Mission effort primarily on rotary-wing aircraft.



### Sling Load Experience

Individual aviators evaluated their total sling load experience and assigned a percentage number to each of the broad, sling load categories -- vehicles, artillery (including ammo), POL and containers. This assigned number represents the percentage of overall sling load experience spent lifting that category of sling load (e.g., vehicle, 40%; artillery, 30%; POL, 20%; and containers, 10%). Figure A-7 presents a composite of the aviator responses. Detailed information on specific items of Army equipment within the framework of the broad categories is furnished in subsequent sections.

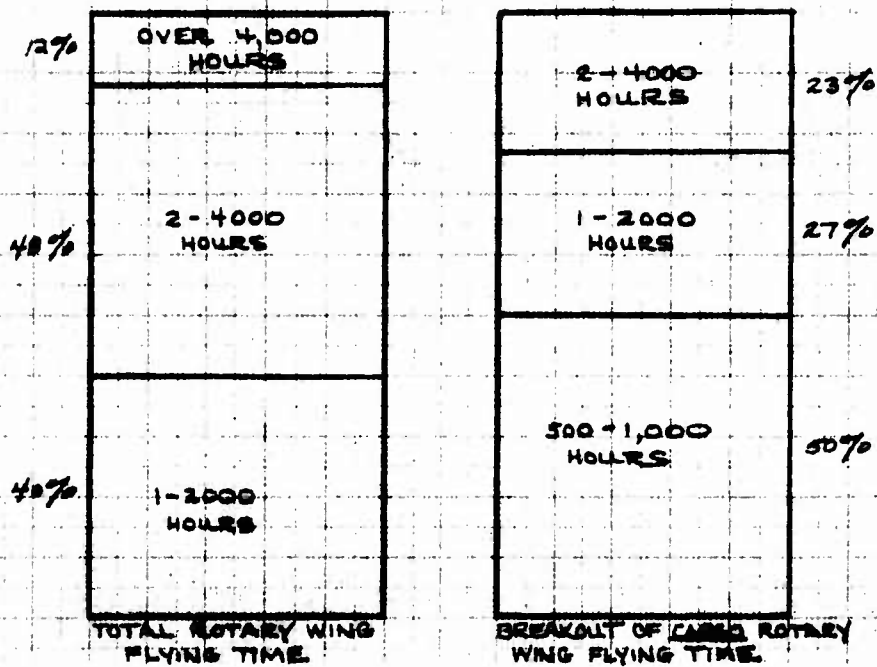


Figure A-1. Summary of Army Aviator Rotary-Wing Flying Time.  
(Sample Size 40 Aviators)

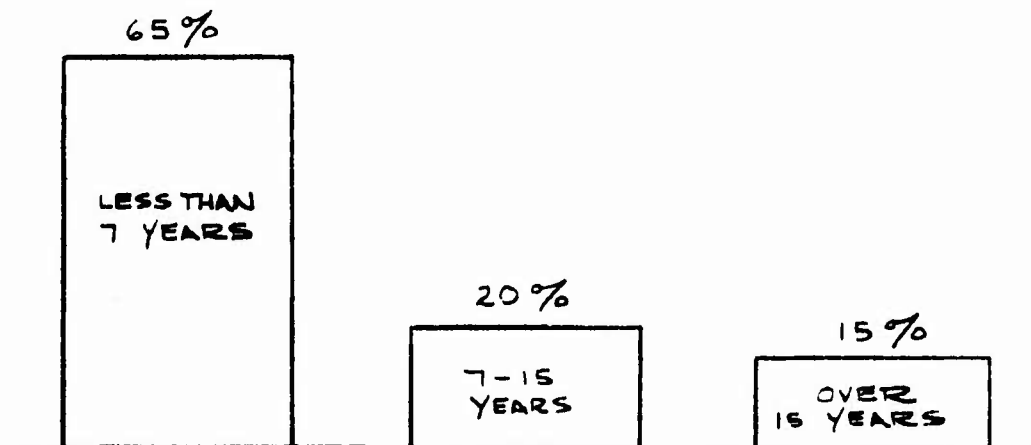


Figure A-2. Years of Rated Service.

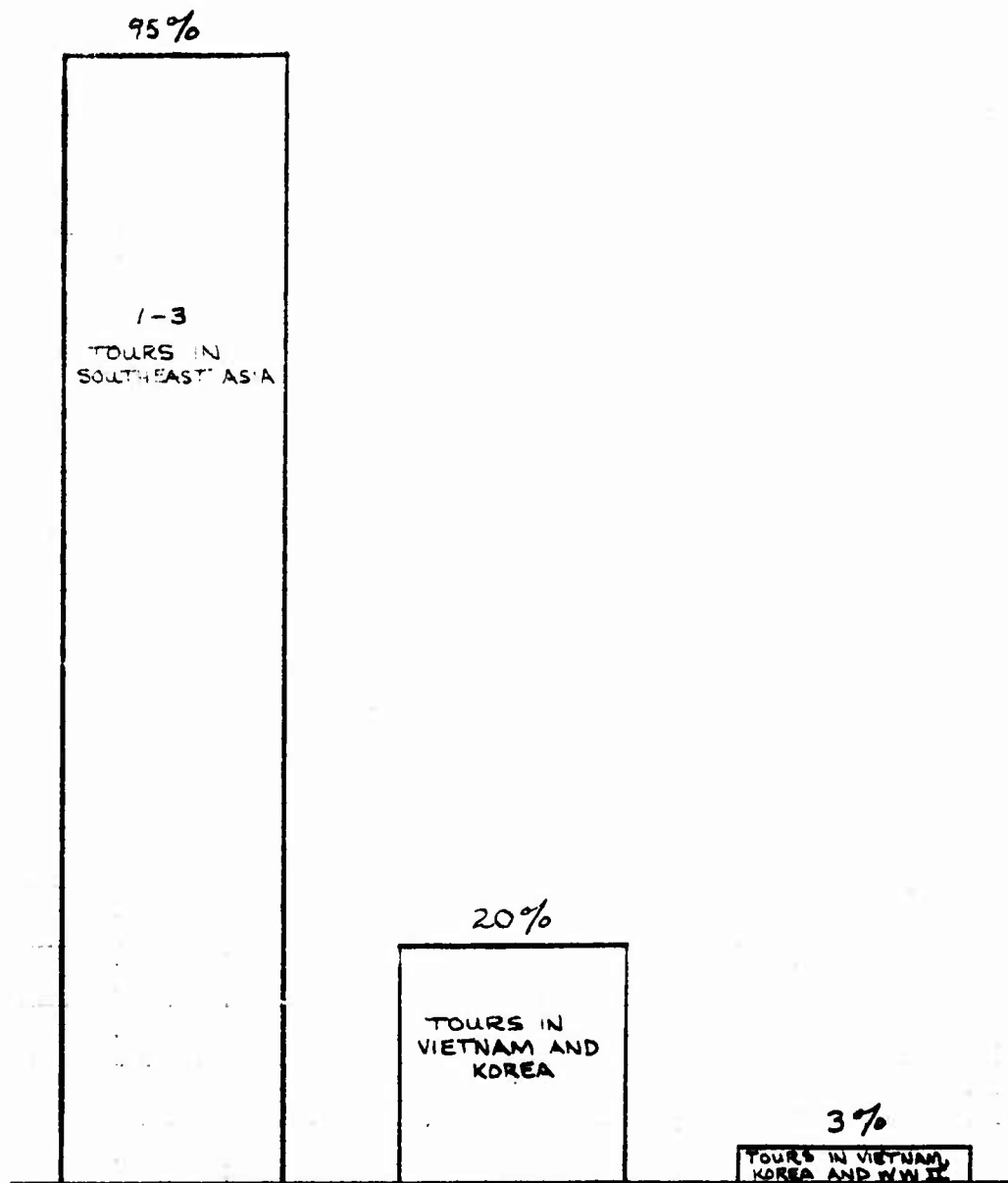


Figure A-3. Combat Experience as Army Aviator.

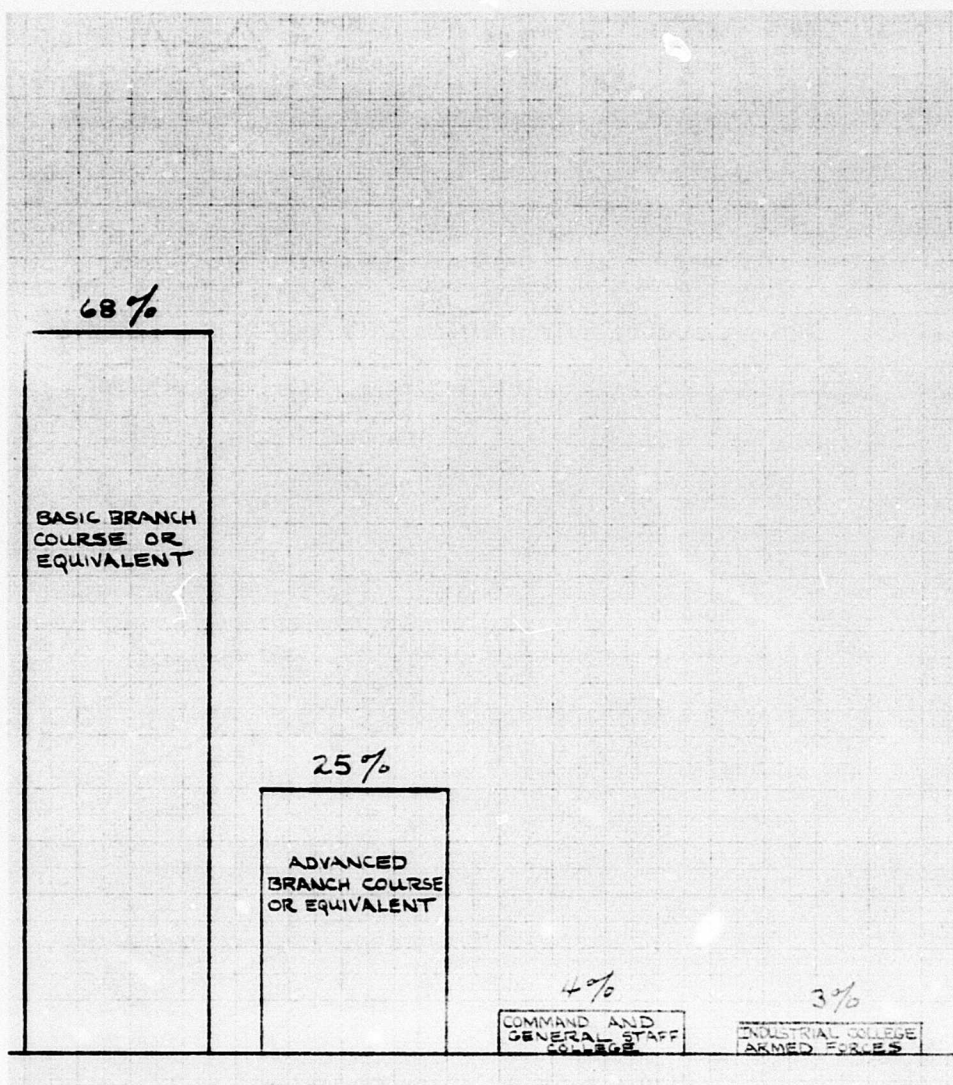


Figure A-4. Combat Experience as Army Aviator.

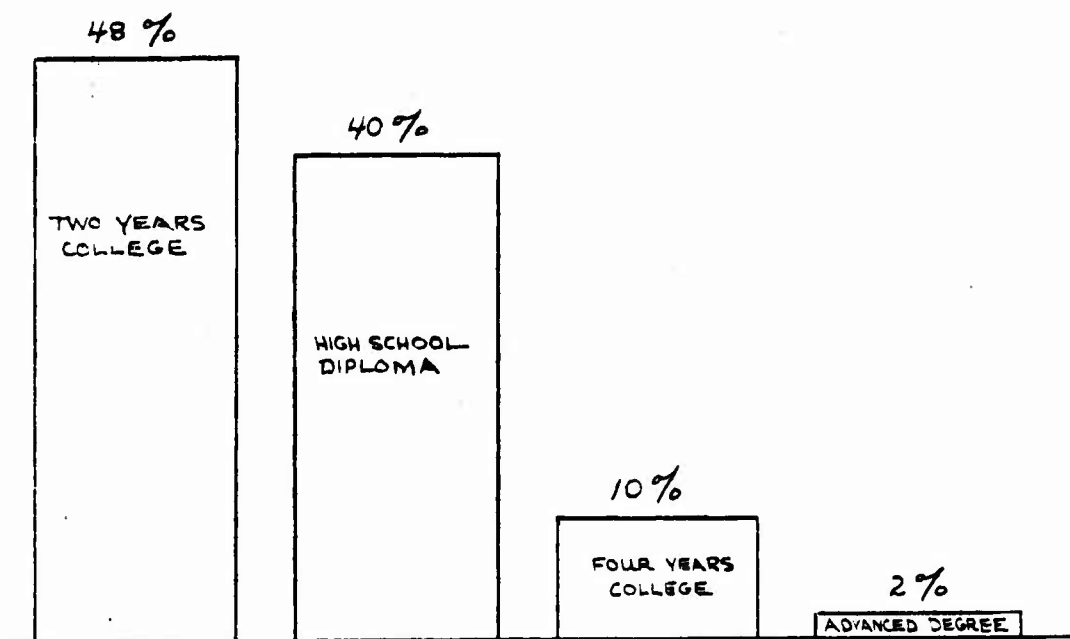


Figure A-5. Military Education.

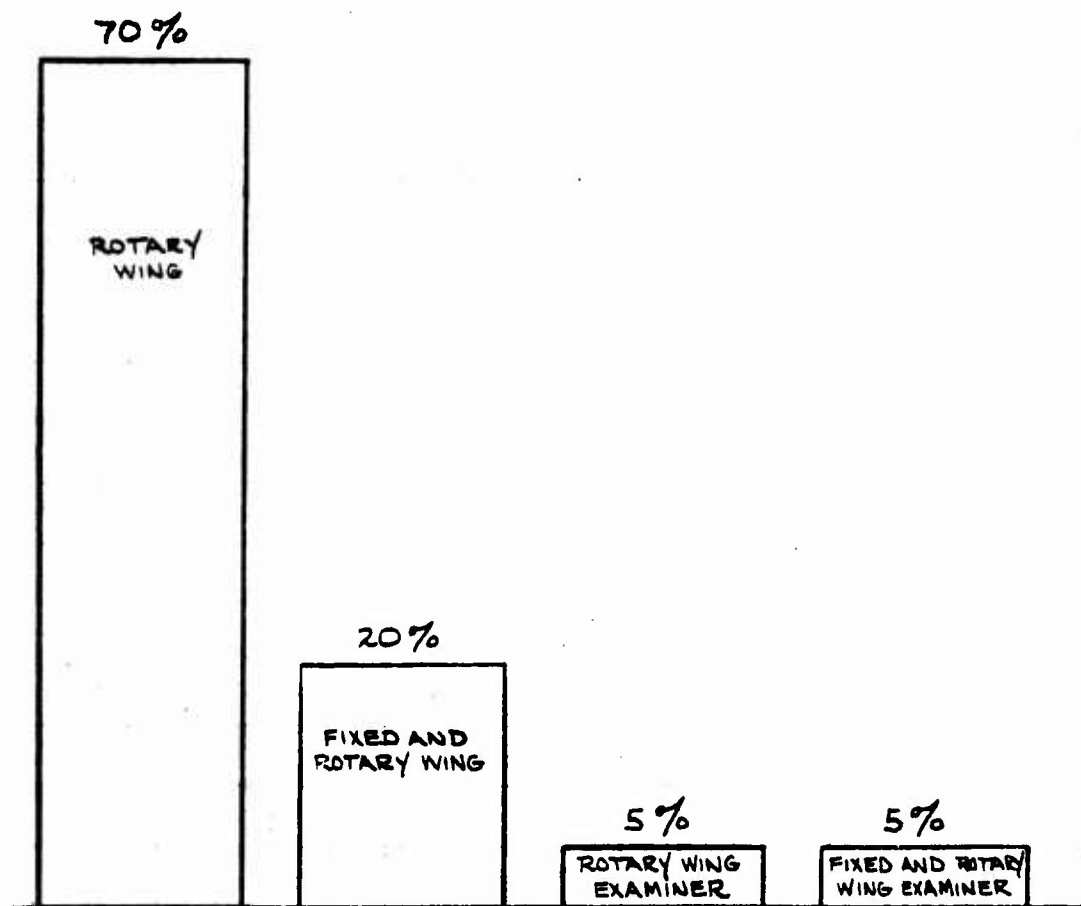


Figure A-6. Instrument Qualification.

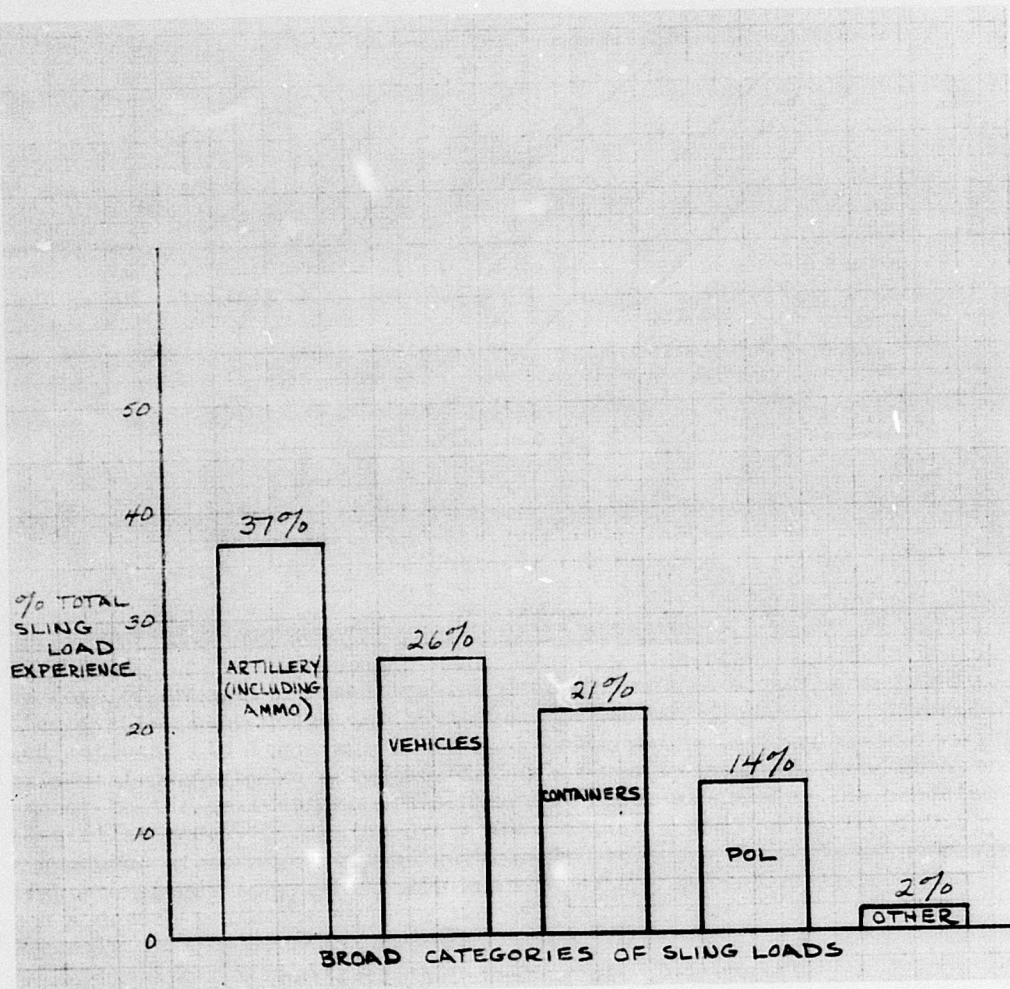


Figure A-7. Composite of Army Sling Load Experience.

### Load Category

The next step following selection of the four broad sling load categories previously described was to assign items of Army equipment that are continually lifted as sling loads to each of the broad categories. Shopping lists of loads were included in the aviator questionnaire. These lists were refined by the interviewees.

### Typical Vehicular Sling Loads

Tables A-1 and A-2 present the vehicular loads, in descending order, that were most frequently carried as sling loads by CH-47 and CH-54 helicopters.

TABLE A-1. CH-47 VEHICULAR SLING LOADS	
Item	Quantity and Weight
1-1/2-ton water trailer	1 @ 6300 lb
Downed aircraft	1 @ 2-8000 lb
3/4-ton truck (5700 lb w/o winch)	1 @ 5700 lb w/o winch
1/4-ton truck (2350 lb)	1 @ 2350 lb
Mule 1/2-ton, M274 (900 lb)	2 @ 900 lb
1-1/2-ton trailer (2750 empty)	1 @ 5750 lb
Sectionalized bulldozer	Assembled weight, 16000 lb
Other	Variable

TABLE A-2. CH-54 VEHICULAR SLING LOADS	
Item	Quantity and Weight
Downed aircraft	1 @ 4-15000 lb
2-1/2-ton truck cargo	1 @ 12365 lb
1-1/2-ton water trailer	2 @ 6300 lb each
M113 armored personnel carrier	1 @ 19300 lb
Sectionalized bulldozer	1 @ 16000 lb
3/4-ton truck	1 @ 5700 lb w/o winch
Rough terrain forklift	2 @ 5600 lb each
Other	Variable

### Typical Artillery Sling Loads

Tables A-3 and A-4 present the artillery loads (including ammo), in descending order of lift, that were most frequently carried by CH-47 and CH-54 helicopters.



TABLE A-3. CH-47 ARTILLERY SLING LOADS	
Item	Quantity and Weight
M-102 Howitzer	1 @ 3100 lb plus 1450 lb ammo
M-101 Howitzer w/shields	1 @ 4990 lb plus 1450 lb ammo
M-101 Howitzer w/o shields	1 @ 4600 lb plus 1450 lb ammo
Ammunition	Variable to 8000 lb

TABLE A-4. CH-54 ARTILLERY SLING LOADS	
Item	Quantity and Weight
155 MM Howitzer, M114A1	1 @ 12,950 lb plus 3000 lb ammo
M-102 Howitzer	1 @ 3100 lb plus 12900 lb ammo
M-101 Howitzer w/shields	1 @ 4990 lb plus 11000 lb ammo
M-101 Howitzer w/o shields	1 @ 4600 lb plus 11000 lb ammo

Typical Petroleum, Oil, Lubricants (POL) Loads

Tables A-5 and A-6 reflect the POL loads, in descending order of lift, that were most frequently lifted by CH-47 and CH-54 helicopters.

TABLE A-5. CH-47 POL SLING LOADS	
Item	Quantity and Weight
55-gal drums of gasoline	21 drums @ 373 lb ea
55-gal drums of JP/4	19 drums @ 410 lb ea
500 gal collapsible drums of gasoline	2 drums @3300 lb ea
500-gal collapsible drums of JP/4	2 drums @3550 lb ea

TABLE A-6. CH-54 POL SLING LOADS	
Item	Quantity and Weight
500-gal collapsible drums of gasoline	4 drums @3300 lb ea
500-gal collapsible drums of JP/4	4 drums @ 3550 lb ea
500-gal collapsible drums of diesel	4 drums @ 3800 lb ea

### Typical Container Loads

Tables A-7 and A-8 present the container loads, in descending order of lift, that were most frequently lifted by CH-47 and CH-54 helicopters.

TABLE A-7. CH-47 CONTAINER SLING LOADS	
Item	Quantity and Weight
CONEX	2 @ 3000 lb ea
Airmobile Maintenance Shop Sets	2-3 @ 2000 lb ea
MILVAN	5 @ 8000 lb ea

TABLE A-8. CH-54 CONTAINER SLING LOADS	
Item	Quantity and Weight
CONEX	3-4 @ 3000 lb ea
MILVAN	1 @ 8000-16,000 lb ea
Airmobile Maintenance Shop Sets	3-5 @ 2000 lb ea

### Operational Variables

Analysis of the aviator responses revealed a consensus that greater weights than those listed could have been safely lifted on a day-to-day basis. The constraining factor was unit SOP's which specified allowable cargo loads and airspeeds. Since SOP's are normally based on considerable operational experience, including the accident rate, the quantities and weights are considered realistic for combat operations, albeit they may be conservative in some cases.

### Airspeed and Altitude Considerations

In deference to time/manpower constraints, the next step subsequent to assignment of frequently carried sling loads to the four broad categories was to narrow the study scope by addressing airspeed/altitude ranges only for the load in each of the four broad categories that was most frequently lifted. Although limited data were secured on the older, piston-powered helicopters (CH-34, CH-21 and CH-37), the data displays to follow will consider only the CH-47 and CH-54. These aircraft constitute the backbone of the active Army cargo helicopter fleet.

### Vehicular Loads

The CH-47 vehicular load most frequently lifted was the 1-1/2-ton water trailer. Factors influencing this selection are that the CH-47's are organic to divisional sized Army units, thus normally committed in direct support of division combat activities. Additionally, the physical environment in Southeast Asia is tropical, thus creating a recurring heavy demand for potable water for the troops. Figures A-8 and A-9 present the airspeed and altitude ranges for the CH-47 while lifting 1-1/2-ton water trailers. The majority of flights were accomplished at 80 knots in the 2000-to 2500-foot altitude spectrum.

The CH-54 vehicular load most frequently lifted was downed aircraft. This selection reflects the greater payload of the CH-54 vis-a-vis the CH-47, and the fact that while CH-54 units may be attached to divisional sized units, they are normally available for general support of a wide tactical area of operations. Figures A-10 and A-11 portray airspeed and altitude ranges for the CH-54 while lifting downed aircraft. The majority of downed aircraft evacuations were conducted at airspeeds of 60 knots and below, at 1500 feet or less above the ground.

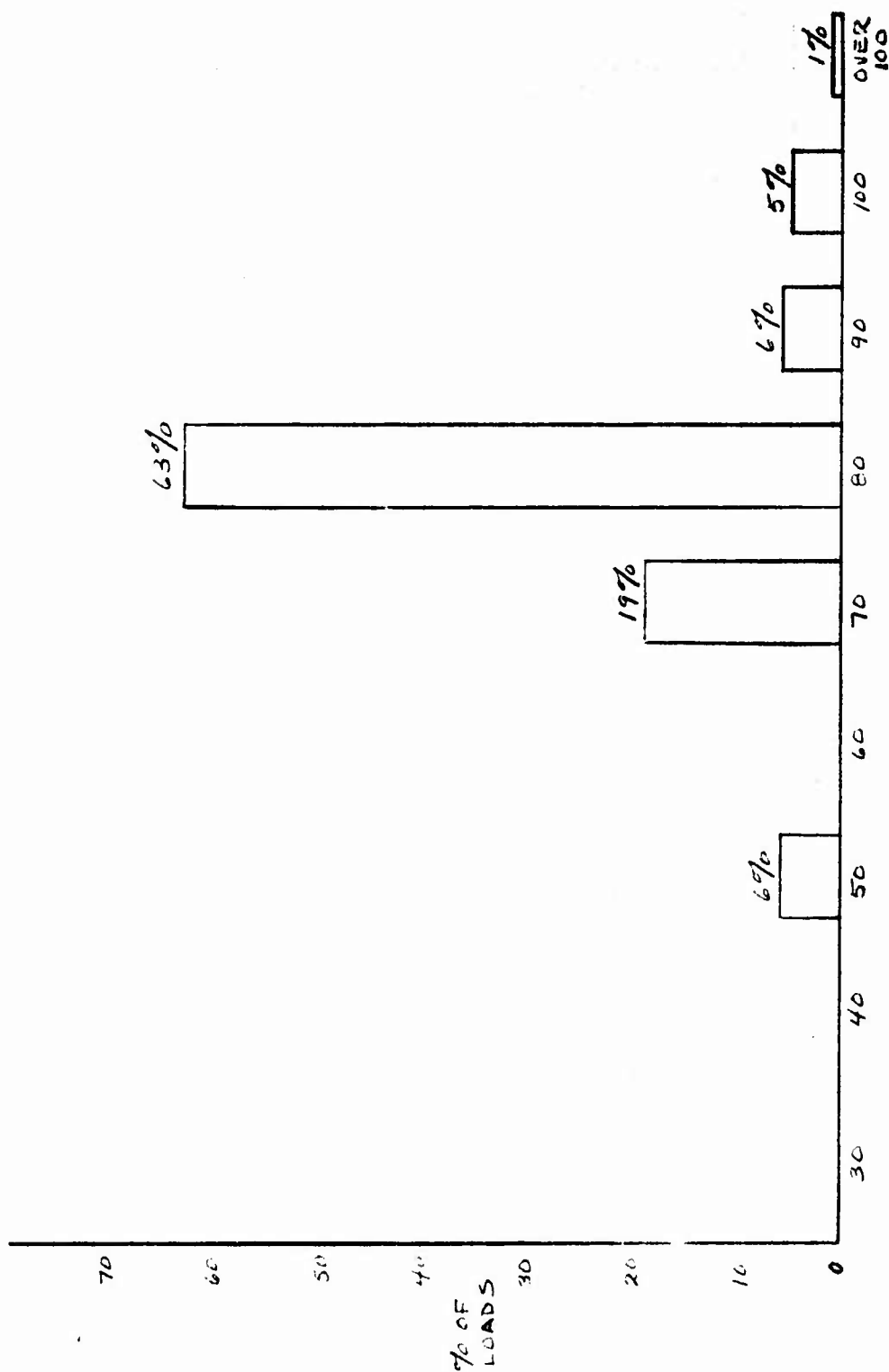


Figure A-8. Airspeed Range for Vehicular Load CH-47.  
(1-1/2-Ton Water Trailer)

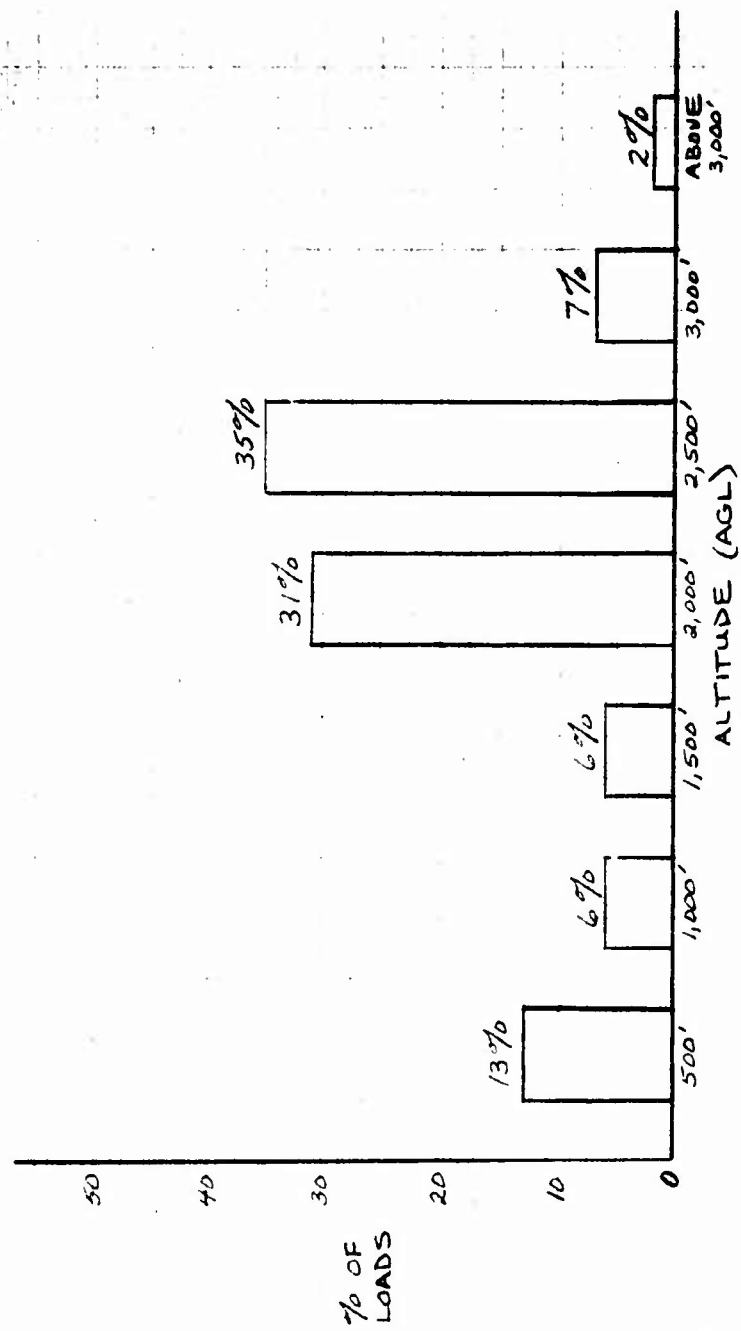


Figure A-9. Altitude Range for Vehicular Load CH-47.  
(1-1/2-Ton Water Trailer)

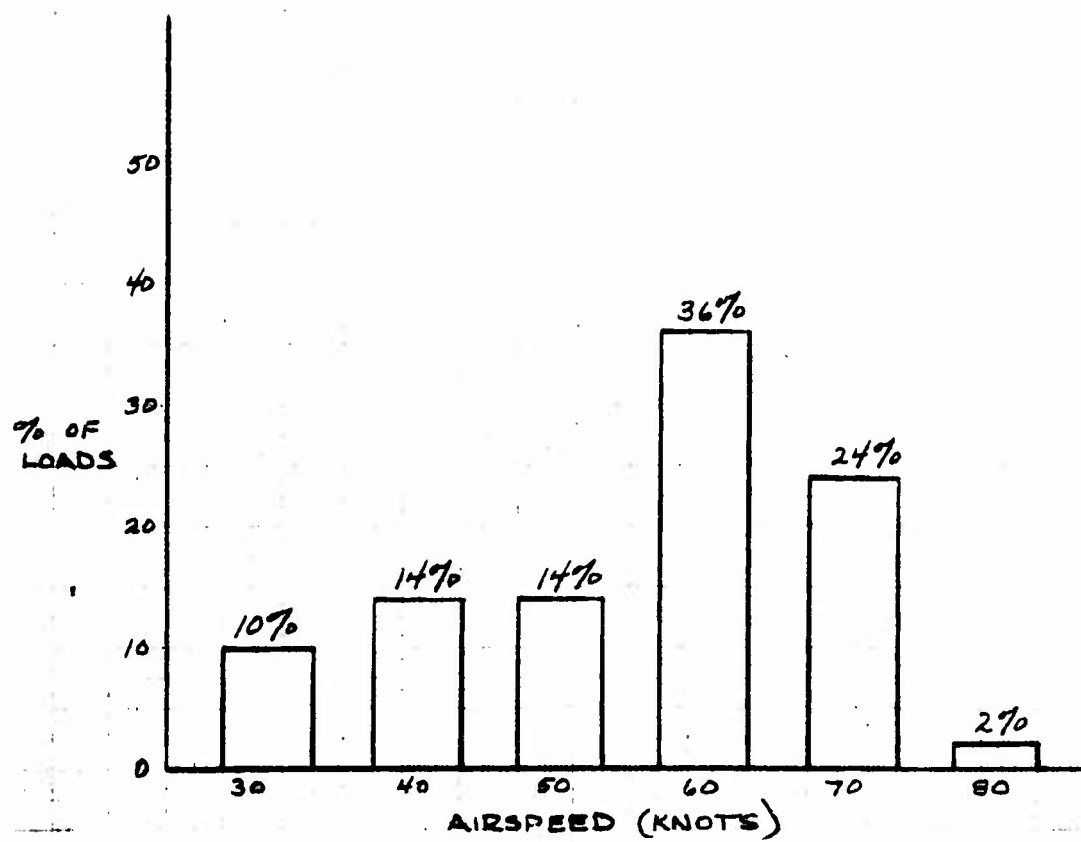


Figure A-10. Airspeed Range for Vehicular Load CH-47.  
(Downed Aircraft)

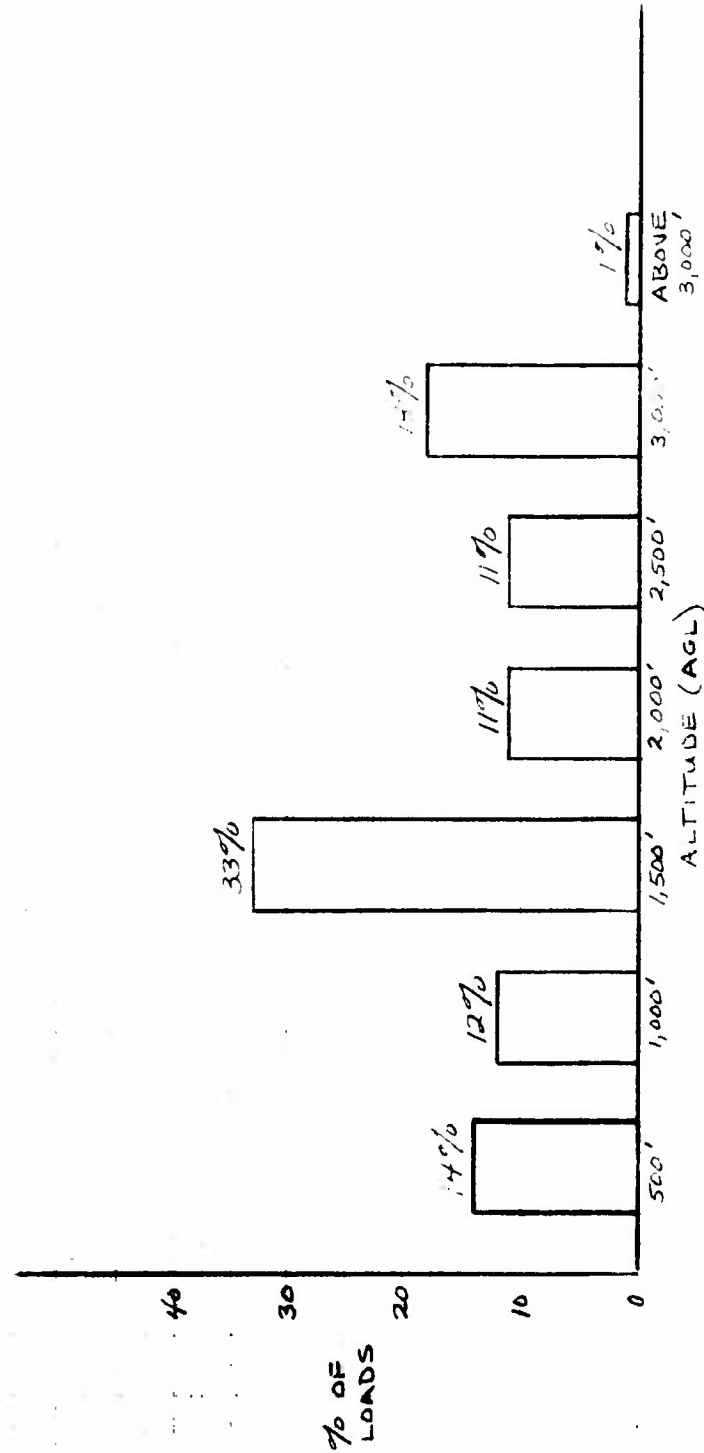


Figure A-11. Altitude Range for Vehicular Load (F-47. (Downed Aircraft))

### Artillery Loads

Artillery sling loads are mainly accompanied by a piggyback load of ammunition (see Figure A-12 for an artist's concept). The CH-47 load most frequently lifted was the M102 Howitzer. Figures A-13 and A-14 display airspeed and altitude ranges for this load. The bulk of the loads were flown at 80 knots or more, in the 2000- to 3000-foot altitude range.

The CH-54 artillery load most frequently lifted was the 155mm Howitzer. The preferred airspeeds were 60 to 70 knots with a somewhat unusual altitude range of 1500 and 3000 feet. Discussions with Army aviator personnel revealed that this altitude spread stemmed directly from enemy activity in a sector. Thus, 1500 feet was used in a cold sector and 3000 feet in a hot sector. The latter altitude was a compromise between being high enough to avoid small-arms fire and not so high as to present a favorable target for anti-aircraft weapons. Figures A-15 and A-16 provide additional information.

### POL Loads

Analysis of POL loads carried by the CH-47 and CH-54 revealed a dichotomy in the equipment used for containing POL products during transport. For example, the CH-47 load most often lifted was 55-gallon drums of gasoline, whereas the CH-54 load was 500-gallon collapsible drums of gasoline. The reasons for this split into the two modes are keyed to the difference in aircraft lift capability, but more importantly, the CH-47s are used for retail supply delivery of 55-gallon drums directly to Army units in the forward edge of the battle area. The CH-54 with its greater weight carrying capability normally delivers the 500-gallon collapsible drums of gasoline on a wholesale supply basis to supply points within the division rear. Figures A-17 and A-18 reflect that the airspeed/altitude ranges for POL loads were mainly in the 70- to 80-knot range at altitudes of 3000 to 4000 feet above the ground. Figures A-19 and A-20 reflect similar data on the CH-54. The bulk of CH-54 POL loads were flown at an airspeed of 70 knots at 1500 feet above the ground.

### Container Loads

The container load most frequently lifted was the CONEX for both the CH-47 and CH-54 helicopters. Figures A-21 and A-22 reflect that the majority of the CH-47 loads were flown at 40-50 knots airspeed at 2500 to 3000 feet above the ground.

Figures A-23 and A-24 present airspeed and altitude information on the CH-54. The majority of CONEX loads were flown at an airspeed of 40-50 knots. The altitude range split evenly at 1500 feet. Fifty percent were flown at or below 1500 feet and fifty percent above this to an upper limit of 3000 feet above the ground. The altitude spread is attributed again to enemy activity in the area of operations. The loads were flown at higher altitudes when the flying area became "hot".



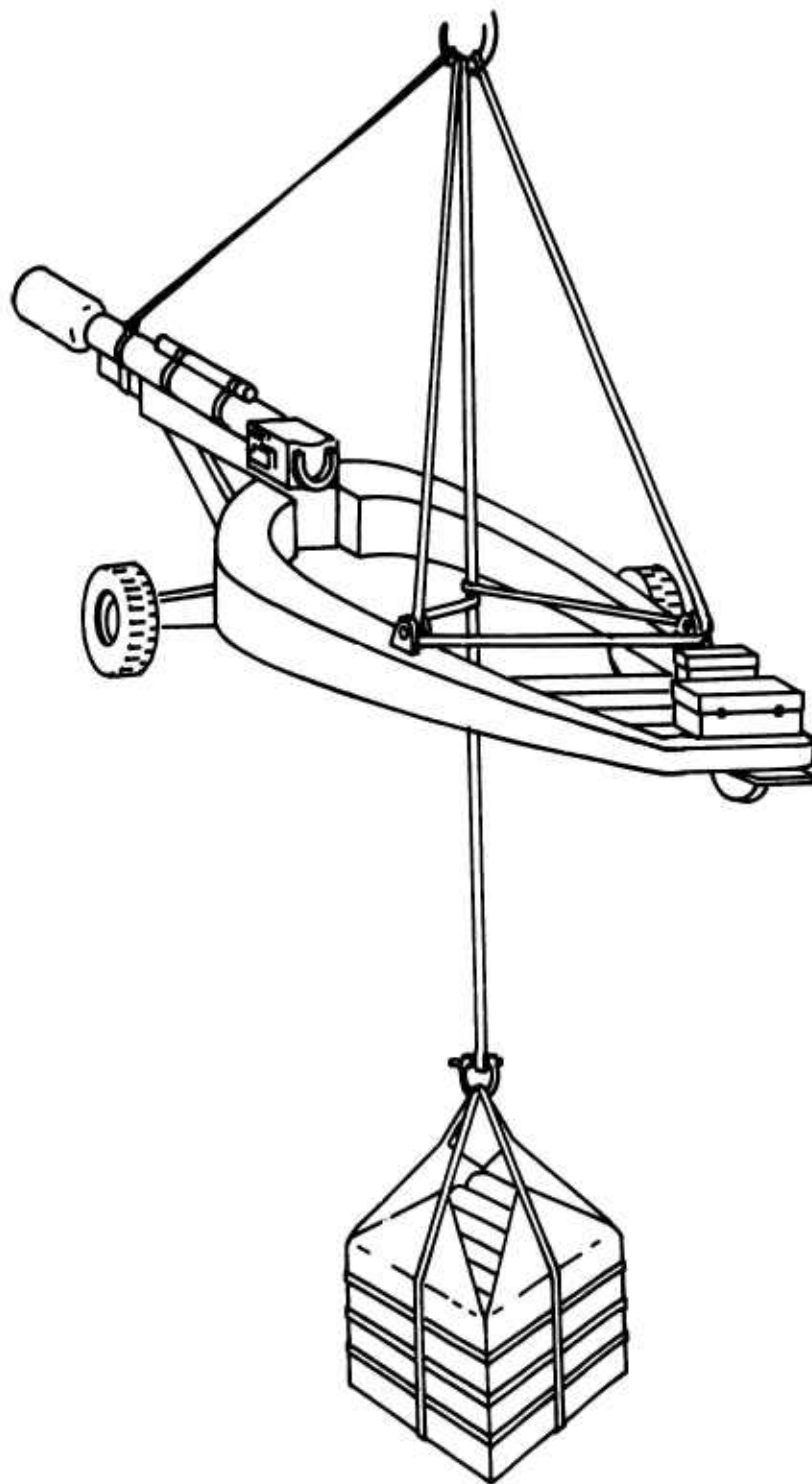


Figure A-12. M102 Howitzer With Piggyback.

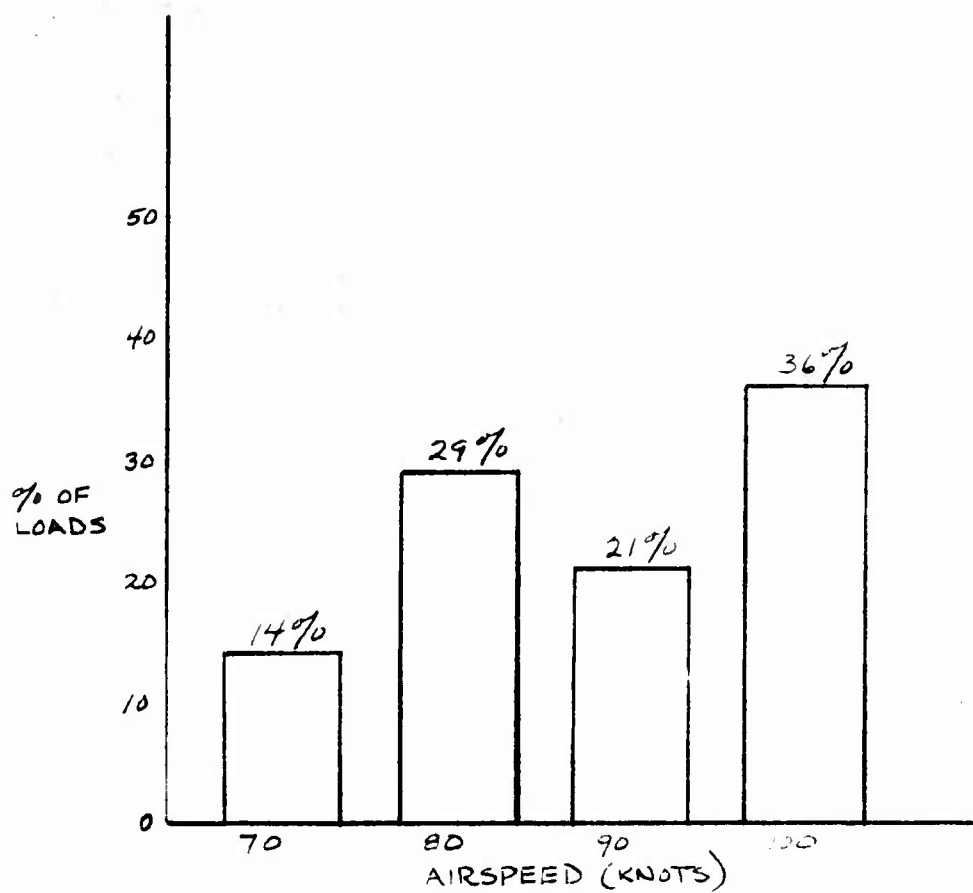


Figure A-13. Airspeed Range for Artillery Load CH-47.  
(Howitzer, 105 mm Towed, M102)

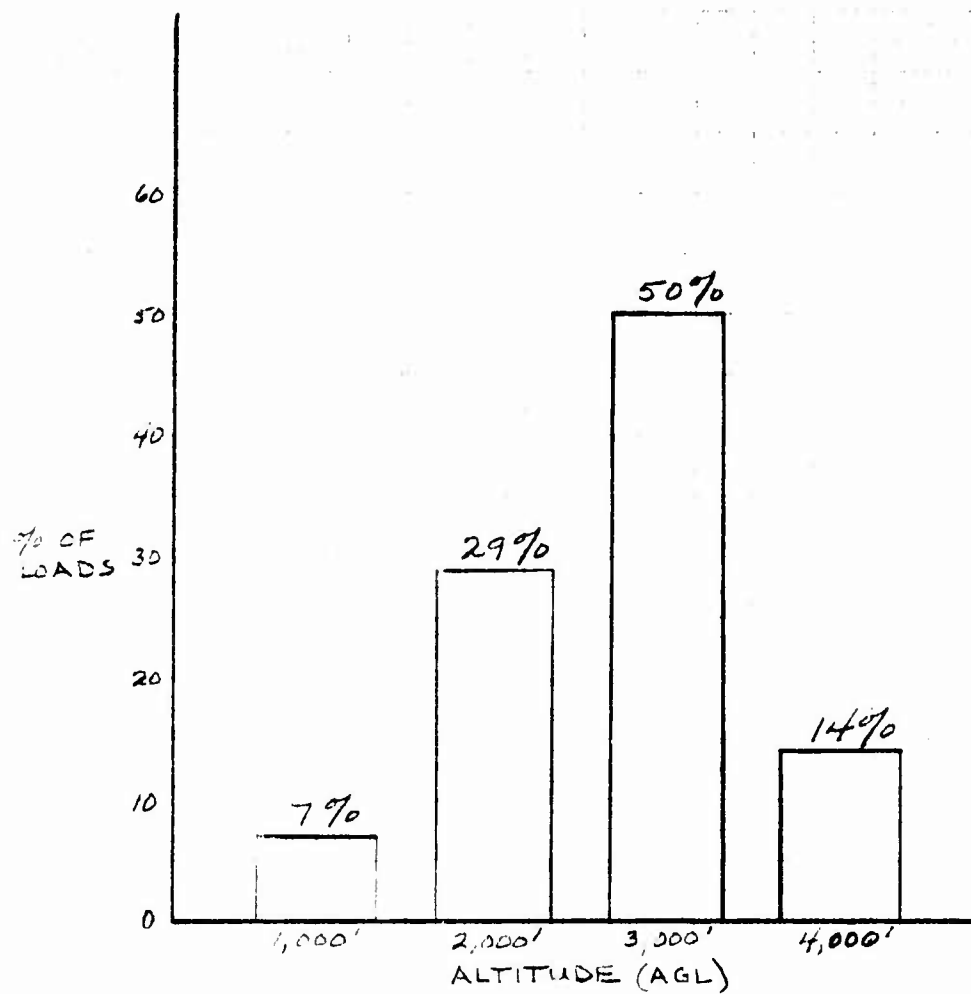


Figure A-14. Altitude Range for Artillery Load CH-47.  
(Howitzer, 105 mm Towed, M102)

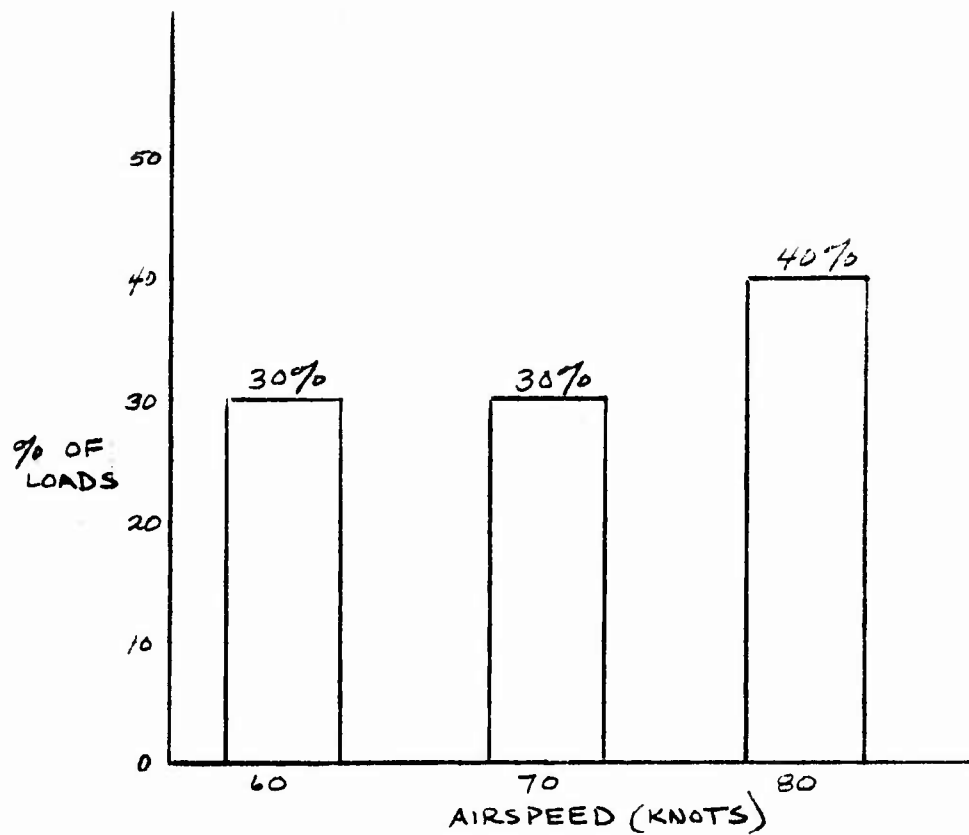


Figure A-15. Airspeed Range for Artillery Load CH-47.  
(155 Howitzer, Towed, M14A1)

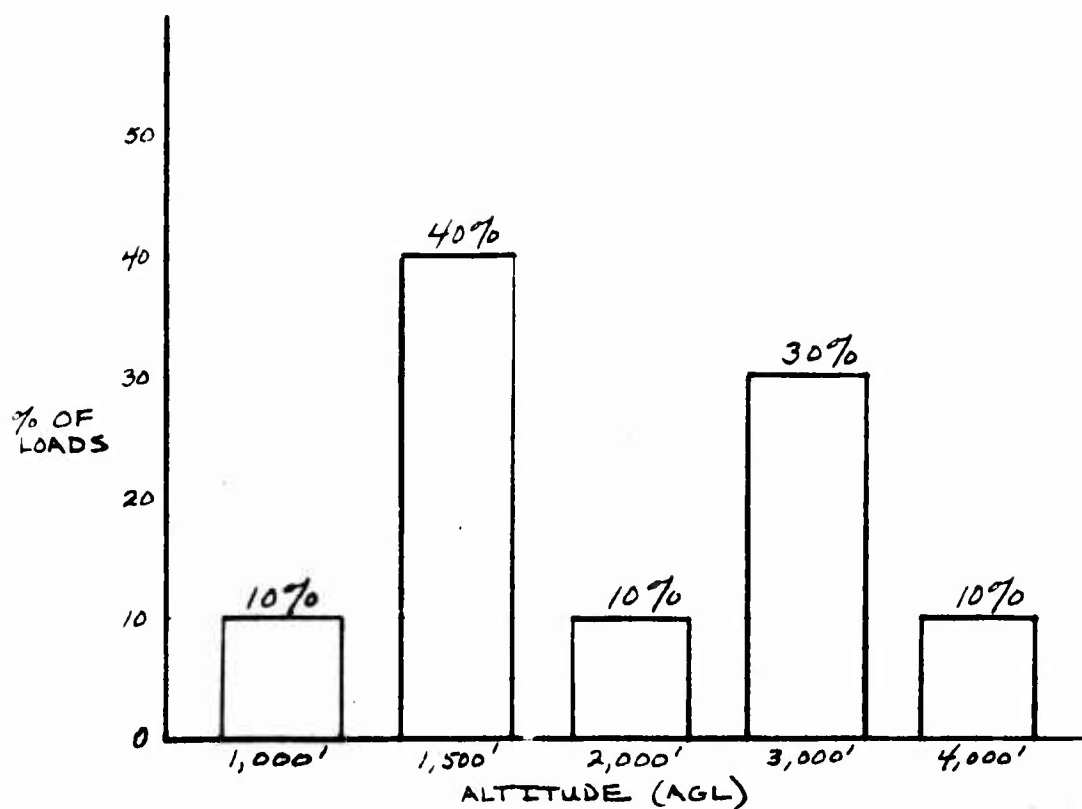


Figure A-16. Altitude Range for Artillery Load CH-47.  
(155 mm Howitzer)

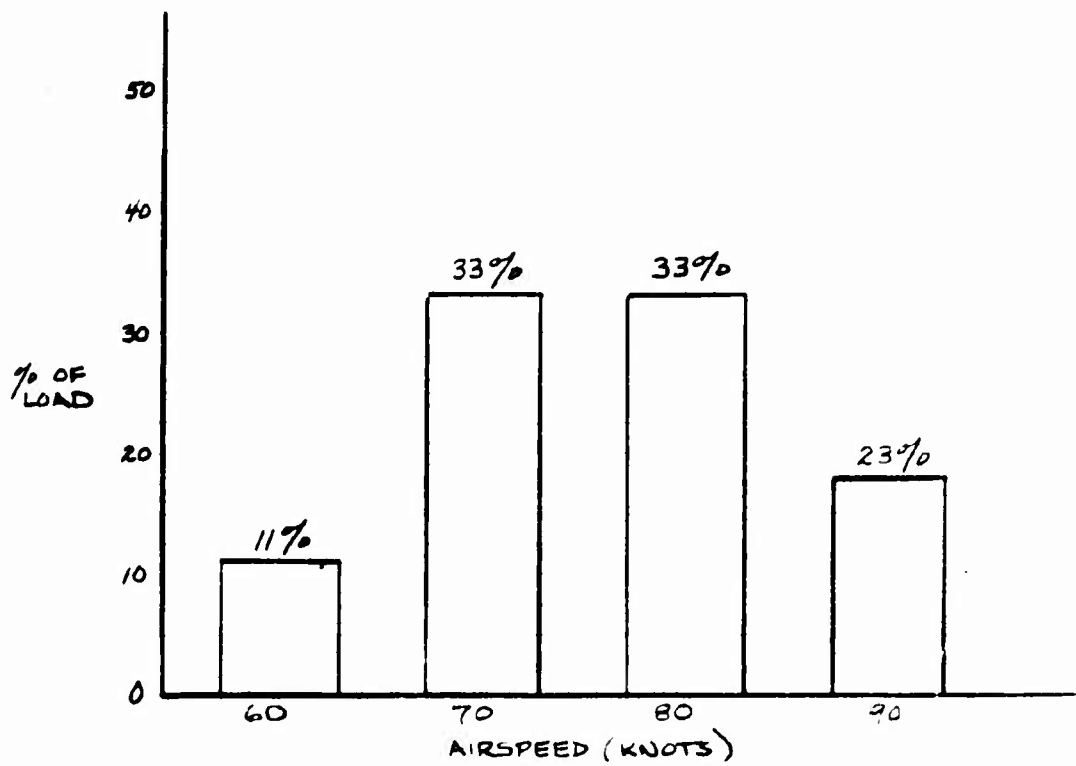


Figure A-17. Airspeed Range for POL Load CH-47.  
(55-Gallon Drums - Gasoline)

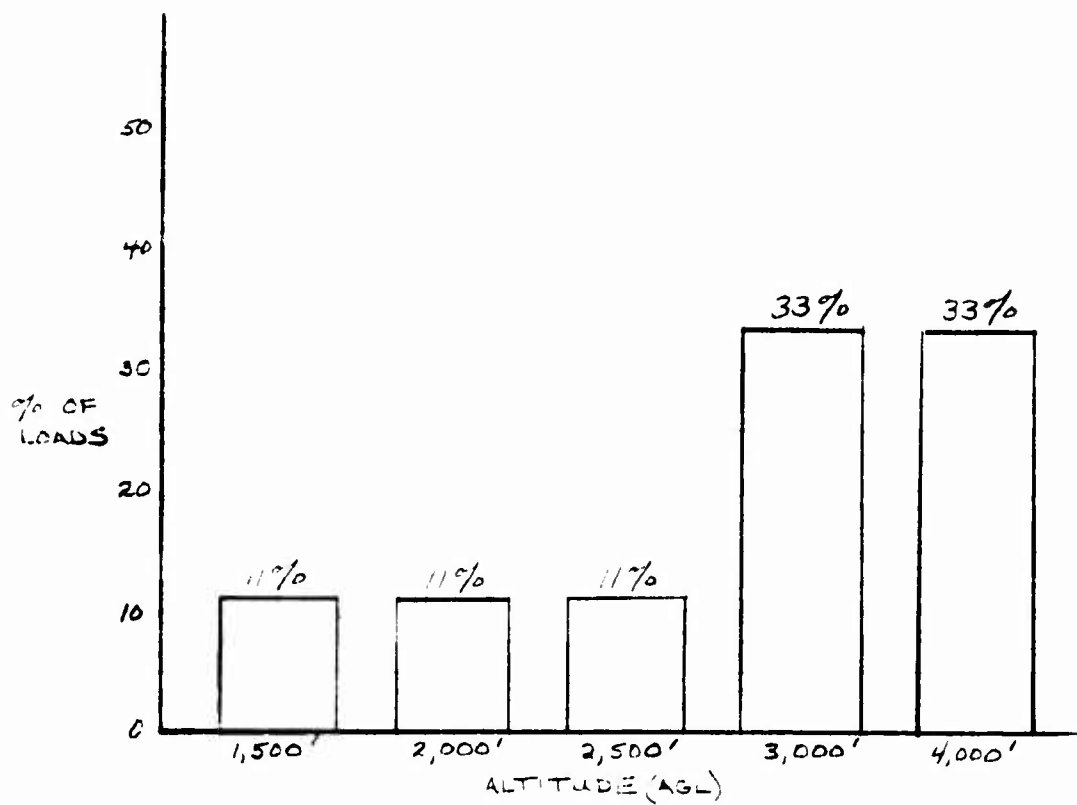


Figure A-18. Altitude Range for POL Load CH-47.  
(55-Gallon Drums - Gasoline)

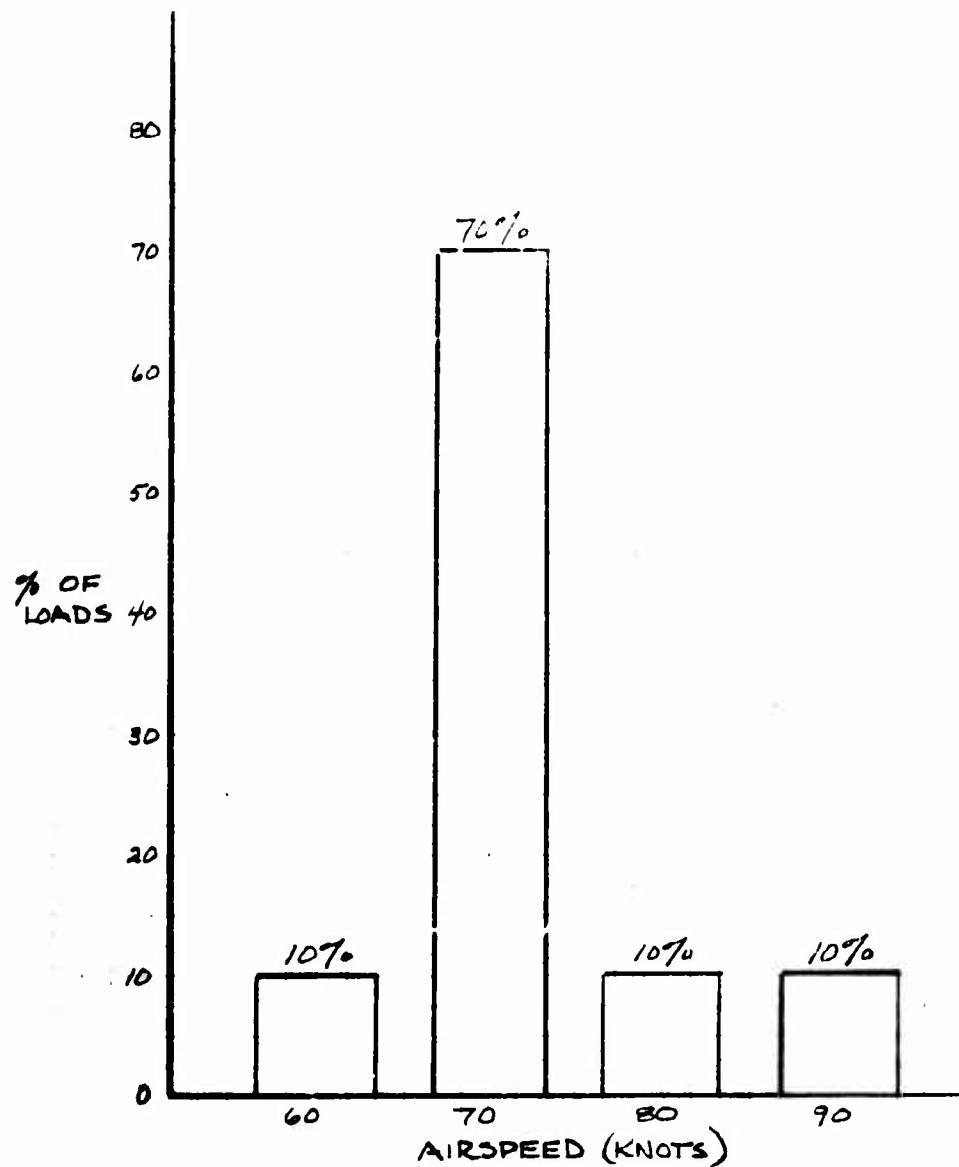


Figure A-19. Airspeed Range for POL Load CH-54.  
(500-Gallon Collapsible Bags - Gasoline)



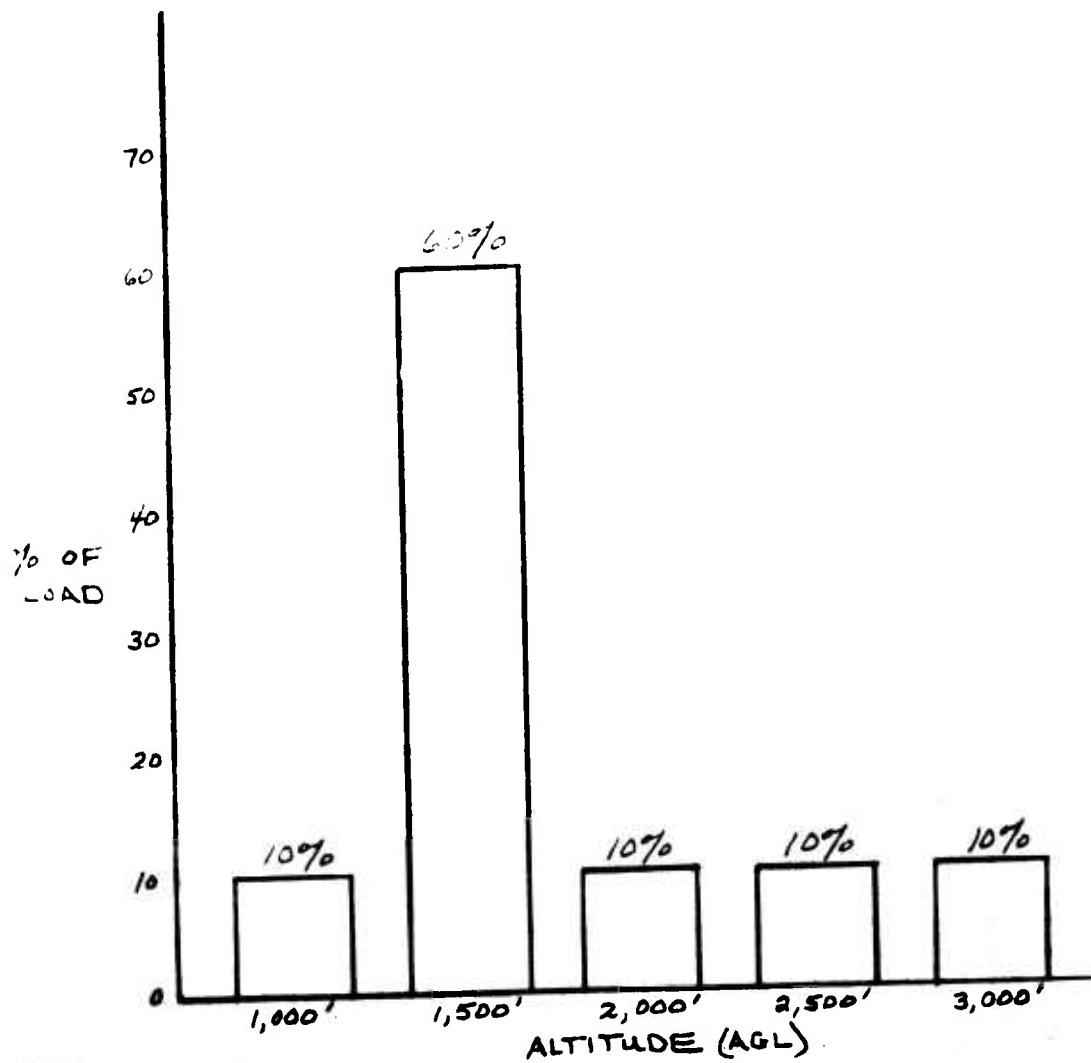


Figure A-20. Altitude Range for POL Load CH-54.  
(500-Gallon Collapsible Bags - Gasoline)

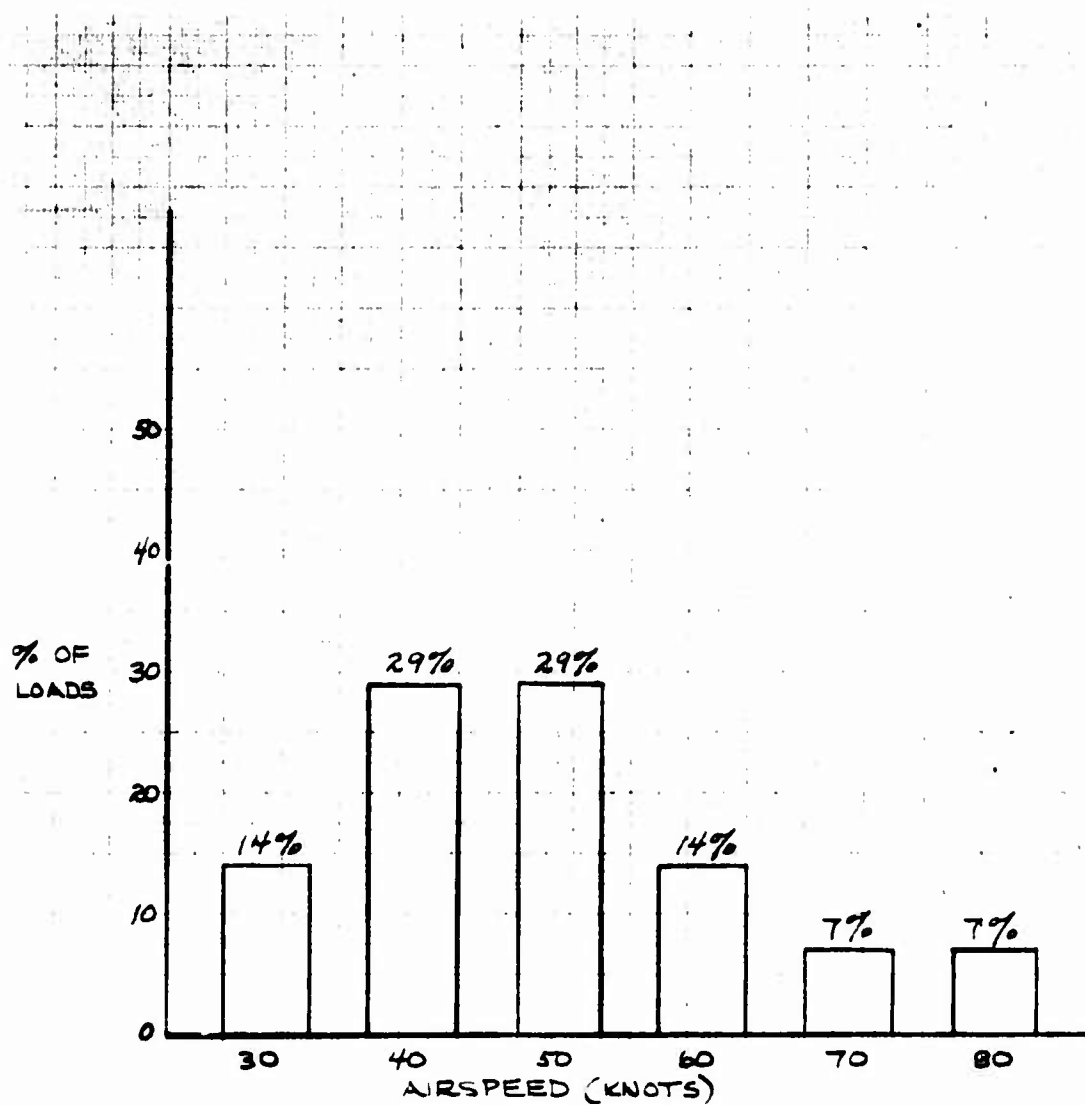


Figure A-21. Airspeed Range for Container Load CH-47.  
(Conex)

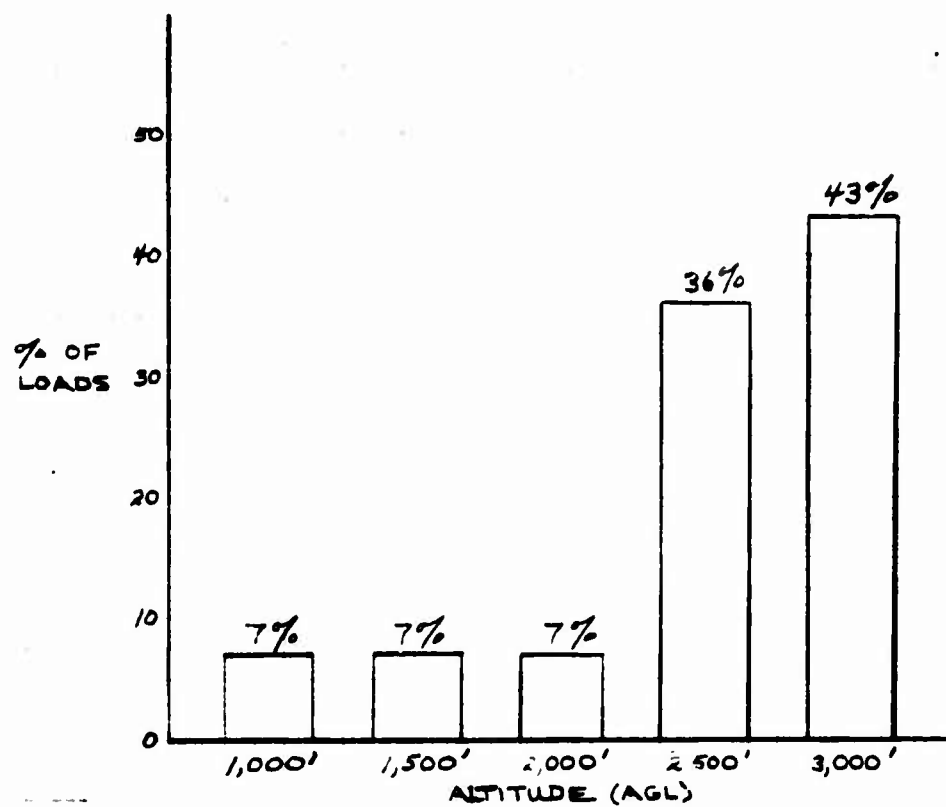


Figure A-22. Altitude Range for Container Load CH-47.  
(Conex)

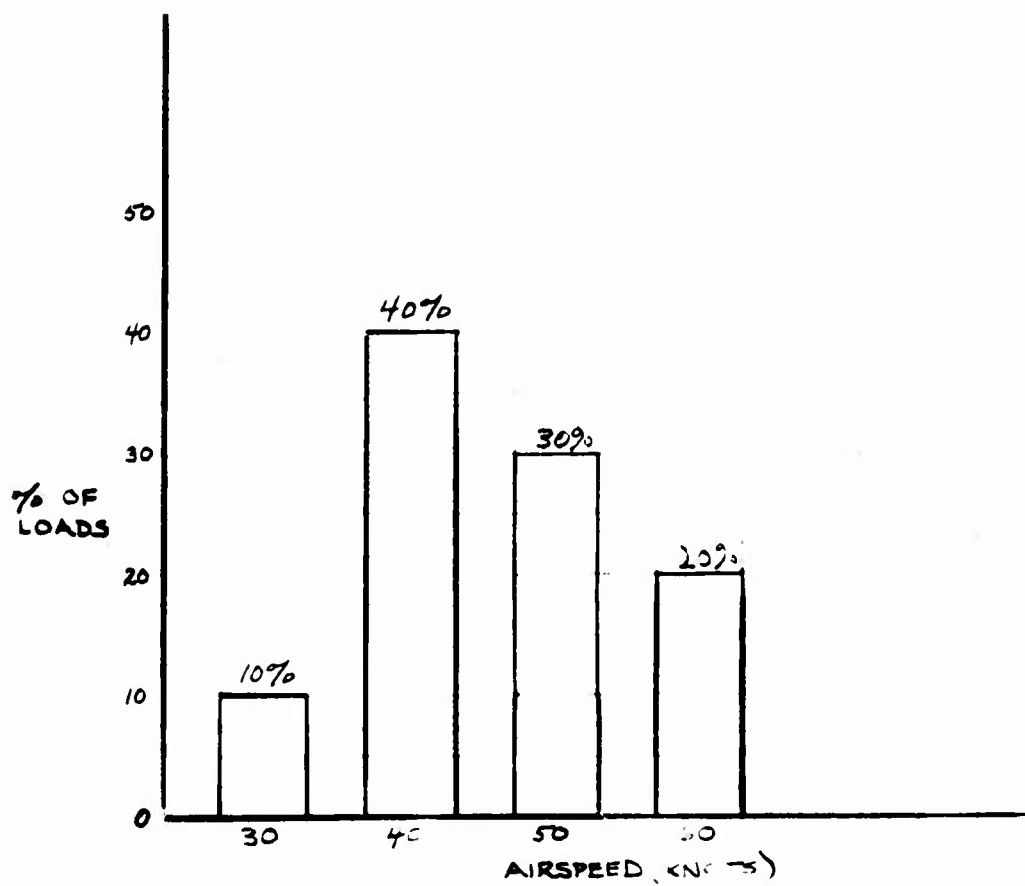


Figure A-23. Airspeed Range for Container Load CH-54.  
(Conex)

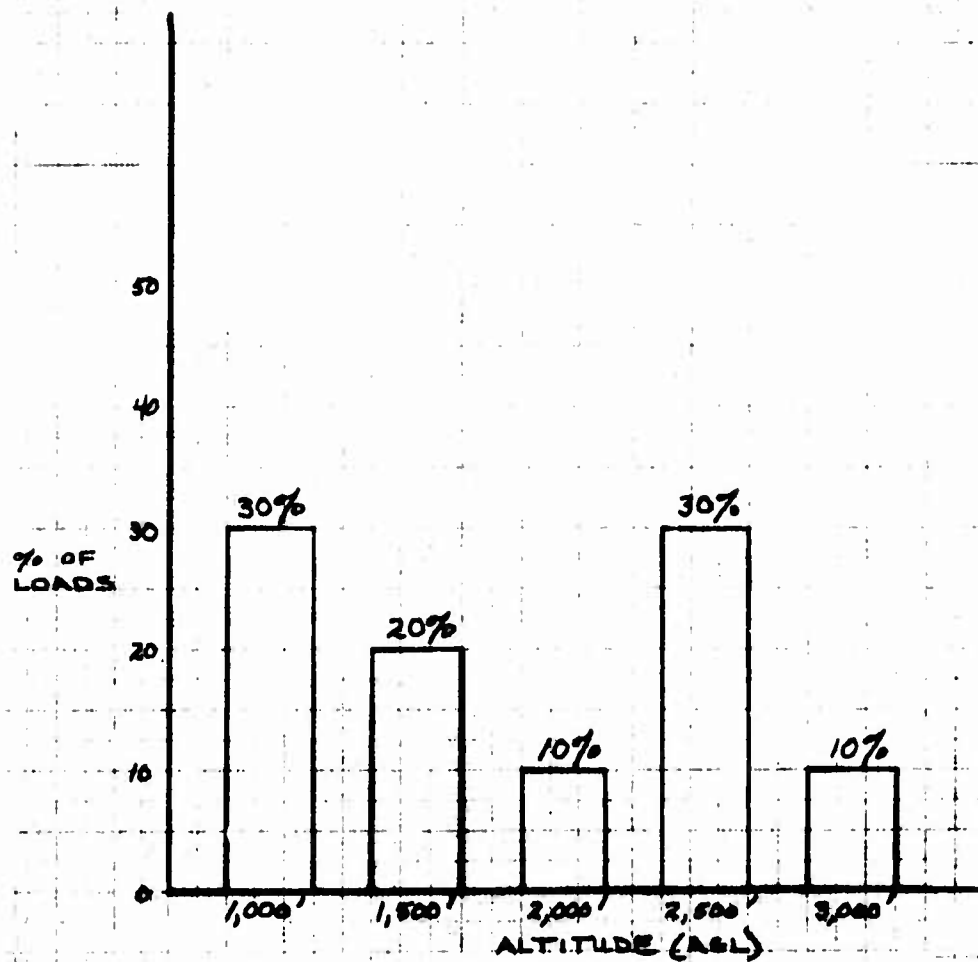


Figure A-24. Altitude Range for Container Load CH-54.  
(Conex)

### Load Weights and Airspeed

Figures A-25 and A-26 (CH-47 and CH-54) present data on weights normally lifted for the four broad categories of load and the airspeed at which they were flown.

### Aerial Delivery Slings and Nets

In determining the slings and nets used during external load operations, the items have been identified as a generic group. This approach was selected because of the multitude of slings of varying lengths and load capabilities in the Army inventory. For example, Federal Stock Class 1670 contains over 14 individual slings. Regardless of the sling length and capacity used for a particular load, the slings are attached to the helicopter hook by an endless sling which is better known as a "doughnut." The doughnut serves two main purposes: to facilitate hooking the load to the helicopter cargo hook, and to reduce the possibility of injury to the hookup man on the ground from static electricity buildup which may discharge when the cargo hook is touched. Table A-9 provides information on slings and nets normally used for lifting the four broad categories of sling loads. Subsequent sections of this report will address specific sling lengths and their impact on external load operations.

TABLE A-9. SLINGS AND NETS	
Load Category	Sling and/or Net Used
Vehicles	Sling, cargo, aerial delivery
Artillery	Sling, cargo, aerial delivery
POL	Sling, cargo, net
Containers	Sling, cargo, aerial delivery

### Stabilization Techniques and Devices

Questions 3c(5), (6), (7) and (8) of the questionnaire requested data on techniques and devices used to stabilize the four broad categories of sling loads. The flying technique commonly used by the aviators interviewed, when encountering load instability, was to reduce airspeed, start a gradual climb or descent, and in the CH-54, momentarily turn off the aircraft stabilization system. Table A-10 summarizes the rigging techniques and devices used to stabilize the loads.

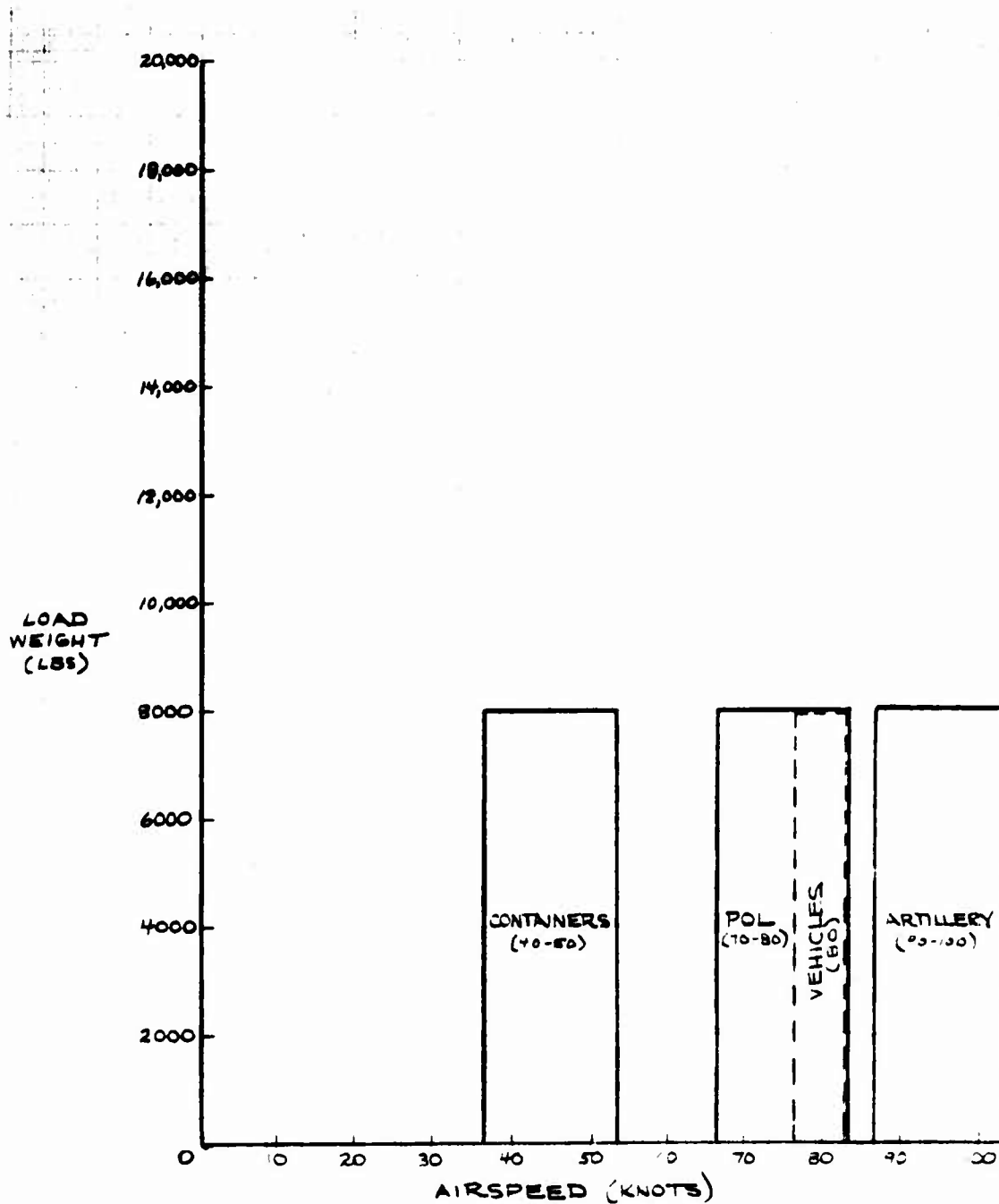


Figure A-25. CH-47 Average Load Weights and Airspeeds.

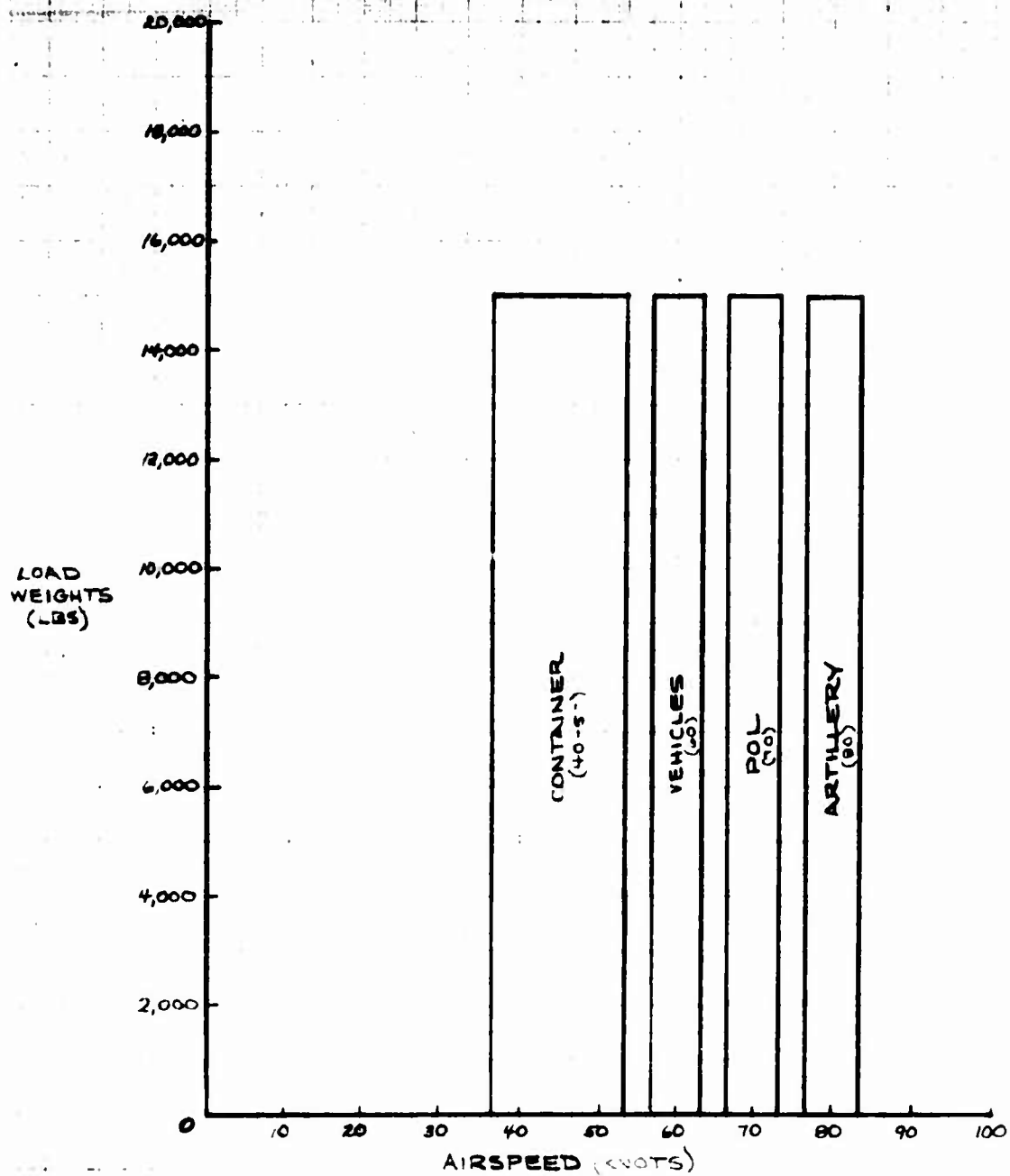


Figure A-26. CH-54 Average Load Weights and Airspeeds.



TABLE A-10. LOAD STABILIZATION DEVICES AND RIGGING TECHNIQUES	
Load Category	Device/Rigging Technique Used
Vehicles	Varying sling length Multipoint suspension Drogue chute Piggyback load
Artillery	Varying sling length Multipoint suspension Piggyback load
POL	Varying sling length Multipoint suspension
Containers	Multipoint suspension Varying sling length Drogue chute

#### Ranking of Individual Load Stability

The next question in the questionnaire asked the aviator to select sling loads in each of the four broad categories that exhibited the most and least stability characteristics in the air. These eight loads are identified in Table A-11.

TABLE A-11. INDIVIDUAL LOAD STABILITY	
Item	Stability Ranking
<u>Vehicles</u>	
2-1/2-ton truck	Most stable
AH-1G	Least stable
<u>Artillery</u>	
155mm Howitzer	Most stable
M102 Howitzer	Least stable
<u>POL</u>	
500-gallon collapsible drums of gasoline	Most stable
55-gallon drums of lube oil	Least stable
<u>Containers</u>	
Airmobile maintenance shops	Most stable
CONEX	Least stable

### Load Shape Impact on Stability

Aviator opinions on the impact of a load's shape on sling load stability are summarized in Tables A-12 and A-13 for tandem and single main rotor configuration helicopters, respectively. The interviewees were requested to rank six load shapes on a scale of 1 to 6 (1 represents the most stable and 6 the least stable shape). Total aviator responses are less than 40 since not all of the personnel were checked out in both aircraft rotor configurations. The numbers in the boxes represent a distribution of the aviator responses.

TABLE A-12. LOAD STABILITY RANKING (TANDEM ROTOR CONFIGURATION)						
LOAD SHAPE	STABILITY RANK ORDER *					
	1	2	3	4	5	6
Cylinder	12	8	4	0	0	4
Egg	4	9	7	2	3	3
Round	9	5	11	1	1	1
Triangle	0	1	1	16	6	4
Rectangle	3	2	2	4	15	2
Square	1	1	4	5	3	14
*1 represents most stable and 6 the least stable load						

TABLE A-13. LOAD STABILITY RANKING (SINGLE MAIN ROTOR CONFIGURATION)						
LOAD SHAPE	STABILITY RANK ORDER*					
	1	2	3	4	5	6
Round	15	7	6	4	2	0
Egg	5	13	7	0	6	4
Cylinder	7	9	11	1	2	5
Triangle	0	2	4	19	4	6
Rectangle	5	0	6	4	13	7
Square	3	3	2	7	7	13
*1 represents most stable and 6 the least stable load						

### Sling Length

Questions 3c(15), (16), (17), (18) and (19) were structured to permit aviator comments on optimum sling lengths, load behavior using varied lengths, and flying techniques used in countering load instability.

### Sling Length

In arriving at an optimum sling length, the first consideration is to use slings of sufficient length to maintain clearance between the load and the underside of the helicopter. The point was continually emphasized by the interviewees that a low-density load normally moves aft and slightly upward during cruising flight conditions, making load/aircraft separation even more critical. Tables A-14 and A-15 present aviator opinions on sling lengths for the four broad categories of loads that normally provide optimum stability. The tables cover single main and tandem-rotor configuration, respectively.

TABLE A-14. SINGLE-MAIN-ROTOR OPTIMUM SLING LENGTHS	
Load Category	Sling Length (ft)
Vehicles	15
Artillery	15
POL	15
Containers	16

TABLE A-15. TANDEM-ROTOR OPTIMUM SLING LENGTHS	
Load Category	Sling Length (ft)
Vehicles	13
Artillery	13
POL	13
Containers	13

### Load Behavior Using Varying Sling Lengths

The aviators consistently agreed that using sling lengths greater than 15 feet induced load instability. This instability is normally sensed from the cockpit and observed by the crew chief or aft-facing aviator (CH-54) as a side-to-side oscillation. The aviators felt much more comfortable, and experienced less load instability by carrying the loads closer to the belly of the aircraft. The limiting factor, as previously mentioned, was the danger of the load striking the aircraft while increasing air-speed and during cruising flight conditions.

In the hover flight mode, the aviators reported that longer sling lengths created a pendulum effect on the load.

In addition to side-to-side oscillation, the aviators reported that lifting low-density loads with sling lengths greater than approximately 15 feet induced yawing movements into the load. Aviators frequently use the term "load hunting" in describing yawing movements. Shorter sling lengths reduced the tendency of the load to yaw. The discussion on sling lengths thus far has been keyed to the usage of equal lengths, fore and aft to the load attachment points. These equal-length slings are then attached by means of a doughnut to the helicopter cargo hook. Another rigging technique, favored by the interviewees as a means of stabilizing loads, is to use longer\* slings to the forward attaching points of a load. Using longer slings on the front of a load provides a slightly negative angle of attack on the front of the load during translation to forward flight and cruise. This dipping of the front of the load results in greatly increased load stability and freedom from both side-to-side oscillation and yawing problems.

#### Instability Sensations in the Cockpit

The most common instability sensations reported by the aviators were the "reverse pendulum" effect, yawing, and induced changes in aircraft pitch.

The reverse pendulum effect in the air is generated by the side-to-side oscillation of the sling load. These forces are sensed in the cockpit as aircraft movement in an opposite direction from the swinging motion of the load. This situation is occasionally encountered in the hover mode during the moment that the load is being initially lifted from the ground. The sensation felt in the cockpit is described as the feeling an individual might experience if seated on a giant, inverted, grandfather clock pendulum.

Yawing sensations felt in the cockpit are described as a "hunting" action whereby the nose of the aircraft yaws from side to side.

Fore-and-aft oscillation of a sling load induces pitch changes into the aircraft attitude, and these are sensed from the cockpit as normal pitch changes, that is, nose-up/nose-down with a varying frequency rate.

#### Flying Techniques To Counter Load Instability

The primary technique for reducing sling load instability of any kind in forward flight is reduction of airspeed. Secondary actions include entering a shallow climb or descent, if permitted by the terrain. A

---

\* Exception is howitzer loads which use shorter lengths to front attaching points to preclude the trail's striking the belly of the aircraft.

tertiary procedure for the CH-54 is to momentarily turn off the AFCS.

The aviators reported that the reverse pendulum effect in the hover mode was best controlled by a slight reduction of collective pitch to place the load back on the ground, then making sure that the helicopter is positioned directly over the load before attempting another lift.

Yawing moments are best controlled by reduction of airspeed and use of the rudder pedals to dampen the oscillation.

Fore-and-aft oscillation is countered by airspeed reduction and by making sure that the aircraft is in trim.

All of the aviators emphasized the requirement for smooth, coordinated flight control movements not only to counter load instability but to preclude aviator-induced instability factors to the load.

#### Development of Flying Technique

Questionnaire questions 3c(20) and (21) dealt with development of flying technique and application thereof under adverse visibility conditions. The factors, in descending order of impact, that influenced development of aviator sling load technique are:

1. Day-to-day routine flying activity
2. Unit instructor pilots
3. Flight school training
4. Discussion with fellow aviators
5. Aircraft accident

The aviators unanimously agreed that poor visibility in an area of operations created problems in sling load stability. They likewise agreed that poor visibility caused an aviator to become tense and try to overcontrol the helicopter. Corrective action is to relax and make flight control inputs very smooth.

#### Sling Load Weight

Question 4 of the questionnaire addressed three areas which included the heaviest sling load lifted by various Army helicopters, changes in aviator technique when lifting an allowable cargo load, and vertical bounce.

### Maximum Sling Load Weight

The maximum sling load lifted by a CH-47B helicopter under operational conditions was reported to be 15,000 lb. The maximum for the CH-54B was 20,000 lb.

### Allowable Cargo Loads (ACL)

Unit SOP's in Southeast Asia normally specified an ACL of 10,000 lb for the CH-47B and 18,000 lb (reduced range) for the CH-54B. The aviators reported that no changes were made in their flying technique except for very smooth flight control inputs when lifting an ACL.

### Vertical Bounce

Fifteen of the forty Army aviators interviewed reported they had experienced vertical bounce while flying sling loads. The majority of flights were being flown at maximum gross weights and high airspeeds, although four cases were reported in the hover mode. The condition was experienced in both CH-47 and CH-54 helicopters. The majority of the pilots believed that vertical bounce was induced by rough handling of the flight controls. Corrective action to eliminate vertical bounce included reduction of airspeed and smooth, coordinated inputs to flight controls.

### Load Suspension Points

The final question in the questionnaire solicited aviator comments on the optimum number of load suspension points for Army helicopters, a projection of the maximum weight that would be lifted by Army helicopters through 1995, and identification of the most unusual sling load lifted by the individual aviator.

### Optimum Number of Load Suspension Points

The consensus of the aviators was that single-point suspension of sling loads was incompatible with airspeeds in excess of 100 knots. The main advantage of single-point suspension is the capability of rapid hookup and release of loads.

The majority of the aviators believed that multipoint suspension up to a maximum of four points for selected loads must be adopted if helicopters are to be used in sling load operations in the 100- to 150-knot airspeed spectrum. They cautioned, however, that multipoint suspension must possess a capability of rapid hookup and release, and a failsafe method of jettisoning the load must be developed.

### Projected Sling Load Weights

The majority of the aviators feel that external sling loads of 30 to 50 short tons will be lifted, by both single-main and tandem-rotor helicopters, as routine loads by the year 1995.

### Unusual Sling Loads

Sling loads lifted ranged from church steeples to live animals.

### Summary and Study Correlation

In summary, analysis of the aviator questionnaire data substantiated the findings of the previous Northrop study, "Inflight Stabilization of Externally Slung Helicopter Loads," Contract DAAJ02-70-C-0067.

Specifically, the data revealed that high-density loads may be lifted at or near cruising airspeeds, whereas low-density loads and those with aerodynamic qualities require a reduction in airspeed. Sling lengths in excess of 15 feet increase load instability, although the longer slings may have to be used for a particular load to prevent damage to the aircraft belly when the load shifts aft and upward during cruising flight. Varying the overall sling lengths and using longer slings on the front attachment points of a load are included in aviation unit SOP's as a means of achieving greater load stability.

Load oscillation is exhibited as side-to-side, fore and aft, yawing, and, on occasion, vertical movements. The primary flying technique in reducing load oscillation is a reduction in airspeed. The interviewees agreed that multi-point suspension was desirable provided hook up/release times could be reduced.

The conclusions of the previous Northrop study were presented in the introductory portion of this report.

To correlate the findings of both study efforts, the matrix on the next page presents the sling loads addressed in the previous study cross-referenced to tables of this report where substantiating data on the loads may be found. In using this matrix, the reader should refer to the Introduction for the previous study conclusions on a specific load, and then to the cross-referenced paragraphs on this report.

### CORRELATION OF LOADS

#### PREVIOUS STUDY DAAJ02-70-C-0067

#### THIS REPORT

Box (8 ft x 8 ft x 20 ft)	Tables IX, X, XI, XII, XIII, XVI and XVII
Box (8 ft x 8 ft x 40 ft)	Tables IX, X, XI, XII, XIII, XVI and XVII
Truck	Tables III, IV, XI, XII, XIII, XVI and XVII
Tank	No data obtained
Armored Personnel Carrier	Tables IV, XI, XII and XVI
Downed Aircraft	Tables III, IV, XII, XVI and XVII



### SPECIAL SLING LOAD PROBLEMS

During the analysis incident to this study, three special problem areas were identified which impact on future Army helicopter sling load operations. These problems are discussed in the following paragraphs.

#### AH-1G Instability

The AH-1G Cobra was continually identified in the questionnaire as a particularly unstable sling load. A detailed examination of the problem was outside the scope of this short study effort, but the problem appears to stem from the aerodynamic behavior of the Cobra's narrow fuselage. The aviator comments indicate that the Cobra executes a violent 180° turn during the initial lift-off from the ground, and continues to oscillate vigorously in the air. Attempts to stabilize the aircraft have met with very limited success.

#### MILVAN Positioning on Marine Craft

Two field maneuvers have been conducted near Fort Story, Virginia, to determine the potential of cargo helicopters to load and off-load container ships. The MILVAN container was the primary container used in the operations. This container measures 7 b 7 by 20 feet and can contain a maximum load of up to 20,000 lb of various supply items. The MILVAN has been successfully extracted from container ship holds by Army helicopters at weights of up to approximately 5,000 lb. The problem with the MILVAN arises when an attempt is made to deposit it in the MILVAN chassis guide jigs from a hover mode. The MILVAN is reported to be very unstable during this phase of sling load operation.

#### CH-54 Aft-Facing Aviator Training

Numerous comments were received from the interviewees concerning the level of proficiency of newly transitioned CH-54 aviators when performing aft-facing aviator duties incident to sling load operations. The consensus was that more training at the aviation school was needed, to include a flight simulator cockpit for the CH-54 aft seat.

## AREAS REQUIRING ADDITIONAL STUDY

In resolving sling load problems with future Army helicopters, particularly the HLH, the three special problem areas outlined above are recommended for further study. A rationale for each area is presented below.

### AH-1G Instability

The Cobra represents a significant quantity of the Army aviation fleet, and its mission makes it a potential candidate for frequent evacuation as a sling load. It is recommended that a study be initiated to identify the Cobra instability problems when being lifted as an external load.

### MILVAN Instability

In view of the fact that the Army has a tremendous investment in MILVAN containers and is attempting to convince the U.S. Navy of the feasibility of loading and off-loading container ships by helicopter, it appears highly desirable to make more effort to resolve the MILVAN instability during loading operations in the hover mode.

### CH-54 Aft Seat Training

The aviation school at Fort Rucker, Alabama, has incorporated a Synthetic Flight Training System (SFTS) into the helicopter training program of instruction. The SFTS is basically a large computer that controls UH-1 and CH-47 cockpit replicas, thus permitting concurrent multiple student training. It appears feasible to incorporate a CH-54 aft-facing cockpit replica into the SFTS. It is recommended that a short study be initiated in this area.

# APPENDIX B ANALOG COMPUTER MECHANIZATION DIAGRAMS

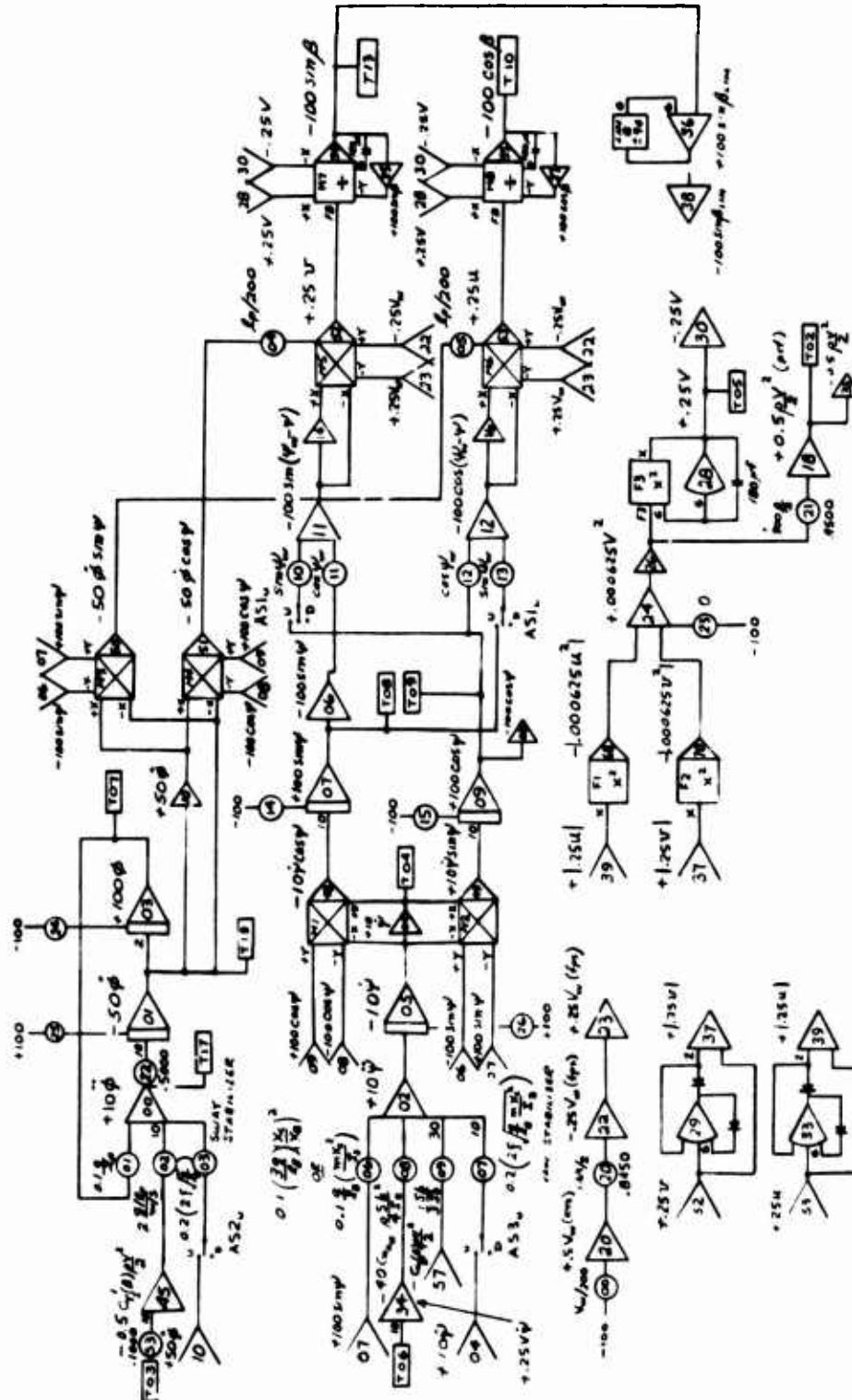
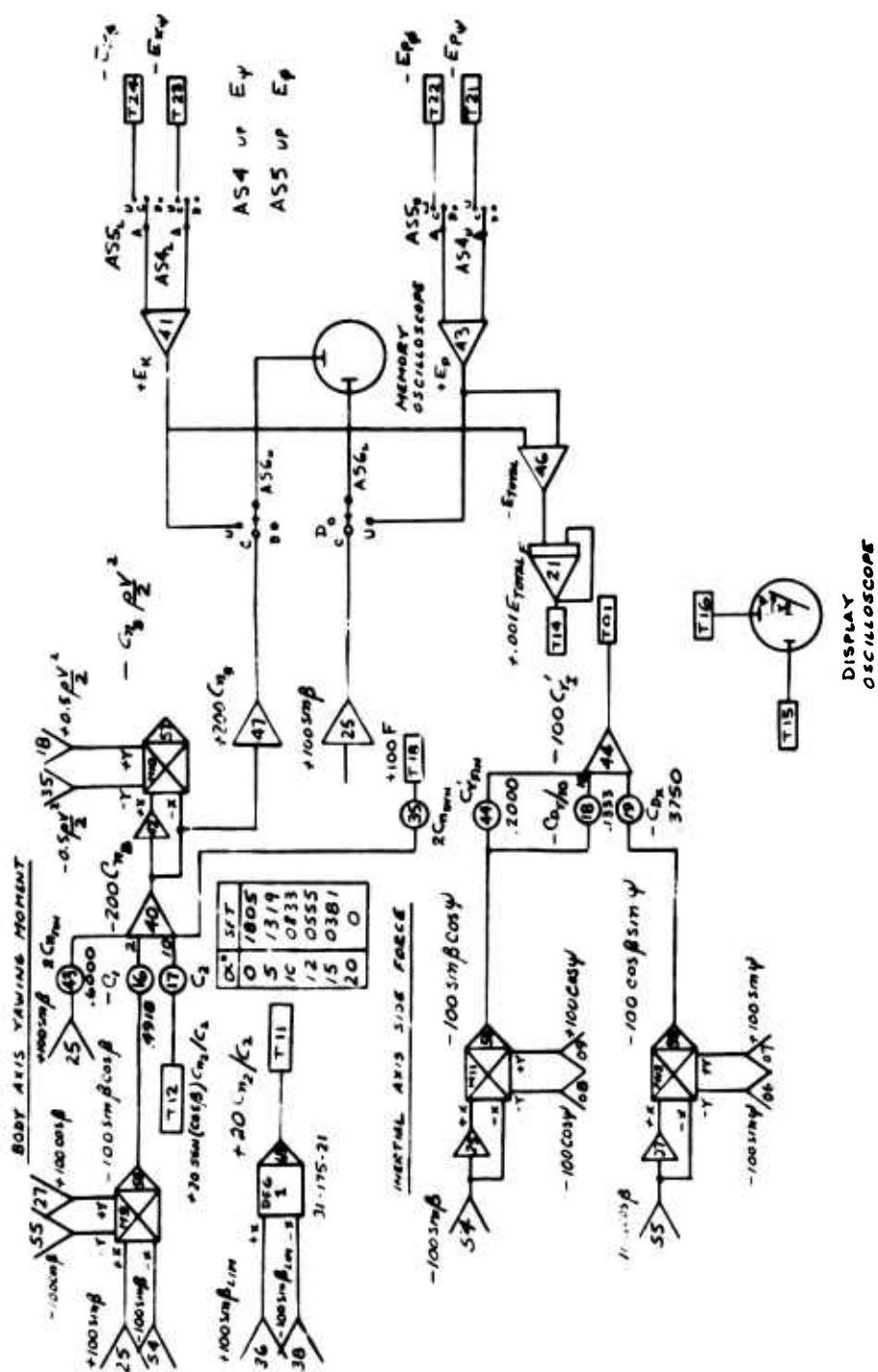


Figure B-1. Sling Load Analysis (Dynamics).





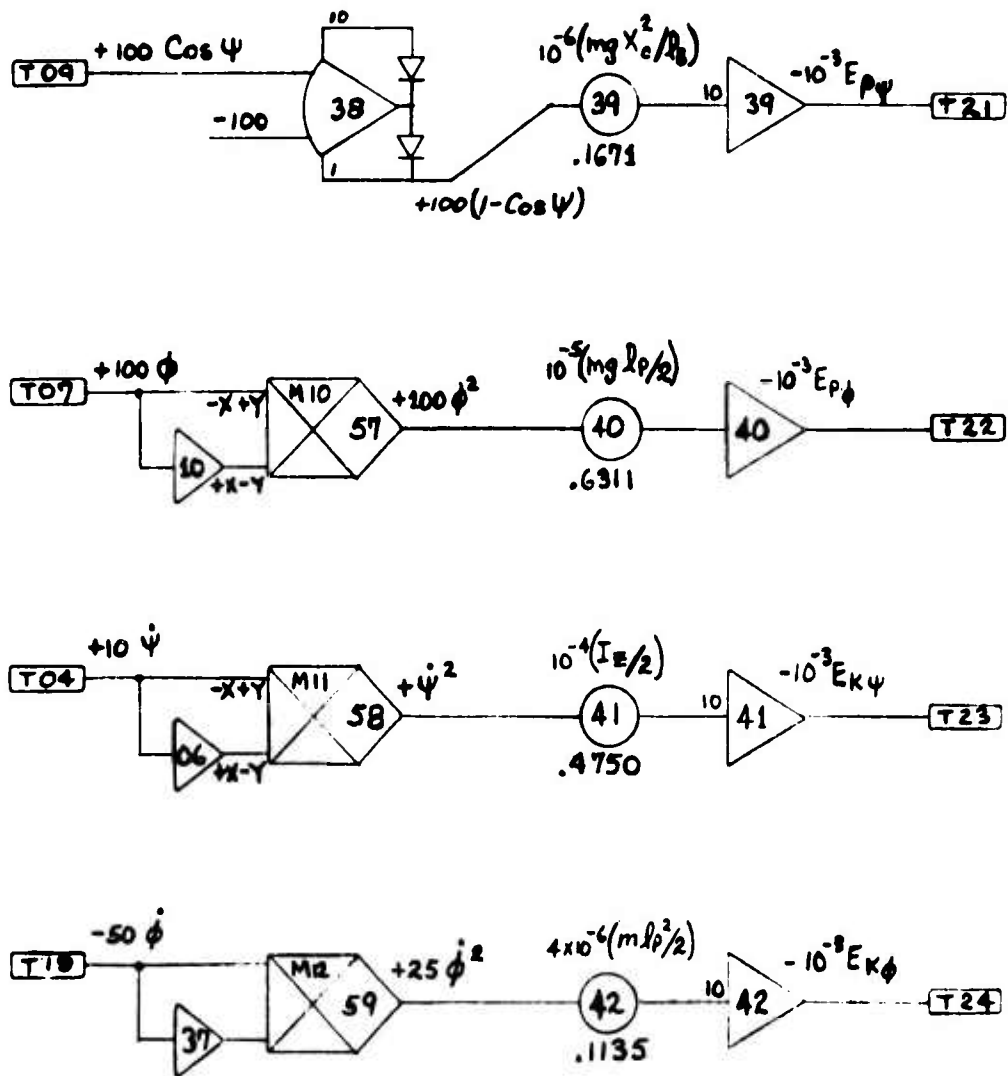


Figure B-4. Sling Load Analysis (Engineering Computation).

## APPENDIX C

### DYNAMIC WIND TUNNEL TEST RUN LOG

#### 0.1 SCALE MILVAN CONTAINER TEST LOG

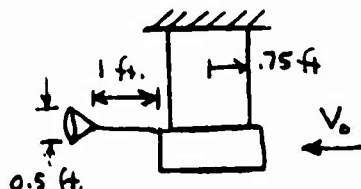
#### Run

1. Photo mapping for airspeed calibration - top of tunnel
2. Photo mapping for airspeed calibration - side of tunnel
3. Initial conditions of  $6^\circ$ ,  $12^\circ$  and  $0^\circ$  ( $\phi_0 = 6^\circ$ ,  $+12^\circ$ ,  $0$ )  $V_0 = 0$
4.  $\alpha = 0^\circ$   $\phi_0 = 6^\circ$   $V_0 = 20\text{KT}$   $X_c = .75$  ft  $\ell_B = 3.11$  ft  
Tufts on rear face oscillate at yaw frequencies,
5.  $\alpha = 0$   $\phi_0 = 6^\circ$   $V_0 = 20\text{KT}$   $X_c = .75$  ft  
Tufts on rear were shortened to prevent tying.
6.  $\alpha = 0^\circ$   $\phi_0 = 0^\circ$   $V_0 = 20\text{KT}$   $X_c = .75$  ft  
No film record  
 $\alpha = 0$   $\phi_0 = 0$   $V_0 = 20\text{KT}$   $X_c = .75$  ft  
 $\tau = 1.62$  sec  $\omega = 3.88$  rad/sec  
This is the bifilar frequency. The computed value for 20KT is 4.6 rad/sec.
7.  $\alpha = 0^\circ$   $\phi_0 = 0^\circ$   $V_0 = 25\text{KT}$   $X_c = .75$  ft  
 $\tau = 1.62^\circ$  sec or the bifilar period again  
The tufts on the rear face point in the direction of motion of the rear face (inertially) possibly slightly leading, yaw rate or  $\dot{\beta}$ .
8.  $\alpha = 0^\circ$   $\phi_0 = 6^\circ$   $V_0 = 25\text{KT}$   $X = .75$  ft  
 $\omega = 3.76$  rad/sec  $\psi_{\max} \approx \pm 30^\circ$
9.  $\alpha = 0^\circ$   $\phi_0 = 0^\circ$   $V_0 = 30\text{KT}$   $X_c = .75$  ft  
Box tended to yaw about forward cable about  $\pm 40^\circ$  at the bifilar frequency.
10.  $\alpha = 0^\circ$   $\phi_0 = 0^\circ$   $V_0 = 35\text{KT}$   $X_c = .75$  ft  
High-frequency oscillations ( $\pm 5^\circ$ ) at small  $\beta$ , then slower oscillations at the bifilar frequency with increasing amplitude ( $\pm 30^\circ$ ).  
Rotation about front cable.

11.  $\alpha=0^\circ$   $\phi_0=0^\circ$   $V_0=40KT$   $X_c=.75$  ft  
 Similar to Run 10  
 Initial frequency observed at  $\sim 6$  rad/sec (1 Hz)  
 which reduced to bifilar frequency as  $\beta$  increased beyond  $\pm 10^\circ$ .
12.  $\alpha=0^\circ$   $\phi_0=0^\circ$   $V_0=20KT$   $X_c=.75$  ft  
 with splitter plate 18" long  
 oscillation  $\omega \approx 1$  Hz fantastic!
13.  $\alpha=0^\circ$   $\phi=6^\circ$   $V=20KT$   
 Great!  $^\circ$  Pendulum mode oscillation with small sideslip; stable.  
 Increased speed to 25KT  $\tau=1.29$  sec  $\omega=4.8$  rad/sec  
       "      "      to 30KT  $\tau=1.21$  sec  $\omega=5.1$  rad/sec  
       "      "      to 40KT  $\tau=1.06$  sec  $\omega=5.82$  rad/sec
14.  $\alpha=0^\circ$   $\phi=6^\circ$   $V=40KT$   $X=.75$  ft  
Stable!  $\tau=1.1^\circ$  sec  $\omega=5.7$  rad/sec
15.  $\alpha=0^\circ$   $\phi=6^\circ$   $V=20KT$   $X=.75$  ft  
 Splitter plate cut to 12" length  
 $\tau=1.5$  sec Stable!  
 Increased speed to 40KT then put in initial condition of  $\phi=6^\circ$   
 Stable!
16.  $\alpha=0^\circ$   $\phi=6^\circ$   $V=20KT$   $X=.75$  ft  
 Splitter plate cut to  $4\frac{3}{4}$ " (half-width of box)  
 Not stable-resembles run with no plate.  
 $\tau=1.116$  sec  $\omega=5.4$  rad/sec for small sideslip
17.  $\alpha=0^\circ$   $\phi=6^\circ$   $V=20KT$   $X=.75$  ft  
 Two half doors on the edges. Stable!
18.  $\alpha=0^\circ$   $\phi=6^\circ$   $V=20KT$   $X=.75$  ft  
 Two quarter doors; oscillations - not stable
19.  $\alpha=0^\circ$   $\phi=6^\circ$   $V_0=20KT$   
 Two quarter doors at  $45^\circ$   
 Oscillations at 1 Hz about  $\pm 30^\circ$  Yaw  $\pm .2$  ft sway  
 both in phase. Rotation about front cable.

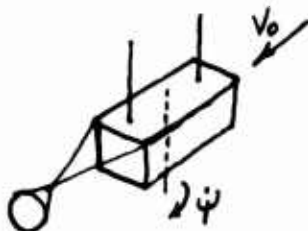


20.  $\alpha=0^\circ$   $\delta=0^\circ$   $V=20KT$   $X_c=.75$  ft  
 With Conical Drag Chute (paper paint filter)  
 0.5 ft diameter, apex 1 ft aft of rear face  
 $X_c=0.75$  ft



Not stable, oscillations at bifilar frequency  
 $\psi_{\max}=\pm 30^\circ$ ,  $\delta=\pm .1$  rad (rotation about the front cable)

21.  $\alpha=0^\circ$   $\delta=0^\circ$   $V=20KT$   $X_c=.75$  ft  
 With conical drag chute suspended by two cables



for +r, the left cable is taut, indicating a  $C_{N_r}$  contribution.  
 Stable for no initial conditions  
 Limit cycle  $6^\circ$  initial conditions @ bifilar frequency

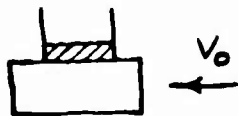
22.  $\alpha=0^\circ$   $\delta_o=6^\circ$   $V_o=20KT$   $X_c=.75$  ft  
 same configuration as Run 21  
 Stabilized to a limit cycle at bifilar frequency  
 after  $\sim 2$  min  $\psi_{\max}=\pm 20^\circ$ , rotation about the CG.  
 Took 15 sec of film of the limit cycle

23.  $\alpha=0^\circ$   $\delta_o=6^\circ$   $V_o=20KT$   $X_c=.75$  ft  
 With aft fin as shown



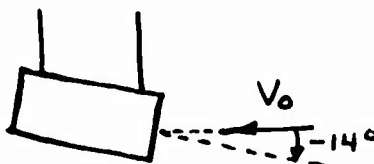
With initial startup, some roll was observed  $\tau=1.59$  sec  
 $\omega=3.92$  rad/sec. When released, bifilar oscillations observed  
 with rotations of  $\pm 30^\circ$   $\psi_{\max}$

24.  $\alpha=0^\circ$   $\delta_o=6^\circ$   $V_o=20KT$   $X_c=.75$  ft



With top surface fence between the cables 2" high  
Oscillates at  $\psi_{\max}=\pm 30^\circ$  at  $\omega=3.74$  rad/sec

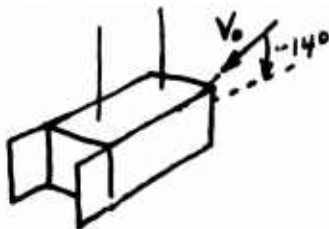
25.  $\alpha=-14^\circ$   $\delta_o=6^\circ$   $V_o=20KT$   $X_c=.75$  ft



Stable! slight oscillation of  $\pm 3^\circ$   $\psi_{\max}$  about forward cable at  
 $\omega=3.85$  rad/sec (bifilar  $\omega$ )  
Increased speed to 30 KT, oscillations  $\psi_{\max}=\pm 20^\circ$   $\omega=3.88$  rad/sec

26.  $\alpha=-14^\circ$   $\delta_o=6^\circ$   $V=40KT$   
Oscillates at  $\psi_{\max}=\pm 30^\circ$  about front cable at bifilar frequency -  
still until the initial condition (IC) was established.  
Stable with no IC.

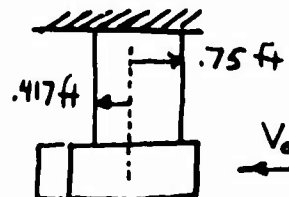
27.  $\alpha=-14^\circ$   $\delta_o=0^\circ$   $V=40KT$   $X_c=.75$  ft  
With two half-width doors<sup>c</sup> at each side at the rear



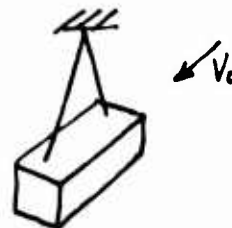
Stable, slight roll oscillations. Some oscillation of yaw at  
bifilar frequency  $\pm 2^\circ$   $\psi_{\max}$

Increased speed to 63KT. Some oscillations tended to build,  
requiring use of the side tethers. Appeared to be stable for  
about 55KTS.

28.  $\alpha=0^\circ$   $\delta=0^\circ$   $V=40KT$   $X_c=.75$  ft  
With side boards.  
Bifilar oscillations  $\psi_{max}=\pm 10^\circ$   
Increased speed to 60KT  
 $\omega=5.4$  rad/sec  $\psi_{max}=\pm 10^\circ$  about front cable.
29.  $\alpha=0^\circ$   $\delta=0^\circ$   $V=60KT$   $X_c=.75$  ft  
 $\omega=5.2$  rad/sec  $\psi=\pm 10^\circ$  With side boards  
 $\omega$  was higher for small perturbations
30.  $\alpha=-10^\circ$   $\delta=6^\circ$   $V=40KT$   $X_c=.75$  ft  
With side boards  
Stable - slight roll oscillations, lateral mode reasonably well damped. Increased speed to 67KTS then put in initial condition of  $\delta=6^\circ$ . Stable, well damped
31.  $\alpha=-10^\circ$   $\delta=6^\circ$   $V=67KT$   $X_c=.75$  ft  
With side boards  
Stable, well damped!  $\zeta=0.3-0.4$
32.  $\alpha=-10^\circ$   $\delta=12^\circ$   $V=67KT$   $X_c=.75$  ft  
With side boards Stable!  $\zeta=0.4$   
Sway mode only excited, yaw about  $1-2^\circ$
33.  $\alpha=-10^\circ$   $\delta=6^\circ$   $V=20KT$   $X_c=.75$  ft  
No Side boards  
Stable sway mode ex. lightly damped  
Increased speed to 30KT. Yaw oscillations excited  $\pm 20^\circ$  at bifilar frequencies.
34.  $\alpha=0^\circ$   $\delta=0^\circ$   $V=10KT$   $X_c=.75$  ft  
No side boards. Smoke study
35.  $\alpha=0^\circ$   $\delta=0^\circ$   $V=10KT$   $X_c=.75$  ft  
Smoke Study with side boards
36.  $\alpha=0^\circ$   $\delta=6^\circ$   $V=30KT$   $X_{cf}=9"$  .75 ft  
With side boards  
 $X_{CR}=5"$  .417 ft
37. Same as 36 but  $V_o=50KT$   
with side boards
38.  $\alpha=0^\circ$   $V_o=30KT$   $\delta=6^\circ$   $X_c=.417$  ft  
With side boards  
oscillations about rear cable



39.  $\alpha = -10^\circ$   $\beta = 6^\circ$   $V_o = 30KT$   $X_c = .417$  ft  
 With side boards  
 Stable  $\zeta \approx 0.3$   
 Increased speed to 40KT still stable  
 " " " 60KT " "
40.  $\alpha = -10^\circ$   $\beta = 6^\circ$   $V_o = 68KT$   $X_c = .417$  ft  
 With side boards
41.  $\alpha = 0^\circ$   $\beta = 6^\circ$   $V_o = 20KT$   $X_c = .417$  ft  
 No side boards  
 Oscillations of  $\pm 20^\circ$   $\psi_{max}$  at bifilar frequency  
 Rotation about C.G.
42.  $\alpha = -10^\circ$   $\beta = 6^\circ$   $V_o = 20KT$   $X_c = .417$  ft  
 No side boards  
 Oscillations of  $\pm 10^\circ$  at bifilar frequency
43.  $\alpha = 0^\circ$   $\beta = 0^\circ$   $V_o = 20KT$   $X_c = 0$   
 Single Cable  $\psi_o \approx 0^\circ$  No side boards  
 Not restrained during tunnel startup. At  $V_o \approx 14KT$   
 turned broadside  $\beta \approx 80^\circ$ . Stable in the broadside configuration.
44.  $\alpha = 0^\circ$   $\beta = 0^\circ$   $V_o = 20KT$  Single Cable  
 No side boards,  $\psi_o \approx -90^\circ$   
 $\tau = 4.66$  sec  $\omega = 1.34$  rad/sec  
 Sway mode unstable
45.  $\alpha = 0^\circ$   $\beta = 0^\circ$   $V_o = 20KT$  Single Cable  
 With side boards  $\psi_o \approx 0^\circ$   
 $\tau = 4.9$  sec @ 17KT  $\omega = 1.28$  rad/sec  
 $\tau = 4.15$  sec @ 20KT  $\psi_{max} = \pm 5^\circ$   
 $\tau = 4.75$  sec @ 20KT  $\psi_{max} = \pm 5^\circ$   
 $\omega = 1.32$  rad/sec  
 Induced large yaw angle, returned to  $\beta \approx 0$
46.  $\alpha = -10^\circ$   $\beta = 0^\circ$   $V_o = 20KT$  Single Cable  
 With side boards  $\psi_o \approx -90^\circ$   
 Stable, returns to  $\beta = 0$  condition
47.  $\alpha = -10^\circ$   $\beta = 0^\circ$   $V_o = 20KT$  Single Cable  
No side boards  
 $\psi_o \approx 0^\circ$   
 At 18KT turned broadside  
 $\tau = 2.3$  sec  $\omega = 2.73$  rad/sec (broadside)  $\psi_{max} = \pm 10^\circ$   
 After a long time 2-3 min. sway mode begins to build.



APPENDIX D

FLIGHT SIMULATOR DESCRIPTION

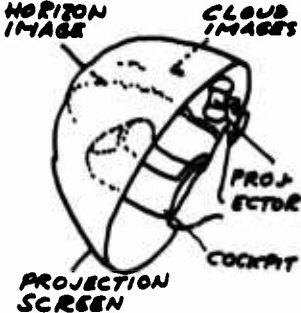
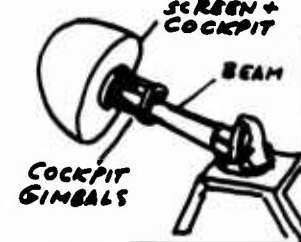
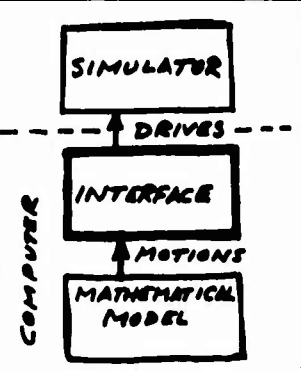
<p><b>BASIC COMPUTER PROGRAM AND COMPUTING COMPLEX</b></p>	<p style="text-align: center;"><u>MATHEMATICAL MODEL</u></p> <p>Full flight envelope representation employing rigid-body equations of motion for helicopter and external load and classical rotor equations or rotor maps. Powerplant and flight control system are accurately modeled, and small perturbation sling load dynamics are complete. Based on the data of Reference 4.</p>
 <p>The diagram shows a perspective view of a cockpit. A large, curved projection screen is positioned in front of the cockpit. Labels include 'HORIZON IMAGE' pointing to the top of the screen, 'CLOUD IMAGES' pointing to the upper part of the screen, 'PROJECTOR' pointing to the screen itself, and 'COCKPIT' pointing to the seat area.</p>	<p style="text-align: center;"><u>VISUAL DISPLAY</u></p> <p>Wide-angle visual system provides 200° wide x 60° high display of the horizon, some sky details, and a featureless brown earth scene. No attitude restrictions. No representation of height. Bandwidth is 4 cycles/second and static thresholds are 0.1 degree. Driven by complex interface based on unpublished Northrop data.</p>
 <p>The diagram shows a beam-type motion base. A large, circular screen is mounted on a gimbal system. A cockpit is attached to the end of a long beam that is supported by a base. Labels include 'SCREEN + COCKPIT' pointing to the screen and cockpit, 'BEAM' pointing to the support arm, and 'COCKPIT GIMBALS' pointing to the base.</p>	<p style="text-align: center;"><u>MOTION SYSTEM</u></p> <p>Five-degree-of-freedom beam-type motion base providing pitch, roll, yaw, heave and lateral sway motions. More than adequate acceleration and rate capability; 4 cycle/second bandwidth. Motion recovery about 40%. Interface is contained in Reference 5.</p>
<ul style="list-style-type: none"> <li>• BASIC INSTRUMENTS</li> <li>• CYCLIC</li> <li>• PEDALS</li> <li>• COLLECTIVE</li> <li>• MODE SWITCHES</li> </ul>	<p style="text-align: center;"><u>INSTRUMENTS &amp; FORCE FEEL SYSTEM</u></p> <p>A full complement of flight instruments is provided together with a cockpit controller force servo system which accurately represents the stick, pedal and collective forces.</p>
 <p>The diagram is a block diagram showing the flow of data. At the bottom is a box labeled 'MATHEMATICAL MODEL'. An arrow labeled 'MOTIONS' points up to a box labeled 'INTERFACE'. From the 'INTERFACE' box, a dashed arrow labeled 'DRIVES' points up to a box labeled 'SIMULATOR'. To the left of the 'INTERFACE' and 'SIMULATOR' boxes, the word 'COMPUTER' is written vertically.</p>	<p style="text-align: center;"><u>INTERFACE COMPUTATIONS</u></p> <p>A complex system of algebraic and differential equations that accept outputs from the equations of motion and calculate the drive commands for each actuator. Compensation is included that produces a matched dynamic response for the whole device. The visual display calculations are based on unpublished Northrop data. The motion system interface is contained in Reference 5.</p>

Figure D-1. Key Properties of the 347 Flight Simulation.

VALIDATION METHOD

1. Static and dynamic comparisons with flight data
2. Subjective evaluation by pilots current in the 347
3. Related analysis of pilot-vehicle dynamics

BASIC CAPABILITY

Able to represent the 347 over its complete operating envelope except near the ground. Sling load is represented accurately for small amplitudes and two-point parallel suspensions.

USES FOR THE PRESENT PROGRAM

The simulation was used to investigate the effects of:

1. Load mass/helicopter mass
2. Load geometry
3. Load suspension system (two-point)
4. SAS feedbacks from load motion sensors
5. Active cable guide actuator concepts

Figure D-1. Continued.

### LIST OF SYMBOLS

A	characteristic equation coefficient, $\frac{qs}{m}$ , ft/sec <sup>2</sup>
B	characteristic equation coefficient, $\frac{qsb}{I_z}$ , lb-ft-sec <sup>2</sup>
b	container width, ft
C	unsteady yawing moment coefficient
C <sub>N</sub>	yawing moment coefficient
C <sub>NB</sub>	yawing moment coefficient due to sideslip, rad
C <sub>YB</sub>	side force coefficient due to sideslip, rad
C <sub>Nr</sub>	yawing moment coefficient due to nondimensional yaw rate $\frac{rb}{2V_o}$
D	differential operator
F <sub>R</sub>	Froude number, $\frac{v_o^2}{lg}$
f	unsteady yawing moment function
g	acceleration of gravity, 32.2 ft/sec <sup>2</sup>
I <sub>z</sub>	yawing moment of inertia, slug-ft <sup>2</sup>
j	$\sqrt{-1}$
l	container length, ft
l <sub>p</sub>	pendulum length, ft
l <sub>B</sub>	bifilar length, ft
m	load mass, slugs
N	yawing moment, lb-ft
Q, q	dynamic pressure, lb/ft <sup>2</sup>

$r$	yaw rate, rad/sec
$S$	container planform area, $i \times b$ , $\text{ft}^2$
$S_T$	Strouhal number, $\frac{\omega b}{V_o}$ , rad
$s$	Laplace operator
$V_o$	airspeed, ft/sec or kt
$W$	load weight, lb
$X_C$	horizontal distance between cable and load center of mass, ft
$X_B$	container half-length, ft
$\alpha$	load angle of attack, deg
$\beta$	load sideslip angle, deg or rad
$\beta_\epsilon$	sideslip error, $\beta_{\text{command}} - \beta$ , rad
$\omega$	frequency, rad/sec
$\omega_\psi$	bifilar frequency, rad/sec
$\omega_\omega$	pendulum frequency, rad/sec
$\sigma$	real part of complex root
$\psi$	load yaw angle, rad or deg
$\phi$	load lateral sway angle, deg or rad
$\rho$	air density, slugs/ $\text{ft}^3$

#### Subscripts

$\phi$	sway axis
$\psi$	yaw axis
max	maximum value

A dot over a quantity indicates differentiation with respect to time